Helsinki University of Technology Publications in Bridge Engineering
Teknillisen korkeakoulun sillanrakennustekniikan julkaisuja
Espoo 2006 TKK-SRT-36

# INFLUENCE OF SHEAR CONNECTORS ON THE ELASTIC BEHAVIOUR OF COMPOSITE GIRDERS

Doctoral Dissertation

**Bertalan Szabó**

TEKNILLINEN KORKEAKOULU
TEKNISKA HÖGSKOLAN
HELSINKI UNIVERSITY OF TECHNOLOGY

Helsinki University of Technology Publications in Bridge Engineering
Teknillisen korkeakoulun sillanrakennustekniikan julkaisuja 36
Espoo 2006

# INFLUENCE OF SHEAR CONNECTORS ON THE ELASTIC BEHAVIOUR OF COMPOSITE GIRDERS

Doctoral Dissertation

**Bertalan Szabó**

Dissertation for the degree of Doctor of Science in Technology to be presented with due permission of the Department of Civil and Environmental Engineering for public examination and debate in Auditorium R1 at Helsinki University of Technology (Espoo, Finland) on the 8th of December, 2006, at 12 noon.

Helsinki University of Technology
Department of Civil and Environmental Engineering
Laboratory of Bridge Engineering

Distribution:
Helsinki University of Technology
Laboratory of Bridge Engineering
P.O. Box 2100
FIN - 02015 TKK
URL:http://www.tkk.fi/Units/Bridge/
Tel. +358-(0)9-451 3701
Fax. +358-(0)9-451 3826
E-mail: srt.sihteerit@tkk.fi



ISBN 951-22-8446-4
ISBN 951-22-8447-2 (PDF)
ISSN 1456-6273

Műegyetemi Kiadó
Budapest 2006

Szabó, B.: Influence of shear connectors on the behaviour of composite girders

**Keywords:** steel-concrete and wood-concrete composite girders, bridge, shear connection, flexible connectors, finite element method, parametric study.

## ABSTRACT

The effect of deformable and rigid connectors and influence of connection parameters on the behaviour of composite girders is examined. Both the elastic and plastic behaviour are discussed, but the former one is the main concern. Deformable connectors cause slip in the joint, which results in redistribution of internal forces and changes in the deformed shape of the beam compared to the connection with rigid connectors.

The aim of this study is to complement the analytical methods and develop numerical models – based on the author's experimental research - capable to provide reliable parametric studies of three-dimensional structural models of composite girders with deformable and rigid connectors.

At first, the partial interaction problem, behaviour of composite girders in the case of various loading types, recent development and real behaviour of connections of composite girders is discussed in the introduction. It is followed by a detailed literature survey serving the purpose of this study. This survey comprises two main parts: analytical and numerical models of composite girders. Among the analytical models, statical and energy methods are considered. The author also developed a new kind of energy method based on variational calculation for determination of shear force distribution of shear connectors of composite girders. The new method is in compliance with the experimental and the latest theoretical investigations. Next, experimental study on steel-concrete and wood-plywood composite girders conducted by the author at the Budapest University of Technology and Economics and Helsinki University of Technology respectively, are presented as well.

Experimental studies are followed by parametric studies based on analytical and finite element analyses in order to examine how changes in the connector stiffness affect the behaviour of composite girders. Based on these parametric studies, new design formulas are developed for design practice. The main results obtained by the author are: development of energy method based on the variation calculation, elaboration of a parametric study for determining the elastic shear force for all cross-sections and spans, use of photoelastic method to verify shear stresses near to the beam end, simulation of temperature effect, and development of a FEM model providing results that show good compliance with experimental results.

# PREFACE

In Hungary steel-concrete composite bridges have been extensively used for a long time. In the last two decades even a Danube bridge was constructed using steel-concrete composite girder, use of this structure though is popular mainly for middle-span bridges. Several composite bridges with such structure are being planned and constructed in Hungary. Besides it is always a possible engineering solution to reinforce an old steel plate girder using a concrete slab. In Finland very intensive activity can be experienced in the field of implementing wood-concrete composite girders since the early 1990's, out of which the Vihantasalmi Bridge is the greatest and most attractive king post composite bridge. To meet the demands of engineering practice, large-scale investigations are being carried out on composite structures both at the Budapest University of Technology and Economics (BUTE) and Helsinki University of Technology (TKK). The development and introduction of Eurocodes also ensured enormous progress in this field.

In the frame of co-operation between the Laboratory of Bridge Engineering (LBE) of TKK and the Department of Structural Engineering (DSE) of BUTE the present author worked at the LBE during the academic year of 1998/1999 conducting experimental tests on wood-based composite girders. This study aims at supplementing these tests and the earliest research work of the author, providing a new method for calculation, and developing new design formulas for design practice, by investigating the behaviour of connectors, and the influence of their behaviour on the stress and strain condition of a steel-concrete and wood-concrete composite girder.

The author expresses his deep gratitude to his supervisor, Professor Aarne Jutila for the opportunity to prepare this study at TKK under his guidance, for his steady encouragement and devoted support throughout the entire research work.

The author also wishes to thank Professor Bo Edlund from Chalmers University of Technology and Dr Matti V. Leskelä from the University of OULU for thoroughly reviewing the study and for their critical remarks concerning the contents and manner of presentation of the text. These comments were considered and are believed to have contributed to the value of the study.

The author is indebted to Professor Miklós Iványi and the late Professor Pál Platthy from the Department of Structural Engineering (DSE) of BUTE for their support facilitating experimental tests on steel-concrete composite girders. Thanks are also offered to the staff of the Laboratories of LBE and DSE. In addition, many other colleagues of the author from TKK and BUTE and from other organizations not nominated herein merit particular thanks for their continuing help, interest and encouragement.

Last but not least, the author would like to thank Ms. Zsuzsanna Zsilák (M.Sc.) for revising the English text of the manuscript at different stages of completion.

Budapest-Espoo, June 2006

Bertalan Szabó

# CONTENTS

# NOTATION

| | |
|---|---|
| $A_a$ | area of beam cross-section |
| $A_c$ | area of slab cross-section |
| $A_a^*$ | area of the top (or bottom) portion of beam cross-sectional area, defined from the section where $b_a$ is measured |
| $A_c^*$ | area of the top (or bottom) portion of slab cross-sectional area, defined from the section where $b_c$ is measured |
| $A_i$ | ideal area of composite cross-section |
| $A_{se}$ | area of longitudinal reinforcement in compression |
| $A_{ap}$ | effective area of profiled steel sheeting |
| $C^*$ | rigidity parameter of composite girder $[C_a \cdot C_c / (C_a + C_c)]$ |
| $C^2(a;b)$ | space of twice continuously differentiable functions |
| $C_a$ | axial stiffness of beam |
| $C_c$ | axial stiffness of slab |
| $D_{abs}$ | bending stiffness of composite girder without interaction between the parts |
| $D_i$ | ideal stiffness for traditional energy method |
| $D_c$ | bending (flexural) rigidity of slab |
| $D_a$ | bending (flexural) rigidity of beam |
| $D_{full}$ | bending stiffness of the composite girder with full interaction |
| $E_a$ | modulus of elasticity of beam |
| $E_c$ | modulus of elasticity of slab |
| $F$ | connector force |
| $F_a$ | contact force between beam and slab |
| $F_{cf}$ | normal force of beam or slab assuming full strength of connection |
| $F_{emb}$ | shear embedment force |
| $F_{est}$ | estimated maximum load |
| $F_{max}$ | maximum force that can be transmitted by a connector |
| $F_{patch}$ | splitting resistance of the concrete prism |
| $F_{sh}$ | shear force acting on the connector |
| $F_{xz}$ | split load in x-z plane |
| $F_{xy}$ | split load in x-y plane |
| $F_y$ | connector force calculated by the finite element model |
| $G$ | shear modulus |
| $I_a$ | moment of inertia of the beam |
| $I_c$ | moment of inertia of the slab |
| $I_i$ | ideal moment of inertia of the composite cross-section |
| $K$ | spring constant of interface layer |
| $L$ | span |
| $L^2(a;b)$ | pace of square-integrable functions |
| $L_i$ | work of internal forces |
| $M$ | bending moment of composite girder |
| $M_{max}$ | maximal bending moment of composite girder |
| $M_0$ | resultant bending moment |
| $M_a, M_c$ | bending moment acting in the beam (sectorial force) |
| $M_{a,pl}$ | bending moment acting in the beam causing plastic failure |
| $M_{apl,Rd}$ | design plastic resistance of the steel beam |
| $M_c$ | bending moment acting in the slab (sectorial force) |
| $M_{Ed}$ | design bending moment |

| | |
|---|---|
| $M_{pl,Rd}$ | design plastic resistance of composite section |
| $M_{sh}$ | bending moment acting on the connector |
| $M_u^{(r)}$ | reduced ultimate moment |
| $M_u$ | ultimate moment |
| $M_z$ | bending moment about z axis |
| $N$ | normal force acting in the beam or slab |
| $N_0$ | axial force obtained with infinitely rigid joint |
| $N_a$ | normal force acting in the beam (sectorial force) |
| $N_c$ | normal force acting in the slab (sectorial force) |
| $N_{full}$ | normal force due to Hawranek-Stenhardt method with respect to full shear connection |
| $P$ | external force, patch loading |
| $R$ | set of real numbers |
| $S$ | statical moment |
| $S_a^*$ | statical moment of the top (or bottom) portion of beam cross-sectional area, defined from the section were $t_a$ is measured |
| $S_c^*$ | statical moment of the top (or bottom) portion of slab cross-sectional area, defined from the section were $t_c$ is measured |
| $T$ | shear force per unit length (shear flow) |
| $T(0)$ | elastic shear flow at support line |
| $T_{full}(0)$ | elementary shear flow at support line |
| $T_1$ | temperature at upper extreme fibre of concrete slab |
| $V$ | shear force |
| $V_l$ | total design longitudinal shear force |
| $X_a$ | axial force in connector |
| $X_{emb}$ | axial embedment force |

| | |
|---|---|
| $a_i$ $(i=1, 2…n)$ | coefficient of Fourier-series |
| $b_a$ | width of bar connector |
| $b_c$ | effective width of concrete slab or width of concrete prism in splitting analysis |
| $b_f$ | distance between loading point of eccentric shear force $F_{sh}$ and interface of steel beam and concrete slab |
| $c$ | spacing between the connectors |
| $c_i$ $(i=1, 2…n)$ | constants |
| $d$ | distance between centre of gravity of slab and beam ($d = d_a + d_c$) |
| $d_a$ | distance between centre of gravity of beam and contact surface |
| $d_c$ | distance between centre of gravity of slab and contact surface |
| $d_{ai}$ | distance between centre of gravity of beam and ideal centre of gravity of composite girder |
| $d_{ci}$ | distance between centre of gravity of slab and ideal centre of gravity of composite girder |
| $d_{ae}$ | distance between centre of gravity of beam and line of connector force |
| $d_{ce}$ | distance between centre of gravity of slab line of connector force |
| $d_t$ | length of splitting crack |
| $e$ | distance from the lower edge of composite girder |
| $e_k$ | eccentricity from interface of connector force in the method of redundant forces |
| $f_{cb}$ | tensile strength of concrete |
| $f_{ck}$ | yield strength of concrete |
| $f_d$ | lateral stress due to constant component of shear flow |

| | |
|---|---|
| $f_{max}$ | maximum lateral stress due to strip load |
| $f_r$ | lateral stress due to varying component of shear flow |
| $f_{sk}$ | yield strength of reinforcement |
| $f_y$ | yield strength of steel |
| $f_{yp}$ | yield strength of profiled steel sheeting |
| $f_e$ | photoelastic constant of the layer |
| $h_a$ | height of connector or prism used in the splitting analysis |
| $h_c$ | depth of concrete slab |
| $h_1$ | part of concrete slab depth |
| $h_2$ | part of steel web depth |
| *i and j* | real numbers |
| $k_x$, $k_y$, $k_z$ | spring stiffness values of connectors in the finite element model |
| $m$ | fringe order of the isochromat |
| $m_{abs}$ | absolute material content |
| $m_{rel}$ | relative material content |
| $n$ | number of partial shear connectors |
| $n_1$ | a limit number of partial shear connectors |
| $n_f$ | number of full shear connectors |
| $p_i(x)$ | member of Fourier-series |
| $q$ | intensity of uniformly distributed load |
| $q_{pl}$ | intensity of uniformly distributed load causing plastic failure |
| $s(x)$ | slip at interface |
| $t$ | time |
| $t_a$ | width of beam cross-sectional area, measured at the point where shear stress is determined |
| $t_c$ | width of slab cross-sectional area, measured at the point where shear stress is determined |
| $u_{a,o}, u_{c,u}$ | longitudinal displacement of the beam and slab, respectively, at interface |
| $u_a, u_c$ | longitudinal displacement of the beam and slab, resp., at center of gravity |
| $u_x$ | displacement in x direction |
| $u_j$, $u_{ij}$, $u_{jj}$ | relative displacements at connectors of composite girder |
| $v_{max}$ | maximal deflection of composite girder |
| $v$ | vertical displacement |
| $x_t$ | length of the lateral zone |
| $x$, $y$, $z$ | directions of coordinate system |
| | |
| $[U]$ | stiffness matrix |
| $[F]$ | force vector |
| $\{u\}$ | displacement vector |
| | |
| $G$, $G^*$ | kernel (function of potential) and modified kernel, respectively |
| $F[N(x)]$ | potential |
| $\Pi$ | potential energy |
| $D$ | a step in the finite difference method |
| $D\boldsymbol{T}$ | temperature difference between beam and slab |
| | |
| $a$ | constants that enable definition of the non-linear connector behaviour curve |
| $a_{stiff}$ | composite stiffness parameter |

| | |
|---|---|
| $a_T$ | coefficient of thermal expansion |
| $b$ | constants that enables definition of the non-linear connector behaviour curve |
| $z$ | ratio $T(0)/T_{full}$ |
| $h = n/n_f$ | degree of shear connection |
| $w$ | constant in the Hawranek-Steinhardt equation |
| $g$ | constant in the Hawranek-Steinhardt equation |
| $g_a, g_c, g_s, g_{ap}$ | partial safety factors for steel beam, concrete slab, reinforcement, profiled steel sheeting |
| $k$ | curvature of the deflection curve |
| $m$ | Poisson's ratio |
| $f$ | rotation of beam or slab |
| $\varphi$ | angle of principal tensile stress |
| $e$ | strain |
| $e_1, e_2$ | principal strains |
| $e_a$ | strain at centre of gravity of beam |
| $e_c$ | strain at centre of gravity of slab |
| $s_1, s_2$ | principal stresses |
| $s_x$ | normal stress |
| $s_{x,c}$ | average normal stress on the slab |
| $s_{measured}$ | measured normal stress |
| $r$ | density |
| $t_{xy}$ | shear stress |

**Abbreviations**

| | |
|---|---|
| BUTE | Budapest University of Technology and Economics |
| C.A | centroidal axis |
| DSE | Department of Structural Engineering |
| DOF | degree of freedom in a finite element |
| LBE | Laboratory of Bridge Engineering of TKK |
| TKK | Helsinki University of Technology |

# 1 INTRODUCTION

## 1.1 Background

In the field of bridge engineering, composite action is commonly utilised in girder-type structures. The steel-concrete combination is the most common one, but concrete-concrete and wood-concrete composite girders are also used. The popularity of composite structures derives from the simple and appropriate structural form, which allows the construction of lightweight but load-carrying structures in an economical way. They can easily be built in sequences of various construction methods. Obviously one of the most challenging parts in these structures are the connections between the two different materials, but also other issues like

- classification of ductility and non-ductility in a more versatile manner than is done in Eurocode 4[1],
- consideration of connection characteristics with respect to span length of the girder,
- consideration of various densities of the connection (also definition of connection density) and their effect on the serviceability characteristics and
- consideration of minimum densities of connection in ultimate limit state analysis

are important from scientific and practical point of view.

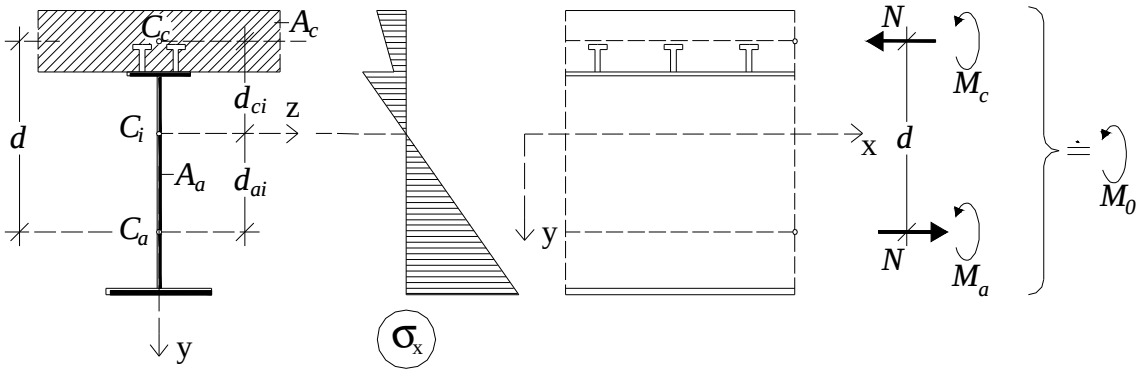


*Fig. 1. A typical composite girder and notation used.*

A typical cross-section of a composite girder is shown in Fig. 1. The girder comprises the beam, the slab and the connectors. In the figure $A_c$ is the cross-section area of the concrete slab, $A_a$ is the cross-section area of the steel beam, $C_c$ is the center of gravity of the concrete slab, $C_i$ is the center of gravity of the composite girder, $C_a$ is the center of gravity of the steel beam, $d_{ci}$ is the distance between the center of gravity of the composite girder and the center of gravity of the concrete slab, $d_{ai}$ is the distance between the center of gravity of the composite girder and the center of gravity of the steel beam, $N$, $M_c$ and $M_a$ are sectorial forces, and $M_0$ is the bending moment acting on the cross-section, which is balanced by bending moments $M_c$ (concrete), $M_a$ (steel) and $N \cdot d$, i.e.

$$M_0 = M_c + M_a + N \cdot d \tag{1}$$

Fig. 1 also shows the coordinate system used in this study.

Fig. 2 gives examples for steel-concrete and wood-concrete composite girders and their connections. This figure confirms as well that the use of composite girders is not at all pushed into the background but is, in fact, becoming more and more wide-spread and extensive.

[1] Eurocode 4 [35] shall mean EN 1994-1-1 in the following part of this study.

Therefore, it is practical to continue the related research work. Although, this study covers only the behaviour of connectors, and the influence of their behaviour on the stress and strain condition of a composite girder, in addition to the research on connectors, it is also necessary to review several other issues and tendencies concerning the investigation of the entire composite girder since the behaviour of the connection may affect that of the entire composite girder.

Although, in the case of steel bridges, reinforced concrete slabs were used as compressed flanges of steel structures, deliberate applications of the first composite bridge structures occurred in the early 1900's in France possessing the most advanced reinforced concrete technology of that time, i.e in the construction of the Canal du Midi near Toulouse and the Chamberly composite bridges, respectively.

Spreading of the composite technology was significantly hindered mainly by the lack of experimental data and theoretical grounds including the problem of the creep of concrete. In the 1930's, however, extensive experimental work related to various connection types in composite structures was commenced in Germany, Sweden, in the USA and other countries. At the same time DISHINGER's main work on the creep of concrete was published in 1937 [31]. This work covered the behaviour of reinforced concrete arches subjected to creep and is applicable to the concrete slab of the composite girder as well.

*Fig. 2. Steel-concrete and wood-concrete composite girders and their connections.*

Following World War II composite structures gained significant importance due to the numerous buildings and structures awaiting refurbishment, and also because of the considerable shortage of steel material. Major construction projects also gave a boost to the research in this field. NEWMARK completed his publication on tests and analyses of

composite beams with incomplete interaction in 1951 [85]. Among other publications like HOISHEN [53] and HAWRANEK-STEINHARDT [52], NEWMARK`s publication forms the basis of the static method used for the calculation of composite girders up to our days. Soon the energy method also appeared in the reference literature as the solution of this problem [53], [55], [94]. These methods consider connectors' linear behaviour.

Since the1950's the number of different solutions of the creep problem has steadily increased. The particular phases in this process are marked by the following names and dates: BUSEMANN 1950 [13], SATTLER 1959 [99], FRITZ 1961 [47], ENGLAND and ILLSTON 1965 [33], NIELSEN 1970 [84], TROST 1968-1973 [120-123], RÜSH, JUNGWIRTH and HILSDORF 1973 [97] and CEB-FIP Model Code Method 1978-1990 [14],[15], [16].

Further research on connections and the surrounding concrete was also carried out. As part of that the interface shear between concrete beam and concrete slab was studied by FENWICK and PAULAY in 1968 [41] and by PAULAY and LOEBER in 1974 [92]. Correspondingly, the behaviour of shear connectors in concrete slab was investigated thoroughly by JOHNSON and OEHLERS [58] and OEHLERS et al. [87], [88], [89] and [90]. In these studies dowel action, longitudinal shear, splitting forces, embedment forces and interaction between shear and axial forces were particularly tackled. These topics are reviewed in detail in Section 2.7.

As in other fields of science, introducing of the finite element method (FEM) led to revolutionary changes in civil engineering. This new tool offered a possibility to analyse structures numerically instead of carrying out relatively expensive laboratory tests. Numerical methods, however, need calibration, and that is why laboratory tests are still needed. Due to this fact Chapter 5 is presented in this study strengthened by two detailed literature surveys (Chapters 2 and 3) and some numerical calculations of the author.

Standards like Eurocode 4 were developed as well [35]. In Eurocode 4 the principle of partial and full shear connection[2] and ductile and non-ductile connectors were introduced for standard composite girders. However, there were no methods recommended for shallow floor composite beams. To fill this gap LESKELÄ carried out research on this topic at the end of the 1990's and early 2000's [75], [76]. The author of the referred study examined the non-ductile connections of shallow floor composite beams, developed the partial connection theory for these structures and studied the influence of connection characteristics with respect to the span length [75], [76]. For the design of steel-concrete composite structural elements of buildings, Eurocode 4 suggests the plastic design in the ultimate limit state and crack width limitation in the serviceability limit state.

The linear partial interaction theory [85], [56] was also developed further. In 1999, differential equations governing the behaviour of simply supported composite girders with partial shear connection were deduced by JASIM [56]. These equations are derived for the case when the distribution of connectors along the span is triangular.

In 1993, a method for the time-dependent analysis of continuous steel-concrete composite girders with deformable shear connectors was developed by DEZI et al. [28], [29]. The mathematical formulation of the problem led to a coupled system of equations, of which two are integral-differential type equations.

[2] Definition of partial and full shear connections can be found in Section 2.6 on page 44.

At the intermediate support regions of continuous composite girders the negative bending moments generate tensile stresses in the concrete slab and compressive stresses in the steel beam. As a result, the mechanical behaviour of these girders is strongly non-linear even for low stress levels, due not only to the slip at the beam-slab interface, but also to cracking in the slab. In addition, the time-dependent behaviour of continuous steel-concrete composite girders causes internal force rearrangement. Due to these reasons several authors studied this problem using standard finite element programs and finite element programs developed by themselves [8], [10], [22], [28], [36], [49], [50], [57], [72], [79], [83]. The tension stiffening effect of cracked concrete was also studied by some authors [36], [79].

Recently DEZI, GARA and LEONI presented a variational approach to resolve the differential equations in an easier manner [30]. The present author also uses this approach in Section 2.4.

## 1.2 Behaviour of connections of composite girders according to earlier studies

Generally speaking, the majority of civil engineering structures consist of girders where the connection between two structural elements can be considered to be deformable instead of being fully rigid. For instance, in railway and highway bridges deformable connections are common between the main beams and cross beams and the cross beams and stringers. In spite of this fact, in practice the deformable connections are usually considered as rigid because of complications in the analysis and minor effect on the final result.

In case of steel-concrete composite highway bridges, the thickness of the reinforced concrete slab varies in a relatively small range and is practically independent of the span of the main girder. This means that in long-span bridges the larger internal forces can be balanced mainly by the increased dimensions of the steel girder only, while the dimensions of the reinforced concrete slab remain practically the same. The result of the increased dimension is that the center of gravity of the composite section tends to move further away from the concrete slab. Therefore, beyond a certain span, the allowable stress in the extreme top fibre of the slab is reached earlier than the allowable tensile stress in the extreme bottom fibre of the steel girder. As a consequence the steel beam cannot be economically utilized. The economy, however, can be improved by using deformable connections and by decreasing the normal force $N$ as suggested by HAWRANEK and STEINHARDT [52]. Other examples are presented in the studies by HOISCHEN [53], HOMBERG [55], SATTLER [100] and STÜSSI [104].

In case of a rigid connection, BODE and SCHANZENBACH examined a composite girder with hot-rolled steel beam and connectors with uniformly distributed spacing using numerical analysis. They found that if the loading force is increased [11], then the connector force diagram (Fig. 3) - initially regular almost in the entire length of the beam except for the support region - becomes irregular. The significant decrease in the connector forces at the beam end cannot be explained by the principles of elementary strength theory either. In practice, connectors are never fully rigid, and there is always some slip between the slab and the steel section. The flexibility of the connectors allows more ductility[3] and a variation in the distribution of longitudinal shear between slab and steel section. Behaviour of deformable connection under increasing load can also be seen in Fig. 3. Small reduction of the connector force at the beam end can be observed in this case as well. The uniformly distributed load $q_{pl}$ causing plastic failure was 56 kN/m.

[3] Definition of ductile and non-ductile connectors can be found in Section 2.6 on page 45.

In addition it is discovered that the maximum connector force does not occur at the first but at the third or fourth connector from the support. JOHNSON and MOLENSTRA [60] came to this conclusion as well (Fig. 4) based on theoretical considerations while ARIBERT [1] – [7], whose curve is also depicted in the figure, conducted experiments and numerical analysis. ARIBERT examined a composite girder (specimen P2 [6]) with hot-rolled steel beam and connectors with uniformly distributed spacing, and the degree of shear connection[4] was approximately 70 %.

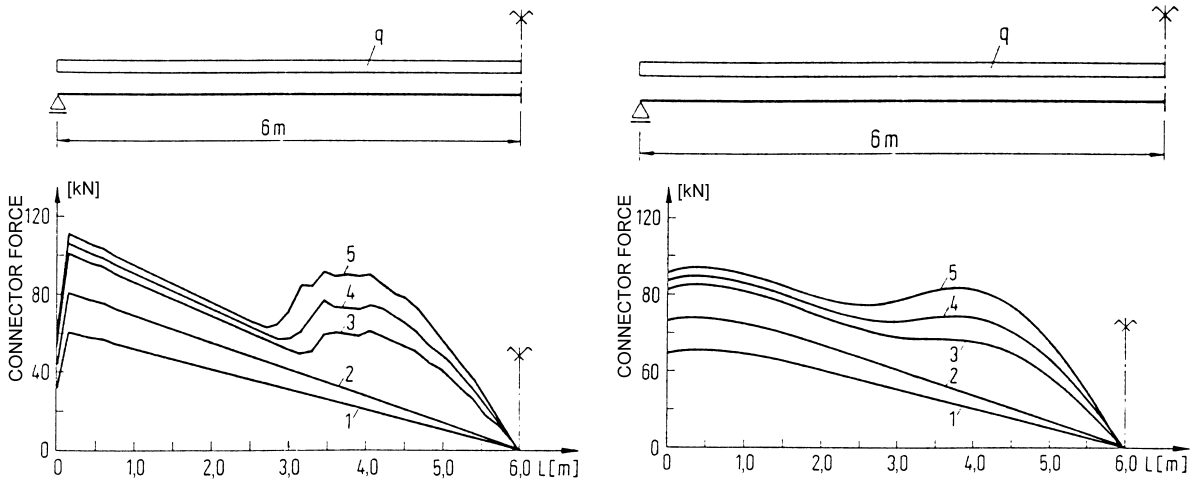


Rigid connection
Curve 1: q =30,0 kN/m = 0,54$q_{pl}$ ,
Curve 2: q =40,0 kN/m = 0,71$q_{pl}$ ,
Curve 3: q =50,0 kN/m = 0,89$q_{pl}$ ,
Curve 4: q =52,5 kN/m = 0,94$q_{pl}$ ,
Curve 5: q =55,0 kN/m = 0,98$q_{pl}$ .

Deformable connection
Curve 1: q =30,0 kN/m = 0,54$q_{pl}$ ,
Curve 2: q =40,0 kN/m = 0,71$q_{pl}$ ,
Curve 3: q =50,0 kN/m = 0,89$q_{pl}$ ,
Curve 4: q =52,5 kN/m = 0,94$q_{pl}$ ,
Curve 5: q =55,0 kN/m = 0,98$q_{pl}$ .

*Fig. 3. Connector forces for rigid and deformable connectors [11].*

The author of this study investigated the problem of decreased connector forces at beam-ends as well both experimentally and analytically [107]. Some simply supported steel-concrete composite beams subjected to gravity loads and 40 $^{o}$C temperature difference were examined. The loading consisted of two knife-edge loads located 125 mm apart from the mid-span. The analytical part of the study was based on the differential equation presented by HAWRANEK-STEINHARDT [52]. When the experimental and calculated shear flow distributions were compared it could be found, that the experimental shear flow at the support line was about the same as the calculated one. A few years later, the author analysed the same test beams by using the Finite Element Method [112]. The connector force distribution obtained by this latest study, expressed as connector shear stress $t_{xy}$, is shown in Fig. 5.

Since the results of these studies are inconsistent with the elementary beam theory (Fig. 3, Fig. 4 and Fig. 5), further studies are needed. The so-called “exact” methods can be re-evaluated in the light of these investigations.

[4] Definition of degree of shear connection can be found in Section 2.6 on page 45.

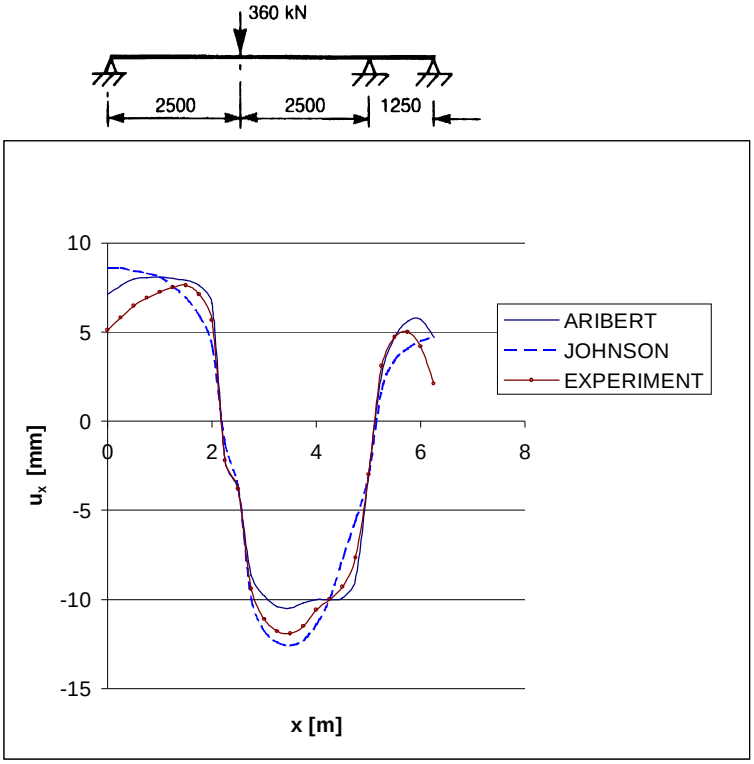


*Fig. 4. Comparison of longitudinal slip values.*

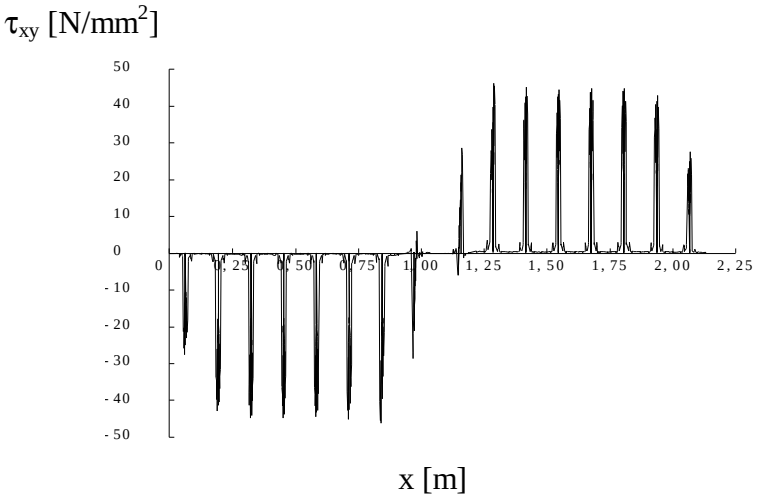


*Fig. 5. Connector force distribution expressed as connector shear stress $t_{xy}$ obtained by the author with a steel-concrete composite girder as function of connector distance x from the girder-end [112].*

## 1.3 Aim of the study

The subject of the study was chosen because of the fact that although there are many research works and publications that deal with the problem of partial and full shear connections[5] of

[5] Definition of partial and full shear connections can be found in Section 2.6 on page 44.

composite girders, there are still significant items in the behaviour of such structural details that have not been sufficiently covered. Some of these items are as follows:

i. the shear force distribution due to temperature difference, creep and shrinkage,
ii. behaviour of the connectors studied by the elementary beam theory especially in the region beyond the support lines,
iii. significant stresses and connector forces in cantilever parts,
iv. partial shear connections.

The aim of this study is to analyse the behaviour of deformable and rigid shear connections of steel-concrete and wood-based composite girders, to develop applicable analytical and numerical methods and to carry out experimental tests for such connections.

When examining the shear force distribution in the support region due to temperature difference, creep and shrinkage (i), because of the several connectors, even a simply supported composite girder is found internally statically indeterminate. These phenomena have not yet been adequately clarified in case of steel-concrete composite girders, with respect to wood-concrete composite girders this kind of investigation just started.

In the elementary beam theory the behaviour of the connectors (ii) is not described correctly and that is why two- or three-dimensional analysis is needed for determining the connector force distribution.

Although unloaded, cantilever parts of a simply supported beam accumulate significant stresses and connector forces (iii), which is in conflict with the traditional bending theory.

Eurocode 4 considers partial shear connections (iv) only, if the cross-sections belong to class 1 or class 2 to Eurocode 3 (real redistribution of plastic moment of cross-sections). If a long-span bridge is considered, the cross-section is of class 3 or 4 under Eurocode 3 [34]. Therefore, shear connections shall be calculated according to the elastic theory instead of considering plastic redistribution of connector forces, which is common practice in the building constructions. This research also aims at analysing the structure being in the elastic state, which still needs to be clarified. The investigations in this field by the author is also supported by the fact that in Finland only elastic theory can be used for the calculation of wood-concrete composite bridges.

The scope of the study covers only simply supported steel-concrete and wood-concrete composite girders with elastic behaviour subjected to static gravity load and/or differential strain (primarily due to temperature difference). However, the overall behaviour of steel-concrete and wood-concrete composite girders is different and that is why these structures are treated separately. In addition, only normal strength concrete and steel materials are considered, with the exception of HSFG bolts.

# 2 ANALYTICAL AND NUMERICAL METHODS RELATED TO COMPOSITE GIRDERS

## 2.1 General flexural theory of composite girders

### 2.1.1 Background

A general analysis of the composite girder requires a complete knowledge of the full stress-strain properties of steel, concrete and shear connection, over the time span being considered. There have been theoretical studies conducted on such a basis, but the use of a computer is absolutely needed because of the complexity of numerical work, and also a less complicated method is required for practical purposes. The numerical work can be facilitated without much damage to accuracy by simplifying assumptions about the properties of the component materials. It is useful to consider first the case of "partial interaction" where deformation of the shear connection produces relative movement between slab and beam. In practice this movement may be of only low significance; consideration of this movement in the analysis will give the measure of its importance.

If slip occurs, the bending stiffness of the composite structure is reduced, which brings the joint towards a deformable shear connection. With zero shear rigidity a state is reached where interaction between the beam and the slab is lost. As a consequence, the two parts act independently in bending. Partial interaction theories based on more or less simplified assumptions have been created. A method developed by NEWMARK [85] is presented here.

For calculation purposes the bending moment acting on the composite beam can be considered as the resultant of sectional forces ($M_a$, $M_c$, $N_a$, $N_c$) acting on the individual steel and concrete components (Fig. 6).

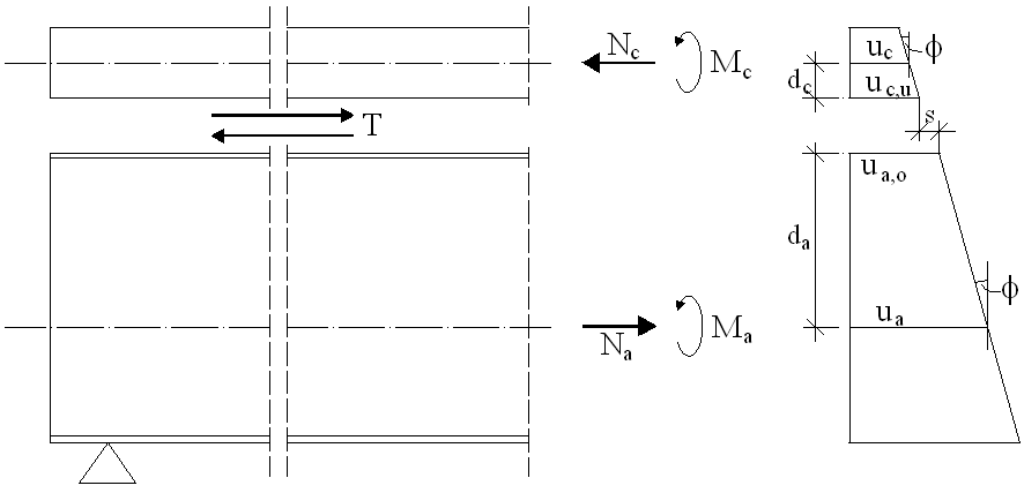


*Fig. 6. Static and kinematical definition of the model.*

The following assumptions are used:

- Instead of discrete shear connection, an equivalent uniform continuous linearly elastic medium is used.
- Initially plane sections remain plane after bending.
- The beam and the slab have the same rotation and curvature.
- The cross-sections of slab and beam are constant over the beam length.
- There is no uplift between beam and slab.

- Both concrete and steel are isotropic elastic materials.

The slip between the steel beam and concrete slab is equal to the difference of the displacement in the axial direction of extreme fibre in the interface of beam and slab (Fig. 6). So,

$$s = u_{a,o} - u_{c,u} \tag{2}$$

where $u_{a,o}$ is the displacement in the axial direction of the extreme fibre of the beam at the interface and $u_{c,u}$ is the displacement in the axial direction of extreme fibre of the slab at the interface.

Considering these displacements as a function of displacements of centres of gravity $u_a$ and $u_c$, the slip is

$$s = u_{a,o} - u_{c,u} = (u_a - f \cdot d_a) - (u_c + f \cdot d_c) = u_a - u_c - f \cdot d \tag{3}$$

where $f$ is the rotation of both the beam and the slab; $d_a$ is the distance between the centre of gravity of the beam and the contact surface; $d_c$ is the distance between the centre of gravity of the slab and the contact surface and $d_a + d_c = d$.

Deriving Equation (3) with respect to x, equation

$$\frac{ds}{dx} = \frac{du_a}{dx} - \frac{du_c}{dx} - \frac{df}{dx} d = e_a - e_c + k \cdot d \tag{4}$$

is obtained. Here $e_a$ means the strain at the centre of gravity of the beam; $e_c$ means the strain at the centre of gravity of the slab and $k = -df/dx$ means the curvature of the deflection curve.

From the moment and horizontal force equilibrium equations it follows that

$$M = M_a + M_c + N \cdot d \tag{5}$$

and

$$N = N_a = -N_c \tag{6}$$

The internal sectorial moments and forces $M_a$, $N_a$, $M_c$ and $N_c$ can be expressed as functions of the axial strains and curvature using internal equilibrium equations

$$N_c = \int_{A_c} s_c dA = \int_{A_c} E_c [e_c - k(y + d_{ci})] dA_c = e_c C_c \tag{7}$$

$$N_a = \int_{A_a} s_a dA = \int_{A_a} E_a [e_a - k(y - d_{ai})] dA_a = e_a C_a \tag{8}$$

$$M_c = \int_{A_c} s_c y dA = \int_{A_c} E_c [e_c - k(y + d_{ci})](y + d_{ci}) dA_c = -kD_c \tag{9}$$

and

$$M_a = \int_{A_a} s_a y dA = \int_{A_a} E_a \left[ e_a - k(y - d_{ai}) \right](y - d_{ai}) dA_a = -kD_a \tag{10}$$

where $C_c$ and $C_a$ are the axial stiffness of beam and slab, respectively, and $D_c$ and $D_a$ are the bending (flexural) stiffness of beam and slab, respectively.

Substituting Equations (6), (7), (8), (9) and (10) into Equation (5) yields to expression

$$M = -kD_a - k \cdot D_c + N \cdot d = -k \cdot D_{abs} + N \cdot d \tag{11}$$

where

$$D_{abs} = D_c + D_a \tag{12}$$

is the bending stiffness of composite girder without interaction between the parts, or, more generally, the bending stiffness of two layered components with no connection.

From Equations (11), (7) and (8) relationships

$$\begin{cases} k = \dfrac{-M + Nd}{D_{abs}} \\ e_c = \dfrac{N_c}{C_c} = -\dfrac{N}{C_c} \\ e_a = \dfrac{N_a}{C_a} = \dfrac{N}{C_a} \end{cases} \tag{13}$$

Substituting Equation (13) into the compatibility Equation (4) results in

$$\begin{aligned} \frac{ds}{dx} &= N\left(\frac{1}{C_a} + \frac{1}{C_c}\right) + kd = N\left(\frac{1}{C_a} + \frac{1}{C_c}\right) + \frac{Nd - M}{D_{abs}} d = \\ &= N\left[\frac{1}{C_a} + \frac{1}{C_c} + \frac{d^2}{D_{abs}}\right] - \frac{Md}{D_{abs}} \end{aligned} \tag{14}$$

Defining $D_{full}$ as the bending stiffness of the composite girder with rigid connection, and defining

$$C^* = \frac{C_a C_c}{C_a + C_c} \tag{15}$$

it is simple to demonstrate that

$$D_{full} = D_{abs} + C^* \cdot d^2 \quad \big|^6 \tag{16}$$

---

[6] Introducing composite stiffness parameter [128] $a_{stiff} = C^* \cdot d^2$, $D_{full}$ can be written as $D_{full} = D_{abs}(1 + a_{stiff})$. This parameter indicates the efficiency of the composite interaction in relation to the parts of the section.

Thus Equation (14) can be written in the form

$$\frac{ds}{dx} - N\frac{1}{C^*}\frac{D_{full}}{D_{abs}} = -\frac{M \cdot d}{D_{abs}} \tag{17}$$

This is the general equation. The unknowns are *s* and *N*.

The constitutive relationship of connectors between the longitudinal shear flow *T*, axial force *N* and slip *s* is

$$T = N' = \frac{dN}{dx} = f(s) \tag{18}$$

where $f(s)$ represents a function of *s*. The resulting equation, obtained by combining Equations (17) and (18), yields to

$$\frac{ds}{dx} - \frac{1}{C^*}\frac{D_{full}}{D_{abs}}\int N'(s)dx = -\frac{M \cdot d}{D_{abs}} \tag{19}$$

### 2.1.2 Modelling of the linear behaviour of connectors

Assuming linear relationship between the longitudinal shear and slip, i.e.

$$T = N' = K \cdot s \tag{20}$$

where *K* is the spring constant of interface layer (compare Equation (18)), and using notation

$$w^2 = \frac{K}{C^*}\frac{D_{full}}{D_{abs}} \tag{21}$$

the general equation can be obtained from Equation (19) in terms of normal force *N* as

$$N'' - w^2 N = -\frac{M \cdot K \cdot d}{D_{abs}} \tag{22}$$

In terms of slip *s* the corresponding differential equation takes the form

$$s'' - w^2 s = -\frac{V \cdot d}{D_{abs}} \tag{23}$$

where $V = dM/dx$ denotes the vertical shear force at the section studied. Normal force *N* can also be formulated as a function of curvature *k*: Thus from Equation (13)

$$N'' = \frac{-q + k'' \cdot D_{abs}}{d} \tag{24}$$

is obtained, where $q = -dV/dx$ denotes the intensity of the uniformly distributed load. Substituting Equation (24) into Equation (22) yields to

$$-q + k'' \cdot D_{abs} - w^2 (M + k \cdot D_{abs}) = -\frac{M \cdot K \cdot d^2}{D_{abs}} \tag{25}$$

from which, by simple steps, equation

$$k'' - w^2 k = w^2 \frac{M}{D_{full}} + \frac{q}{D_{abs}} \tag{26}$$

can be obtained. Equation (26) can be solved directly for statically determinate girders in the knowledge of the moment function. If the problem is statically indeterminate [19], [95], through double derivation a more useful equation

$$k^{IV} - w^2 k'' = -w^2 \frac{q}{D_{full}} + \frac{q''}{D_{abs}} \tag{27}$$

is obtained. Finally, by substituting curvature $k$ by the second derivative of vertical deflection $v''$, equation

$$n^{VI} - w^2 n^{IV} = -w^2 \frac{q}{D_{full}} + \frac{q''}{D_{abs}} \tag{28}$$

is obtained.

In Table 1 the differential equations discussed above are summarised together with boundary conditions valid for a simply supported composite girder.

*Table 1. Different solution possibilities of a simply supported beam with symmetrical load with respect to the mid-span.*

| Unknown quantity | Governing equation | Support | Mid-span |
|---|---|---|---|
| $N$ | $N''(x) - w^2 \cdot N(x) = -\frac{M(x) \cdot K \cdot d}{D_{abs}}$ | $N = 0$ | $N' = 0$ |
| $s$ | $s''(x) - w^2 \cdot s(x) = -\frac{V(x) \cdot d}{D_{abs}}$ | $s' = 0$ | $s = 0$ |
| $k$ | $k''(x) - w^2 \cdot k(x) = w^2 \frac{M(x)}{D_{full}} + \frac{q(x)}{D_{abs}}$ | $k = 0$ | $k' = 0$ |
| $v$ | $v^{IV}(x) - w^2 v''(x) = w^2 \frac{M(x)}{D_{full}} + \frac{q(x)}{D_{abs}}$ | $v = 0$<br>$v'' = 0$ | $v' = 0$<br>$v''' = 0$ |

Reference [52] contains solutions for the axial force and interface shear due to uniformly distributed load, concentrated load, temperature difference and prestressing force on a simply supported beam, which originate from the well-known Hawranek-Steinhardt differential equation

$$\frac{d^2N(x)}{dx^2} - w^2 \cdot N(x) = -g \cdot M(x) \tag{29}$$

where

$$g = \frac{K \cdot d}{D_c + D_a} \tag{30}$$

These equations are valid for multi-material composite cross-sections as well and they were thoroughly discussed by JUTILA [62] and TOMMOLA and JUTILA [118].

When curvature $k$ and shear flow $T(x)$ are known, the internal forces and bending moments can be calculated from Equations (6), (7), (8), (9) and (10). Consequently the internal shear forces $V_a$ and $V_c$ are obtained from equation

$$\begin{cases} V_a = M_a' + T(x) \cdot d_a \\ V_c = M_c' + T(x) \cdot d_c \end{cases} \tag{31}$$

The normal and shear stresses are also shown here, without detailed deduction, as

$$\begin{cases} s_a(x,y) = \dfrac{N_a}{A_a} + \dfrac{M_a}{I_a}(y - d_{ai}) \\ s_c(x,y) = \dfrac{N_c}{A_c} + \dfrac{M_c}{I_c}(y + d_{ci}) \\ t_a(x,y) = \dfrac{V_a \cdot S_a^*}{t_a \cdot I_a} + \dfrac{T(x)}{t_a}\left(\dfrac{A_a^*}{A_a} - \dfrac{S_a^*}{I_a} d_a\right) \\ t_c(x,y) = \dfrac{V_c \cdot S_c^*}{t_c \cdot I_c} + \dfrac{T(x)}{t_c}\left(1 - \dfrac{A_c^*}{A_c} - \dfrac{S_s^*}{I_c} d_c\right) \end{cases} \tag{32}$$

Here $A_a^*$ and $A_c^*$ are the area of the top (or bottom) portion of cross-sectional area, defined from the section where $t_a$ and $t_c$ are measured, $t_a$ and $t_c$ are the width of cross-sectional area, measured at the point where shear stress is to be determined and $S_a^*$ and $S_c^*$ are the statical moment of the top (or bottom) portion of cross-sectional area, defined from the section where $t_a$ and $t_c$ are measured. Subscripts $a$ and $c$ refer to the beam and slab, respectively.

### 2.1.3 Modelling of the non-linear behaviour of connectors

Based on laboratory tests of the behaviour of different connectors it was found out that the connectors in a composite steel-concrete beam show strong non-linear behaviour. When considering the headed-stud connectors, the constitutive law between the force transferred by a single connector $F$ and the slip $s$, as determined by ARIBERT and AL BITAR (1989) [1] and JOHNSON and MOLENSTRA (1991) [60] is

$$F = F_{max}\,(1 - e^{-bs})^a \tag{33}$$

where $F_{max}$ is the maximum force that can be transmitted to the connector, and $a$ and $b$ are two constants that enable definition of the behaviour curve. In Ref. [60] the two following pairs of constants are recommended for studs with shank diameter d = 19 mm:

$$\begin{cases} a = 0{,}558 \\ b = 1\ mm^{-1} \end{cases}$$

and

$$\begin{cases} a = 0{,}959 \\ b = 1{,}535\ mm^{-1} \end{cases}$$

Equation (19) can be used for numerical evaluation of the displacements when the non-linear behaviour of connectors is taken into account. For the effective solution, a constitutive law (load-slip behaviour) concerning the shear connectors should be used, which gives the relationship between the total longitudinal shear force $N'$ and the slip $s$. In particular, the elementary force $dN$ (variation of the force N within length dx) transferred on an elementary part $dx$, which is the first derivate of $N$ with respect to the longitudinal abscissa $x$, relates to the longitudinal force $F$ transferred by a single connector as

$$dN/dx = N' = F/c \tag{34}$$

where $c$ is the spacing between the connectors.

When using Equation (34) it is assumed that the stiffness and strength of connectors can be spread along a certain length of the girder, and so local effects are neglected.

The problem can be solved using the method of finite differences with the constant integration step equal to $\Delta$ [19]. Thus

$$s_{i+1} = s_{i-1} + 2\frac{\Delta}{E \cdot A^*}\frac{D_{full}}{D_{abs}}\sum_{j=0}^{i} N'_j \cdot \Delta + 2\frac{M_i \cdot d}{D_{abs}} \tag{35}$$

where, based on the associated load-slip relationship of the connector,

$$N'_j = N'_j(s_j)$$

After determination of the slip values, $N'$ can be obtained from the constitutive law and by integration of $N$. Finally, the curvature can be calculated using relationship

$$k_i = \frac{-M_i + N_i d_i}{D_{abs}} \tag{36}$$

The deflections are determined by numerical integration.

This method [19] can be applied only to simply supported girders with given loading. For continuous composite girders the solution is suggested in Ref. [60].

## 2.2 Method of redundant forces

The redundant force method has been discussed by some authors, e.g. [74], but here a very ingenious idea is presented for wood-concrete composite girders.

This method [116], [118] is derived for wood beam and concrete slab but in general can be applied to composite girders made of two layers which are connected together by discrete, deformable shear connectors of linear stiffness properties and arbitrary and varying spacing and stiffness. No separation and friction between layers is assumed and the shear deformations of individual layers are neglected.

The analysis procedure is based on the method of redundant shear forces at connectors. Therefore, slip compatibility equations for each connector cross-section are needed. For slip compatibility, it is necessary to formulate equations for longitudinal slip between wood and concrete layers due to unit connector force and vertical loading on the girder. In the following the idea of how the slip and compatibility equations are derived is presented.

The layers of the composite girder are connected by only one connector at the left hand support (Fig. 7). All other connectors are supposed to be removed. When a connector force at the interface of the layers is applied, a contact force along the interface is needed to prevent a separation between layers (Fig. 7a and 7b).

The contact force $F_a$ between layers is necessary because the shear force couple alone causes different curvature to layers. The different curvatures cause a gap between wood and concrete and compatibility would not be satisfied. In other words, the contact force corrects the bending moments for both layers to be in proportion to their bending stiffness. If the connector shear force is moved in vertical direction by some amount $e_k$, it is possible to find a position where the shear force couple causes exactly the same curvature to both layers and no contact forces are needed anymore to satisfy the compatibility. Then one of the initial assumptions of “No disjunction between layers” is automatically satisfied (Fig. 7c). Because of a new vertical position of shear force couple, the contact forces are eliminated and it is possible to write the slip equations in a very simple way. The shear force couple causes axial force and bending moment in layers. By using the conventional beam bending theory it is possible to calculate edge fibre strain for wood and concrete at the interface surface. The slip between layers at any cross-section is simply the sum of difference of interlayer slips between edge fibres of layers and the slip at the connector at the left hand support.

For slip compatibility equation the slip caused by the external loading on the girder is needed (Fig. 8). The external vertical loading causes no axial force or shear force in the left hand connector, which means that the slip at the left end of the girder is zero. Therefore, the slip between layers is only caused by the accumulating bending strain difference along the interface surface. Again, the slip at any cross-section due to any vertical loading is related to the strain difference at the edge fibres of the layers. The initial assumption of ”no disjunction between layers” is secured by sharing the total bending moment between the two layers in proportion to their bending stiffness.

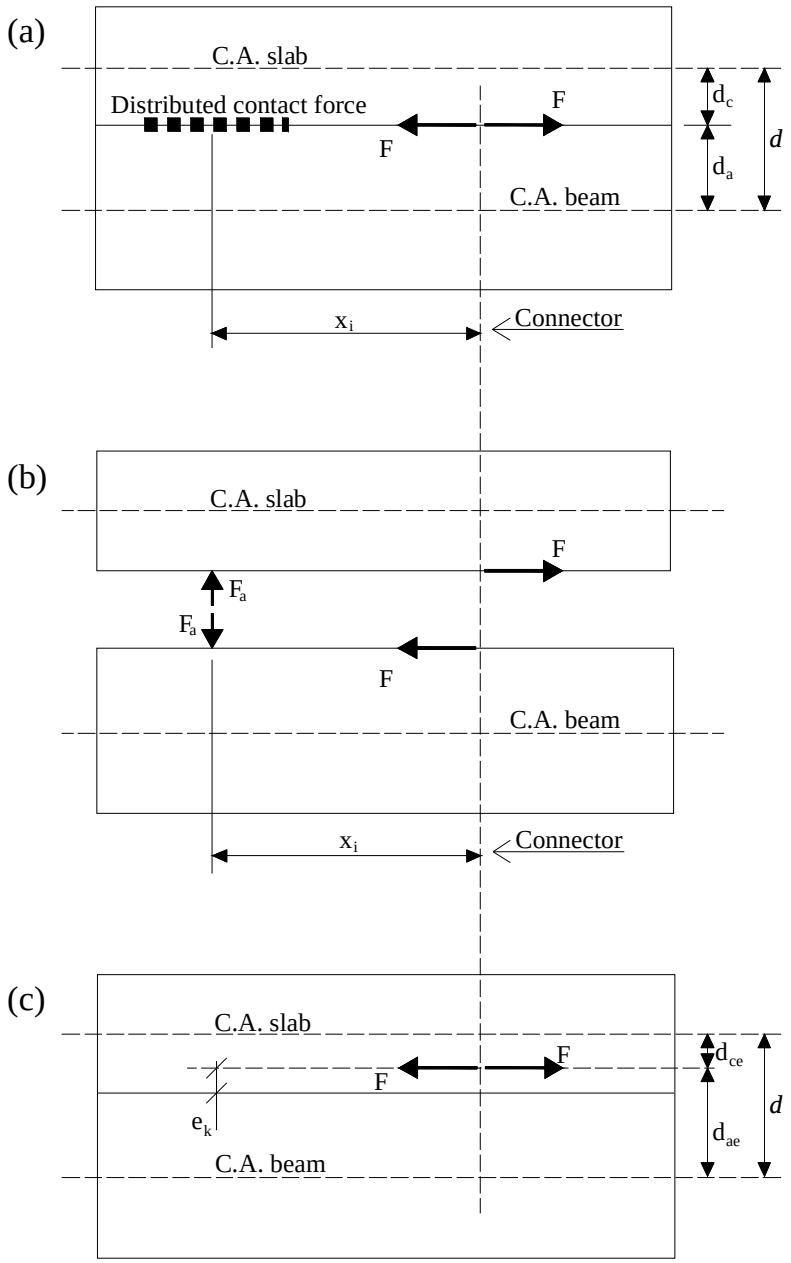


*Fig. 7. A section of composite girder, a) layers together, b) layers separated – free body system and c) contact forces eliminated by repositioning the connector force F.*

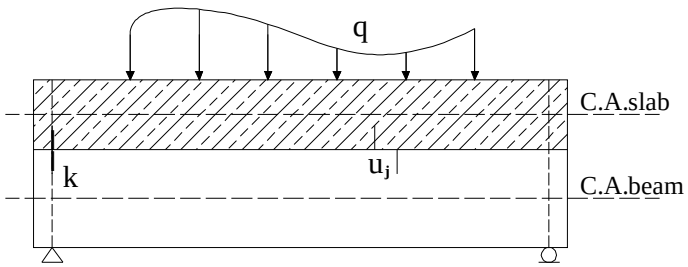


*Fig. 8. A composite girder subjected to unit shear force between layers and an arbitrary external load q.*

For a composite girder that is supplied with n + 1 shear connectors (including the one at the left hand support), the slip compatibility condition for connector j is written as

$$F_j\left(u_{jj}+\frac{1}{k_j}\right)+\sum_{i+1}^{n}F_i\cdot u_{ji(j\neq 1)}=-u_j \tag{37}$$

where $F_i$; and $F_j$ are the connector forces acting at connector *i* and *j*, respectively.

Having written slip compatibility condition for all connectors *j = 1 ... n*, the set of equations

$$\begin{bmatrix} u_{11}+\frac{1}{k_1} & u_{12} & . & . & u_{1n} \\ u_{21} & u_{22}+\frac{1}{k_2} & . & . & u_{2n} \\ & & & & \\ . & & . & & . \\ . & & & . & . \\ u_{n1} & & & & u_{nn}+\frac{1}{k_n} \end{bmatrix} \times \begin{Bmatrix} F_1 \\ F_2 \\ . \\ . \\ F_n \end{Bmatrix} = - \begin{Bmatrix} u_1 \\ u_2 \\ . \\ . \\ u_2 \end{Bmatrix} \tag{38}$$

is obtained. When written in matrix form it reads

$$[U] * [F] = -\{u\} \tag{39}$$

The connector forces are

$$\{F\} = -[U]^{-1} * \{u\} \tag{40}$$

The stresses of wood and concrete layers are obtained by summing the stresses caused by connector forces and external loading. The deflections are obtained using conventional beam theory.

The author has checked this method by LUSAS finite element program. The present method was applied to a simply supported wood-concrete composite girder with 20 m span subjected to uniformly distributed load 8 kN/m and concentrated load 2 x 200 kN with 2 m spacing centrally to the mid-span (Fig. 9).

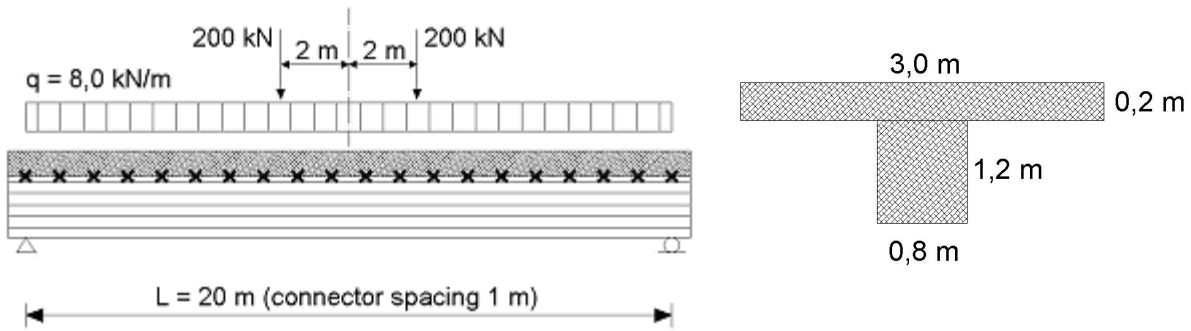


*Fig. 9. Elevation, cross-section and loading of the wood-concrete composite girder studied.*

The beam cross-section was 0,8 m x 1,2 m and that of the slab was 0,2 m x 3,0 m. The layers were connected by 21 deformable shear connectors (l m spacing). The connectors had equal

stiffness value of 100 MN/m. The elastic modulus value was 10000 MN/m$^2$ for wood and 30000 MN/m$^2$ for concrete. In Fig. 10 a very good agreement can be observed between the two results. The difference between maximum shear forces given by the two methods are within one percent. The biggest difference was at the first connector, where the FEM-analysis gave considerably lower shear force. This is due to the fact that TOMMOLA and JUTILA [118] determined forces using the elementary beam theory while in the FEM-analysis the forces are calculated on the basis of a 3D model.

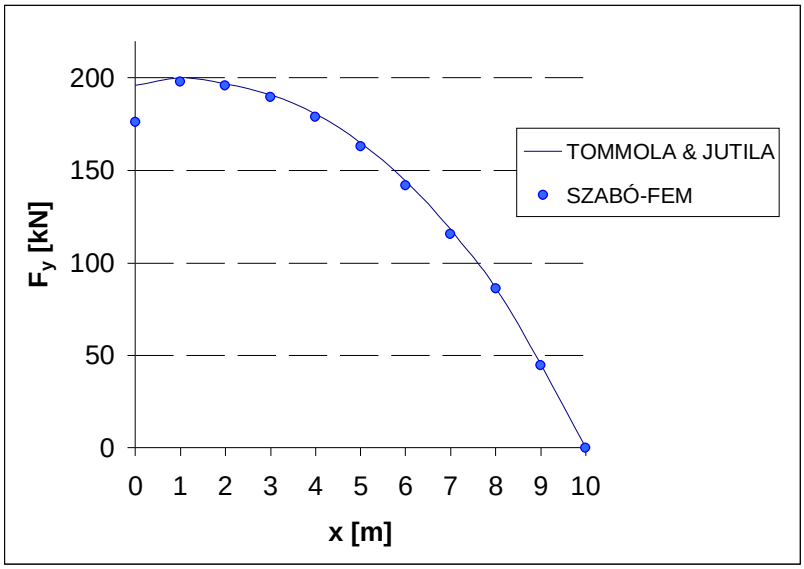


*Fig. 10. Comparison of connector forces along the left half girder.*

## 2.3 Traditional energy method

In addition to the statical methods, traditional energy method can be applied to solve the stress and deformation state of composite girders with elastic connectors, which are replaced by a continuous, elastic layer. This latter method was developed and discussed by several authors [53], [55], [94]. In the following the traditional energy method for simply supported and continuous composite girders is presented.

As well as in case of statical methods, it is also expedient to handle the sectional forces ($M_a$, $M_c$, $N_a$, $N_c$) acting on the individual steel and concrete components separately for the purpose of the traditional energy method.

The potential energy function is given as

$$P = \sum_{i=1}^{i=n} P_i \cdot v(x_i) + \int_0^L q(x) \cdot v(x) dx - L_i \tag{41}$$

where $P$ is the potential energy, $P_i$ and $q(x)$ are the external forces, $v$ is the displacement and $L_i$ is the work of internal forces.

The first two parts of Equation (41) refer to the work of the external forces. They can be determined e.g. by the Ritz method [96]. The following method is focused on the calculation of work of the internal forces $L_i$.

Using the definition of HOISCHEN [53], the change of the length of elastic layer $s(x)$ (Fig. 11) is

$$s(x) = T(x)/K \tag{42}$$

where $K$ is the spring constant of interface layer and $T(x)$ is the shear force per unit length. Determining the longitudinal strain as the difference between the horizontal strains of the connected elements (Figs. 6 and 11) leads to equation

$$\frac{ds(x)}{dx} = \frac{1}{K}\frac{dT(x)}{dx} = \frac{\Delta d\, u_{a,o}}{dx} - \frac{\Delta d\, u_{c,u}}{dx} \tag{43}$$

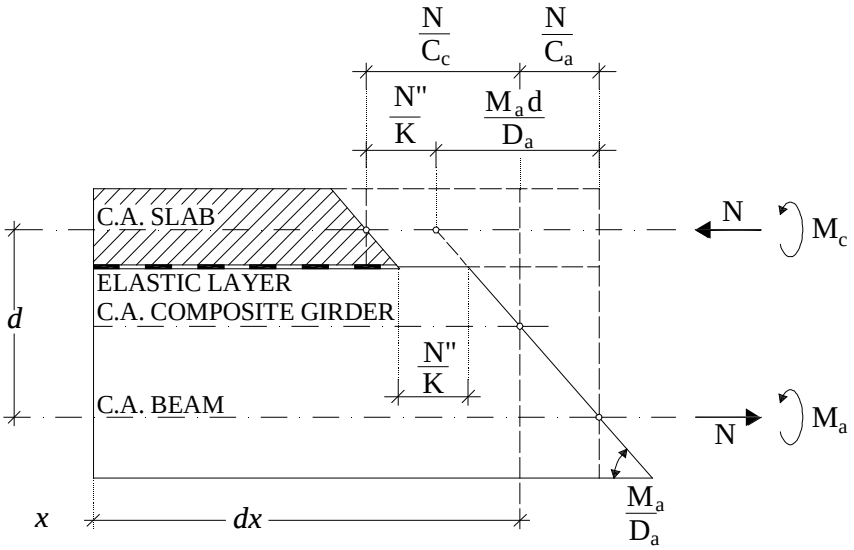


*Fig. 11. An elementary part of composite girder and relative displacements.*

Considering that

$$\frac{Dd\, u_{a,o}}{dx} = \frac{N(x)}{C_a} - \frac{M_a(x)}{D_a} d_a \tag{44}$$

$$\frac{Dd\, u_{c,u}}{dx} = -\frac{N(x)}{C_c} + \frac{M_c(x)}{D_c} d_c \tag{45}$$

and

$$\frac{M_c(x)}{D_c} = \frac{M_a(x)}{D_a} \tag{46}$$

i.e. the equality of the rotations, and taking into account Equations (15) and (18), Equation (43) can be rewritten in form

$$N(x)\frac{1}{C^*} - M_a(x)\frac{d}{D_a} = \frac{1}{K}\frac{d^2N(x)}{dx^2} \tag{47}$$

The physical meaning of the three different parts of Equation (47) is clearly seen in Fig. 11. The first term represents the relative displacement between the center of gravity points of the

beam and the slab due to axial force N. The second term represents the same displacement due to bending moment. The term on the right hand side represents the relative slip at the interface of the two materials. Consequently, the total internal work is

$$L_i = \frac{1}{2}\int_0^L \frac{M_a^2}{D_a}dx + \frac{1}{2}\int_0^L \frac{M_c^2}{D_c}dx + \frac{1}{2}\int_0^L \frac{1}{C^*}N^2 dx + \frac{1}{2}\int_0^L \frac{1}{K}N \cdot N^{"} dx \tag{48}$$

Due to the moment-curvature relationship in flexural girders and the theory of small deformations

$$M_a(x) = -D_a v^{"}(x) \tag{49}$$

and

$$M_c(x) = -D_c v^{"}(x) \tag{50}$$

and by introducing ratio

$$g(x) = \frac{M_a(x)}{N(x)} \tag{51}$$

the normal force expression

$$N(x) = -\frac{D_a v^{"}(x)}{g(x)} \tag{52}$$

can be obtained. Consequently

$$N^{"}(x) = \left(-\frac{D_a v^{"}(x)}{g(x)}\right)^{"} \tag{53}$$

Thus the internal work (Equation (49)), when Equations (49), (50), (51), (52) and (53) are taken into account, takes the form

$$L_i = \frac{D_{abs}}{2}\int_0^L \left[v^{"}(x)\right]^2 dx + \frac{D_a^2}{2 \cdot C^*}\int_0^L \left[\frac{v^{"}(x)}{g(x)}\right]^2 dx - \frac{D_a}{2 \cdot K}\int_0^L \frac{v^{"}(x)}{g(x)}\left[-\frac{D_a \cdot v^{"}(x)}{g(x)}\right]^2 dx \tag{54}$$

Knowing the internal work, the potential energy function (Equation (41)) can be utilised. For convenience deflection *v(x)* can be expressed as a series of functions

$$v(x) \approx c_1 f_1(x) + c_2 f_2(x) + ... \tag{55}$$

where functions $f_1(x)$, $f_2(x)$… are to be chosen so that the boundary conditions of the problem are fulfilled. Coefficients $c_1$, $c_2$… are determined so, that the minimum of the potential energy is reached, i.e.

$$\begin{cases} \dfrac{\partial P}{\partial c_1} = 0 \\ \dfrac{\partial P}{\partial c_2} = 0 \\ \\ \ldots = 0 \end{cases} \tag{56}$$

(Ritz-method [96]). Equations (55), (49), (50) and (52) then lead to the deflection and the internal forces and bending moments of the girder studied.

From the general solution a single solution may be resolved for the case of a simply supported beam with one concentrated load at mid-span cross-section (Fig 12).

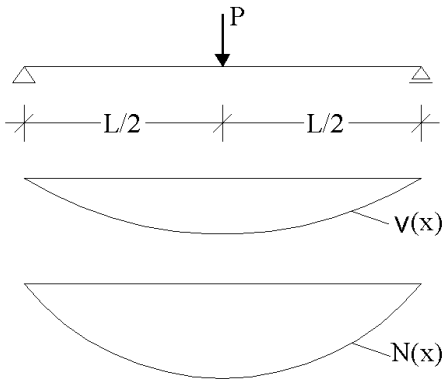


*Fig. 12. The simply supported beam used for demonstrating application of the energy method. Concentrated load at mid-span cross-section.*

Presenting deflection *v(x)* and normal force *N(x)* approximately as a single sinus function of coordinate *x*, i.e.

$$v(x) = c_1 \sin\frac{px}{L} \tag{57}$$

and

$$N(x) = a_1 \cdot \sin\frac{px}{L} \tag{58}$$

respectively, where $a_1$ is a Fourier series coefficient, and considering Equations (47), (51), (57) and (58), a new formulation for ratio *g(x)*, i.e.

$$g(x) = \left[\frac{1}{C^*} + \frac{p^2}{K \cdot L^2}\right]\frac{D_a}{d} \tag{59}$$

can be obtained. As seen coefficient $a_1$ is eliminated, because $\dfrac{N''(x)}{N(x)} = -\dfrac{p^2}{L^2}$.

Thus the internal work (Equation (48)) in this simplified case is reduced to

$$L_i = \frac{c_1^2}{2}\left[\int_0^L D_{abs}\left(\frac{p}{L}\right)^4 \sin^2\frac{px}{L}\,dx + \frac{1}{C^*}\int_0^L\left(\frac{D_a}{g}\right)^2\left(\frac{p}{L}\right)^4 \sin^2\frac{px}{L}\,dx + \right.$$

$$\left. + \frac{1}{K}\int_0^l\left(\frac{D_a}{g}\right)^2\left(\frac{p}{L}\right)^4 \sin^2\frac{px}{L}\,dx\right] = \frac{p^4}{L^3}\frac{c_1^2}{4}\left(D_{abs} + \frac{d^2}{\frac{1}{C^*} + \frac{p^2}{L^2}\frac{1}{K}}\right) \tag{60}$$

Considering that in the present case $\sin\frac{px}{L} = 1$ at the mid-span, the potential function (41) is simplified to

$$P = c_1 \cdot P - L_i \tag{61}$$

Using condition Equation (56) the expression of constant $c_1$ yields to

$$c_1 = \frac{\frac{2}{p^4}PL^3}{D_i} \tag{62}$$

where

$$D_i = D_{abs} + \frac{d^2}{\frac{1}{C^*} + \frac{p^2}{L^2}\frac{1}{K}} \tag{63}$$

Then by Equations (57), (52), (49) and (50) the deflection function $v(x)$, normal force $N(x)$ and bending moments $M_a(x)$ and $M_c(x)$, respectively, are available.

Further statically determinate structures can be solved in the same way and in each case the ideal stiffness $D_i$ (Equation (63)) will be the same expression.

Statically indeterminate structures can be calculated in traditional way using this ideal stiffness $D_i$ of the composite girder.

Methods containing Sections 2.1 and 2.3 assume the connectors to act as a continuous elastic layer, in contrast with the method of redundant forces where discrete connectors are taken into consideration.

## 2.4 Advanced energy method based on variational calculation

In this section advanced energy method developed by the present author is presented and discussed. This method is based on variational calculation and referred as the Author's Energy Method in the following part of this study.

A significant part of natural phenomena is equivalent to some extreme value problem. For example in physics the mechanical equilibrium is achieved when the energy of the system is at minimum. The total statical energy (exclusive of kinetic energy) of an elastic body is the sum of the deformation energy and the potential energy. Displacement field in the equilibrium state is of such characteristics where the total static energy is minimized (e.g. deflection of a beam and geometry of a membrane stretched on a frame).

The functions describing the displacement (deformation) form part of the core function standing after the volume integral providing the global sum of the energy. In this case we need these functions to minimize the integral value (integral principle). In general, common or partial differential equations based on local equilibrium can also be developed for these functions. It can be practical to use a method when appropriate integral principle is sought for the differential equation of a particular problem.

There are two possible solutions of the boundary value problem:

- conventional solution on the basis of the differential equation (e.g. using differential method)
- minimizing the energy integral (e.g. by iterative correction).

Of course, the core function in the integral principle can be transformed into the differential equation. It is most commonly achieved using the Euler-Lagrange equation

$$\frac{\partial G\,(x, N\,, N^{'})}{\partial N} - \frac{d}{dx}\frac{\partial G\,(x, N\,, N^{'})}{\partial N^{'}} = 0 \tag{64}$$

from variational calculation [43], [86], [124].

The variational principles date back to the 18th century [48], [96]. Recently, however, they have been commonly and widely used for example for the development of the finite element method and the various elements applied therein.

The fact that the traditional energy methods presented by HOISCHEN [53], HOMBERG [55] and PLATTHY [94] do not provide solution for composite girders subjected to temperature difference, inspired the author to develop an energy method for such structures as well.

On the basis of Equation (64) the author developed the following method.

**THEOREM:** Differential Equation (29) is the Euler-Lagrange equation of

$$F\left[N(x)\right] \;=\; \int_{0}^{L} G\left[N(x)\right]dx \;\;\rightarrow\;\; \min_{N(x)} \tag{65}$$

which is an integral minimum problem. Here the functional $F\ [N(x)]$ with the appropriate kernel function $G\ [N(x)]$ is

$$\Phi[N(x)] = \underbrace{\int_0^L \left[ \frac{1}{2}\left( N(x)\frac{d^2N}{dx^2} - \omega^2 \cdot N^2(x) \right) + N(x)\cdot\gamma\cdot M(x) \right] dx}_{\Gamma[N(x)]} \tag{66}$$

**Proof:** The first part of functional (66) after partial integration is

$$\int_0^L \frac{1}{2}\left( N(x)\frac{d^2N(x)}{dx^2} \right) dx = \frac{1}{2}\left\{ \left[ N(x)\frac{dN(x)}{dx} \right]_0^L - \int_0^L \left[ \frac{dN(x)}{dx} \right]^2 dx \right\} \tag{67}$$

out of which expression

$$\left[ N(x)\frac{dN(x)}{dx} \right]_0^L = 0 \tag{68}$$

because $N$ fulfills the boundary conditions ($N(0)=N(L)=0$) of a simply supported beam. Thus Equation (68) leads to equation

$$\Phi[N(x)] = \underbrace{\int_0^L \left\{ \frac{1}{2}\left[ -\left( \frac{dN(x)}{dx} \right)^2 - \omega^2\cdot N^2(x) \right] + N(x)\cdot\gamma\cdot M(x) \right\} dx}_{\Gamma^*[N(x)]} \rightarrow \quad \min. \tag{69}$$

By derivating kernel function $G^*[N(x)]$ of Equation (69) with respect to $N'$ leads to equation

$$\frac{\partial G}{\partial N'} = -\frac{dN(x)}{dx} \tag{70}$$

By derivating kernel function $G^*[N(x)]$ of Equation (69) with respect to $N$ leads to equation

$$\frac{\partial G}{\partial N} = -w^2\cdot N(x) + g\cdot M(x) \tag{71}$$

Substituting Equations (70) and (71) to Euler-Lagrange Equation (64) differential Equation (29) is obtained. So the theorem is fulfilled.

In order to solve Equation (66), the normal force is approximated by Fourier series

$$N(x) = \sum_{i=1}^{\infty} a_i \sin\frac{ipx}{L} = \sum_{i=1}^{\infty} a_i\, p_i(x) \tag{72}$$

where the real numbers $a_i$ are unknowns ( $a_i \in R$), $p_i(x)$ are twice continuously differentiable functions ( $p_i(x) \in C^2(a;b)$ ), and $p_i(x)$ are square-integrable functions ($p_i(x)$ $\hat{I}$ $L^2(a;b)$) on the actual interval of the space variable $x$. Here $R$ is a set of real numbers, $C^2(a;b)$ is the space of twice continuously differentiable functions and $L^2(a;b)$ is the space of square-integrable functions.

When $N(x)$ is truncated at $n$, then

$$N(x) \approx \sum_{i=1}^{n} a_i \sin\frac{ipx}{L} = \sum_{i=1}^{n} a_i\, p_i(x) \tag{73}$$

Presenting Equation (66) in another form yields to equation

$$\Phi = \int_0^L N(x)\left[\frac{1}{2}\left(\frac{d^2N(x)}{dx^2} - w^2 \cdot N(x)\right) + g \cdot M(x)\right]dx \to \min. \tag{74}$$

Substituting $N(x)$ from Equation (73) yields to equation

$$\begin{aligned}&\Phi[a_1, a_2, \mathbf{K}\, a_n] \;=\\ &= \int_0^L \left\{\left[\frac{1}{2}\left(\sum_{i=1}^{n} a_i\, p_i''(x) - w^2 \sum_{i=1}^{n} a_i\, p_i(x)\right) + g \cdot M(x)\right]\sum_{j=1}^{n} a_j\, p_j(x)\right\}dx \to \min_{a_1, a_2, \mathbf{L}, a_n}\end{aligned} \tag{75}$$

which after arranging the terms can be expressed as

$$\begin{aligned}&\Phi = \sum_{j=1}^{n}\sum_{i=1}^{n} a_i a_j \frac{1}{2}\int_0^L p_i''(x)\, p_j(x)dx - w^2 \sum_{j=1}^{n}\sum_{i=1}^{n} a_i a_j \frac{1}{2}\int_0^L p_i(x)\, p_j(x)dx +\\ &+ g\sum_{j=1}^{n} a_j \int_0^L M(x)\, p_j(x)dx \;\to \min_{a_1, a_2, \mathbf{L}, a_n}\end{aligned} \tag{76}$$

By integrating the first member of Equation (76) partially yields to equation

$$\begin{aligned}&\Phi = \sum_{j=1}^{n}\sum_{i=1}^{n} a_i a_j \frac{1}{2}\int_0^L \left\{\left[p_i'(x)\, p_j(x)\right]_0^L - \int_0^L p_i'(x)\, p_j'(x)dx\right\} +\\ &- w^2 \sum_{j=1}^{n}\sum_{i=1}^{n} a_i a_j \frac{1}{2}\int_0^L p_i(x)\, p_j(x)dx + g\sum_{i=1}^{n} a_j \int_0^L M(x)\, p_j(x)dx \;\to \min_{a_1, a_2, \mathbf{L}, a_n}\end{aligned} \tag{77}$$

out of which expression

$$\left[p_i'(x)\, p_j(x)\right]_0^L = 0 \tag{78}$$

is obtained, because the Fourier series fulfills the boundary conditions of the simply supported beam.

Thus Equation (77) will be

$$\begin{aligned}&F = -\sum_{j=1}^{n}\sum_{i=1}^{n} a_i a_j \frac{1}{2}\int_0^L p_i'(x)\, p_j'(x)dx - w^2 \sum_{j=1}^{n}\sum_{i=1}^{n} a_i a_j \frac{1}{2}\int_0^L p_i(x)\, p_j(x)dx +\\ &+ g\sum_{i=1}^{n} a_j \int_0^L M(x)\, p_j(x)dx \;\to\; \min\end{aligned} \tag{79}$$

Eliminating $p_i$, $p_j$, $p_i'$ and $p_j'$ by using Equation (73) and taking into account just the first three values of $i$ and $j$ ($i = 1,2,3$, $j = 1,2,3$), Equation (79) can be expressed in form

$$
\begin{aligned}
F = &-\frac{1}{2}\left[ a_1^2 \int_0^L \left( \cos\frac{p}{L}x \right)^2 dx + a_1 a_2 \int_0^L \frac{p}{L}\cos\frac{p}{L}x \cdot 2\frac{p}{L}\cos 2\frac{p}{L}x\,dx + \right. \\
&+ a_1 a_3 \int_0^L \frac{p}{L}\cos\frac{p}{L}x \cdot 3\frac{p}{L}\cos 3\frac{p}{L}x\,dx + a_2 a_1 \int_0^L 2\frac{p}{L}\cos 2\frac{p}{L}x \cdot \frac{p}{L}\cos\frac{p}{L}x\,dx + \\
&+ a_2^2 \int_0^L \left( 2\cos 2\frac{p}{L}x \right)^2 dx + a_2 a_3 \int_0^L 2\frac{p}{L}\cos 2\frac{p}{L}x \cdot 3\frac{p}{L}\cos 3\frac{p}{L}x\,dx + \\
&\left. + a_3 a_1 \int_0^L 3\frac{p}{L}\cos 3\frac{p}{L}x \cdot \frac{p}{L}\cos\frac{p}{L}x\,dx + a_3 a_2 \int_0^L 3\frac{p}{L}\cos 3\frac{p}{L}x \cdot 2\frac{p}{L}\cos 2\frac{p}{L}x\,dx \right] + \\
&- w^2 \left[ a_1^2 \int_0^L \left( \sin\frac{p}{L}x \right)^2 dx + a_1 a_2 \int_0^L \sin\frac{p}{L}x \cdot \sin 2\frac{p}{L}x\,dx + \right. \\
&+ a_1 a_3 \int_0^L \sin\frac{p}{L}x \cdot \sin 3\frac{p}{L}x\,dx + a_2 a_1 \int_0^L \sin 2\frac{p}{L}x \cdot \sin\frac{p}{L}x\,dx + \\
&+ a_2^2 \int_0^L \left( \sin 2\frac{p}{L}x \right)^2 dx + a_2 \cdot a_3 \int_0^L \sin 2\frac{p}{L}x \cdot \sin 3\frac{p}{L}x\,dx + \\
&+ a_3 a_1 \int_0^L \sin 3\frac{p}{L}x \cdot \sin\frac{p}{L}x\,dx + a_3 a_2 \int_0^L \sin 3\frac{p}{L}x \cdot \sin 2\frac{p}{L}x\,dx + \\
&\left. + a_3^2 \int_0^L \left( \sin 3\frac{p}{L}x \right)^2 dx \right] + \\
&+ g\left[ a_1 \int_0^L M(x)\sin\frac{p}{L}x\,dx + a_2 \int_0^L M(x)\sin 2\frac{p}{L}x\,dx + a_3 \int_0^L M(x)\sin 3\frac{p}{L}x\,dx \right] \rightarrow \text{min!}
\end{aligned}
\tag{80}
$$

The necessary condition for the local minimum of the functional $F(a_1, a_2 \ldots a_n)$ is that its partial derivatives are equal to zero, i.e.

$$\frac{\partial F}{\partial a_i} = 0 \qquad (i = 1, 2, \ldots n) \tag{81}$$

When considering that, Equation (81) leads to $n$ equations from which the appropriate Fourier coefficients $(a_1, a_2 \ldots a_n)$ used in the expression of normal force $N(x)$ (Equation (73)) can be determined.

Let us illustrate the procedure in the case when $n = 3$. Thus

$$\frac{\partial F}{\partial a_1} = 0$$

yields to equation

$$-\left[a_1\int_0^L\left(\cos\frac{p}{L}x\right)^2dx+a_2\int_0^L\left(\frac{p}{L}\right)^2\cos\frac{p}{L}x\cdot 2\cos 2\frac{p}{L}x\,dx+\right.$$
$$\left.+a_3\int_0^L\left(\frac{p}{L}\right)^2\cos\frac{p}{L}x\cdot 3\cos 3\frac{p}{L}x\,dx\right]-w^2\left[a_1\int_0^L\left(\sin\frac{p}{L}x\right)^2dx+\right. \quad (82)$$
$$\left.a_2\int_0^L\sin\frac{p}{L}x\cdot\sin 2\frac{p}{L}x\,dx+\ a_3\int_0^L\sin\frac{p}{L}x\cdot\cos 3\frac{p}{L}x\,dx\right]+g\int_0^L M(x)\sin\frac{p}{L}x\,dx=0$$

Similarly condition

$$\frac{\partial F}{\partial a_2}=0$$

yields to equation

$$-\left[a_1\int_0^L\left(\frac{p}{L}\right)^2\cos\frac{p}{L}x\cdot 2\cos 2\frac{p}{L}xdx+a_2\int_0^L\left(2\left(\frac{p}{L}\right)^2\cos 2\frac{p}{L}x\right)^2dx+\right.$$
$$\left.+a_3\int_0^L\left(\frac{p}{L}\right)^2\cos 2\frac{p}{L}x\cdot 3\cos 3\frac{p}{L}xdx\right]- \quad (83)$$
$$-w^2\left[a_1\int_0^L\sin\frac{p}{L}x\cdot\sin 2\frac{p}{L}xdx+a_2\int_0^L\left(\sin 2\frac{p}{L}x\right)^2dx+a_3\int_0^{Ll}\sin 2\frac{p}{L}x\cdot\sin 3\frac{p}{L}xdx\right]+$$
$$+g\int_0^L M(x)\sin 2\frac{p}{L}xdx=0$$

Finally condition

$$\frac{\partial F}{\partial a_3}=0$$

yields to equation

$$-\left[a_1\int_0^L\left(\frac{p}{L}\right)^2\cos\frac{p}{L}x\cdot 3\cos 3\frac{p}{L}x\,dx+a_2\int_0^L 2\left(\frac{p}{L}\right)^2\cos 2\frac{p}{L}x\cdot 3\cos 3\frac{p}{L}x\,dx+\right.$$
$$\left.+a_3\int_0^L\left(3\left(\frac{p}{L}\right)^2\cos 3\frac{p}{L}x\right)^2dx\right]- \quad (84)$$
$$-w^2\left[a_1\int_0^L\sin\frac{p}{L}x\cdot\sin 3\frac{p}{L}x\,dx+a_2\int_0^L\sin 3\frac{p}{L}x\sin 2\frac{p}{L}x\,dx+a_3\int_0^L\left(\sin 3\frac{p}{L}x\right)^2dx\right]+$$
$$+g\int_0^L M(x)\sin 3\frac{p}{L}x\,dx=0$$

Since the Fourier components *sin(px /L), sin2(px /L), sin3(px /L)* … are orthogonal functions, the following members of Equation (82) are equal to zero, namely

$$\int_0^L \left(\frac{p}{L}\right)^2 \cos\frac{p}{L}x \cdot 2\cos 2\frac{p}{L}x\,dx = 0, \qquad \int_0^L \left(\frac{p}{L}\right)^2 \cos\frac{p}{L}x \cdot 3\cos 3\frac{p}{L}x\,dx = 0,$$

$$\int_0^L \sin\frac{p}{L}x \cdot \sin 2\frac{p}{L}x\,d\,x = 0 \quad \text{and} \qquad \int_0^L \sin\frac{p}{L}x \cdot \cos 3\frac{p}{L}x\,dx = 0$$

Because of that Equation (82) reduces to its final form

$$a_1 \int_0^L \left( \left(\frac{p}{L}\right)^2 \cos\frac{p}{L}x \right)^2 dx + w^2 a_1 \int_0^L \left( \sin\frac{p}{L}x \right)^2 dx = g\int_0^L M(x)\sin\frac{p}{L}x\,dx \tag{85}$$

Similarly Equations (83) and (84) are transformed to

$$\begin{cases} a_2 \int_0^L \left( 2\left(\frac{p}{L}\right)^2 \cos 2\frac{p}{L}x \right)^2 dx + w^2 a_2 \int_0^L \left( \sin 2\frac{p}{L}x \right)^2 dx = g\int_0^L M(x)\sin 2\frac{p}{L}x\;dx \\ a_3 \int_0^L \left( 3\left(\frac{p}{L}\right)^2 \cos 3\frac{p}{L}x \right)^2 dx + w^2 a_3 \int_0^L \left( \sin 3\frac{p}{L}x \right)^2 dx = g\int_0^L M(x)\sin 3\frac{p}{L}x\,dx \end{cases} \tag{86}$$

respectively. Generally

$$a_i \int_0^L \left( i\left(\frac{p}{L}\right)^2 \cos i\frac{p}{L}x \right)^2 dx + w^2 a_i \int_0^L \left( \sin i\frac{p}{L}x \right)^2 dx = g\int_0^L M(x)\sin i\frac{p}{L}x\,dx \tag{87}$$

where *i* undergoes values 1,2,3..*n*.

The last equation presented is applicable not only to temperature difference between the beam and the slab, but to all other load types as well. The resulting normal force shows good compliance with the results obtained by the Hawranek-Steinhardt method. The Author's Energy Method can be extended to statically indeterminate structures as well. The advantage of this method is that calculation can be carried out using standard engineering softwares (e.g. MathCad) that are able to handle this kind of equations which simplifies the calculation process extensively.

The present method was applied to a simply supported steel-concrete composite girder with 2 m span subjected to temperature difference 40 $^{o}$C, tested by the author experimentally (see Chapter 4, Specimens S4 and S5, Fig. 37). The detailed calculation is presented in the Appendix. As Fig. 13 shows, very good agreement is observed between the normal forces

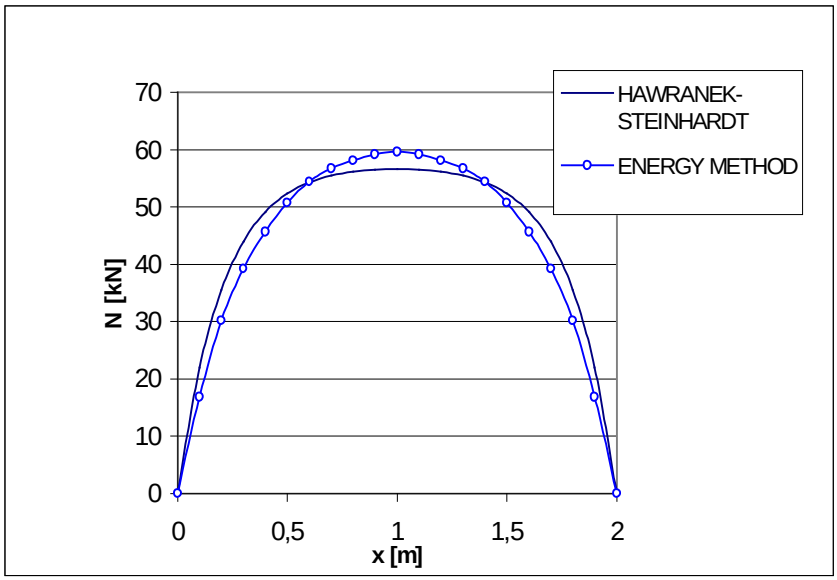


*Fig. 13. Normal force distribution due to temperature difference 40 $^{o}$C along the length of girder studied in Chapter 4 (Fig. 37).*

calculated using the Hawranek-Steinhardt method and the Author's Energy Method, but significant difference can be experienced in the shear forces per unit length especially near the support region (Fig. 14). That is why a finite element method (LUSAS software package) is invoked to interpret the curves as well. The results of LUSAS are in good correlation with the Author's Energy Method.

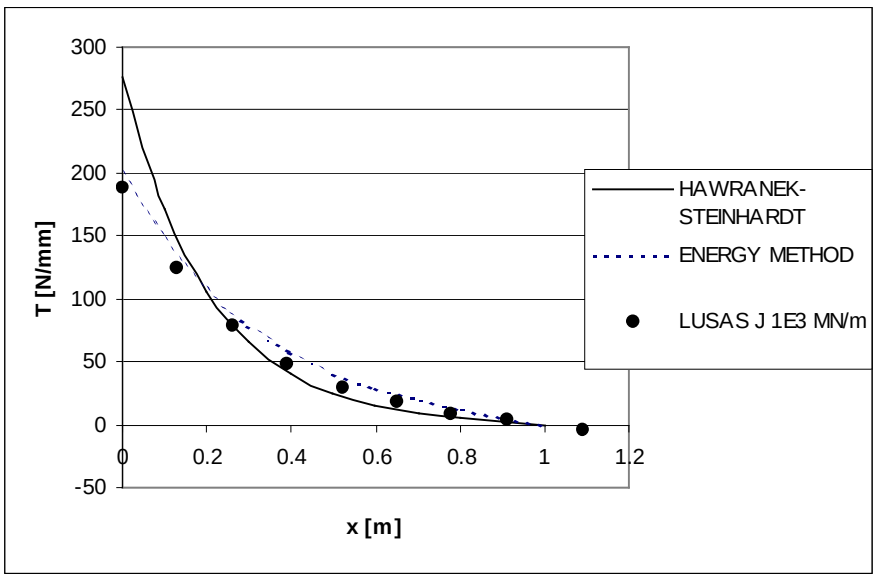


*Fig. 14. Distribution of longitudinal shear force on a unit length due to temperature difference 40 $^{o}$C. The diagrams on the left half of the span shown in the girder studied in Chapter 4 (Fig. 37).*

## 2.5 Numerical methods

Experimental investigation is essential for developing the fundamental background, which is used for validating all theoretical approaches. Experimental research, however, has a limited scope by its very nature. The parametric investigations can be carried out using numerical

simulation which also facilitates to determine the influence of each factor.

Basically three branches of numerical methods are used, the so-called folded plate method, finite difference formulation, and finite element method.

Important things are validation and calibration of numerical models which are capable of simulating the joint response in composite girders accurately enough. Using the numerical modelling technique it is possible to determine the significant factors that influence the joint response. This is needed for the development of simplified prediction procedures that would be used in design practice.

Originally the folded plate theory was developed to analyse isotropic thin-walled prismatic structures (e.g. roofs and bridges) [51], [27], [67]. This theory, however, also facilitates the analysis of composite beams and can be used to determine the effects of a deformable connection between the concrete slab and the steel girder [68], [69].

For the purpose of the folded plate analysis, the composite girder discussed in Ref. [68] was modelled using rectangular elements connected along the longitudinal joints. The concrete slab, flanges and web of the steel girder were idealised by regular folded plate elements. The concrete slab is connected to the top flange by a “special element”, which is similar to the orthotropic element used in the finite strip method.

In the next paragraphs, investigations carried out by finite difference method are summarised.

In 1999 MANFREDI et al. (1999) [79] and in 2000 FABBROCINO et al. [36] developed a refined model of steel-concrete composite girder subjected to negative bending. This model is characterized by two slips, which occur at the steel beam - concrete slab interface and at the reinforcement - concrete in tension interface. In this way both the deformability of the shear connectors and the tension stiffening effect of concrete can be analysed. The differential equations governing the model are solved by finite difference method. The solution of the problem can be obtained up to failure of the composite girder. The results obtained by this method were in good conformity with the experimental ones. Therefore, these program capabilities characterizing the interactions between steel beam and concrete slab and between reinforcement and concrete in tension can properly simulate the real behaviour of the beams. In addition, the proposed model seems to be most suitable for evaluating the rotation capacity of continuous composite girders at the negative bending regions when the ductility of reinforcing bars is considered as well.

In 2001 the finite difference method was also used by DEZI et al. [30] to analyse the shear-lag effect in composite beams with deformable shear connectors taking into account the long-term behaviour of the concrete. In this work variational approach was used to handle the differential equations in an easy way [30]. The author applies this approach as well in Section 2.4, where the unknown normal force function N(x) is approximated using a finite Fourier series of *n* terms, then the Hawranek-Steinhardt differential equation is transformed to *n* linear equations, where the unknowns are the Fourier coefficients. The Fourier term functions are chosen to satisfy the boundary conditions of a simply supported beam. The method is applied to a simply supported composite beam subjected to a 40 $^{o}$C temperature difference between steel and concrete.

In the next paragraphs investigations carried out by finite element method are summarised.

In 1986 a composite beam finite element was developed by LESKELÄ [74]. He also analysed the displacement and force state of the composite girder. In the same year, ARIBERT [2]

developed finite elements of his own for composite girders.

Other finite element method calculations were carried out by KŘÍSTEK et al. (1987) [69], [126]. The composite girders were modelled as a group of simple rod elements. The steel beam is presented by a line element, which embodies the material and geometrical properties of the beam. The concrete slab is supposed to be linearly elastic and also a line element in the centroid is used to represent the slab. The concrete slab is connected to the steel beam through very stiff fictitious connectors that are also modelled by rod elements having the same bending stiffness as the real connectors. The push-out test specimens were also modelled by KŘÍSTEK et al. [69] in this way.

Standard finite element programs are commonly used in structural engineering to model the composite girders. Earlier the three-dimensional (3D) analysis led to computation difficulties because of limited software and hardware facilities. Therefore, two-dimensional (2D) models were adopted. Nowadays the computer hardware capabilities are almost unlimited for use.

In 1999, JURKIEWIEZ et al. [61] implemented a new module in the CASTEM 2000 finite element program. This module is based on the theory of linear viscoelasticity. It applies to composite structures made of elastic or viscoelastic materials, such as wood, concrete, etc. A specific algorithm was also implemented in this program to take into account the phases of construction.

In 2004, the behaviour of steel-concrete composite girders with different degrees of shear connection was investigated by NIE et al. [83]. The girder was subjected to negative bending moment. Firstly, an analytical model for predicting the maximum deflection of the composite girder at the serviceability limit state was developed considering different degrees of shear connection. Secondly, to verify the reliability of the analytical model and the equations, three composite girders were tested. Meanwhile, the general-purpose finite element software ANSYS was used to investigate the behaviour of the girder. The non-linear properties of the constituent materials, crushing of concrete, and slips at the steel beam -concrete slab and concrete slab - reinforcement interface were considered. In this study similar methodology as in Ref. [83] was used, an analytical model was developed (model for the Author's Energy Method) and experimental investigations were carried out. The results were verified both analytically and by using a finite element model based on LUSAS software. The author also investigated the influence of different degrees of shear connection on the behaviour of the entire composite girder by changing the connector stiffness and using different types of connectors.

In 2005, using ABAQUS software package, LAM and EL-LOBODY [73] developed a finite element model with solid elements (Fig. 15) to simulate the load-slip characteristics of headed shear studs in a concrete slab. The model takes into account the linear and non-linear material properties of the concrete and shear in the studs. The finite element results agreed well with the results obtained from the experimental push-out tests. All failure modes were accurately predicted by the finite element model developed. In the future the application of this type of finite element models may eliminate the need for expensive push-out tests for determining the shear capacity of the connectors. To investigate the influence of shear connectors on the composite girder, the author contributed by presenting in this study a similar finite element model based on solid elements and use of a LUSAS software package. This model is presented in detail in Chapter 5.

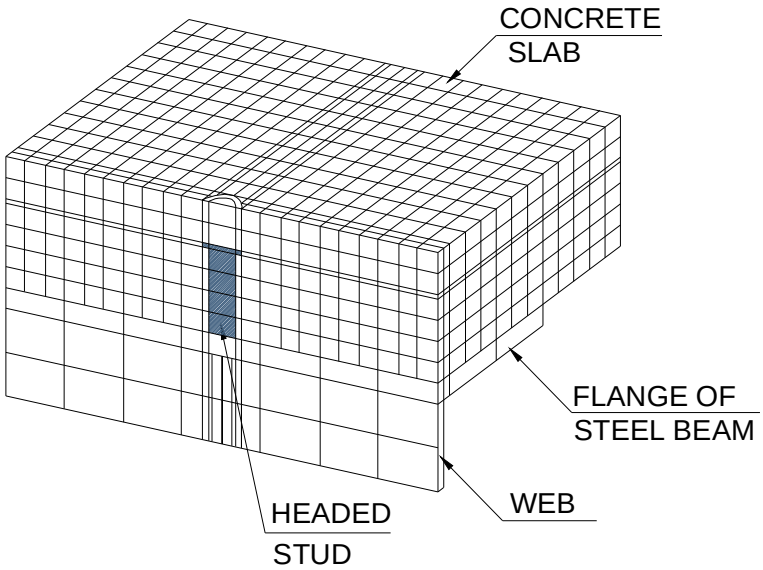


*Fig. 15. Finite element model with solid elements (made by ABAQUS program package).*

In the next paragraphs investigations carried out using one or two-dimensional finite element methods are summarised.

The use of two- and three-dimensional continuum elements for the analysis of composite girders requires the solution of a large number of equations. To reduce the computational effort, several researchers have used one-dimensional composite beam elements only. For studying the instantaneous, long-term and non-linear behaviour of composite girders, displacement-based, force-based and mixed finite elements are developed. Some studies indicate that the use of force-based elements, in which the elemental internal forces are the principal unknowns, can improve the accuracy of numerical results to a significant extent [81], [98]. Unlike displacement-based finite elements, the mixed formulation avoids the nodal force discontinuities [38], [39] and [40], in addition, the mixed approach is used to ensure more accurate solutions in the non-linear range [22].

In 1993, a composite beam finite element with a continuous spring model was used by DANIELS and CRISINEL [24] for the non-linear strength analysis of composite slabs. This beam element is based on the displacement approach with 10 nodal degrees of freedom (10DOF). The constitutive law for concrete is able to handle the tension stiffening effect as well.

In 1998 SALARI et al. [98] developed a composite beam finite element using the force method. This element consists of two line element components connected by a continuous interface element, which accounts for the deformations of the shear connectors. The bond force along the interface is approximated by a cubic interpolation function.

In 1999, GATTESCO [49] presented a non-linear, displacement-based composite beam finite element. This element consists of two line element components connected by discrete spring elements. The stress-strain constitutive relationships available in the literature are used in the procedure. Since the shear transfer between concrete slab and steel beam occurs only through connectors (in the absence of bond), the composite girders can be studied with partial shear connections which normally means large connector pitches. The arc-length method [20] implemented in this procedure allows the collapse load to be reached in structures where the load-deflection curve shows either a perfectly plastic or a softening behaviour. The program, in contrast to many other similar procedures, allows

consideration of bonding at the steel - concrete interface. In addition, this program also allows investigation of the inelastic response of continuous composite girders with complete or partial shear connections.

In 2000, AYOUB and FILIPPOU [9] developed an inelastic beam element for the non-linear analysis of steel-concrete composite girders with partial shear connection. This analysis allows both monotonic and cyclic loads. The element is developed using a two-field mixed formulation with independent approximation of internal forces and transverse displacements. The non-linear response of the composite girder is derived from a layer discretization of the cross-section with non-linear, uniaxial stress-strain relation of the constituent materials. The partial interaction between concrete slab and steel beam through shear connectors is accounted for by an interface element with distributed force transfer characteristics.

In 2000, SEBASTIAN and McCONNEL [102] developed an advanced non-linear finite-element program for the analysis of general steel-concrete composite structures including composite space trusses. Finite elements were used to represent the concrete slab and steel beam which allowed the ribbed composite slabs of reinforced concrete on profiled steel sheeting to be modelled. The concrete slab was modelled using two-dimensional elements, non-linear elastic isotropic material properties before cracking and non-linear orthotropic properties thereafter. For the steel beam a one-dimensional element was selected and initially elastic material properties as well as strain-hardening capabilities after yielding were applied. A special stub element with non-linear shear force-slip relationship was used at the concrete slab - steel beam interface to permit modelling of either full or partial shear connector action.

In 2002, FAELLA et al. [39] developed a linear finite element which may be employed in several cases related to the serviceability limit state of steel-concrete composite beams. As a result, effects related to cracking, non-linear behaviour of shear connection and long-term behaviour of concrete can be calculated. The stiffness matrix was derived from Newmark's "exact" differential equation. Therefore, only one finite element per member is needed. Internal nodes are needed only for considering varying geometrical and mechanical properties and when external, concentrated forces are present. A simplified method was also developed by the same authors [40]. This method enables to evaluate deflections of composite girders with non-linearly behaving shear connection.

In 2004, FRAGIACOMO et al. [44] developed a finite element for studying both the short- and long-term structural response of steel-concrete composite beams. In short-term analyses, the structural problem can be solved at each load level up to the collapse. In long-term analyses under the service load, the rheological phenomena (creep and shrinkage) of concrete can be considered in a rigorous manner. The finite element consists of two line element components connected by a continuous interface element, which models the shear connectors. In the long-term analysis, concrete cracking and tension stiffening effect of concrete are modelled. The solution of the non-linear problem is obtained by using an iterative procedure called "modified secant stiffness method". It is particularly effective in long-term non-linear analyses, because it does not suffer from any convergence problem. Using 10DOF elements the disadvantages of displacement formulation are avoided.

DALL'ASTA and ZONA in 2002 [21] and 2004 [22] developed several non-linear finite elements applicable to composite beams. These elements consist of two line element components connected by a continuous interface spring element. In 2002, some displacement-based elements (8DOF, 10DOF and 16DOF) were presented by the same authors [21]. In 2004, non-linear finite elements (10DOF and 16DOF) were developed for

the non-linear analysis of composite girders with deformable shear connection [22]. In this context a new mixed beam element and two previously introduced displacement-based beam elements were initiated and utilized. The following constitutive laws were used:

(i) Elastic-perfect, plastic-hardening law,

(ii) non-linear law suggested by the CEB-FIP Model Code 1990,

(iii) constitutive law of OLLGARD.

The elastic-perfect, plastic-hardening constitutive law (i) was applied to the steel beam and reinforcing bars. The non-linear law suggested by the CEB-FIP Model Code 1990 (ii) was considered for concrete [16]. The constitutive law of OLLGARD (iii) was adopted for the shear connection [91]. The inelastic response of continuous composite girders was also studied. This problem is of practical interest in structural engineering. Due to high slip gradient, strain localizations, slab cracking in the hogging region and concrete softening in the sagging regions it also represents a difficult numerical test for the finite elements used in composite girder analysis.

As it can be seen from above, many kinds of investigations were carried out based on the use of finite difference method and different types of finite elements were developed by several authors to tackle the problem of composite girders. In the future their results can be incorporated into the standard finite element software packages to improve the accuracy and efficiency of composite girder analysis.

## 2.6 Methods based on Eurocode 4

Since the present study also covers connectors with linear behaviour, the relevant investigations conducted for the Eurocode standards should be introduced here as well. For example, in Eurocode 4 [35] the slip between beam and slab is taken into consideration – indirectly – against the standards used before Eurocode 4. The slip is taken into consideration in the investigation of present author, NIE et al. [82] and WANG [125].

According to JOHNSON and MOLENSTRA [60], "for a given beam, loading and design method, 'full shear connection' is defined as the least number of connectors, such that the bending resistance of the beam would not be increased, if more connectors were provided" (Fig. 16).

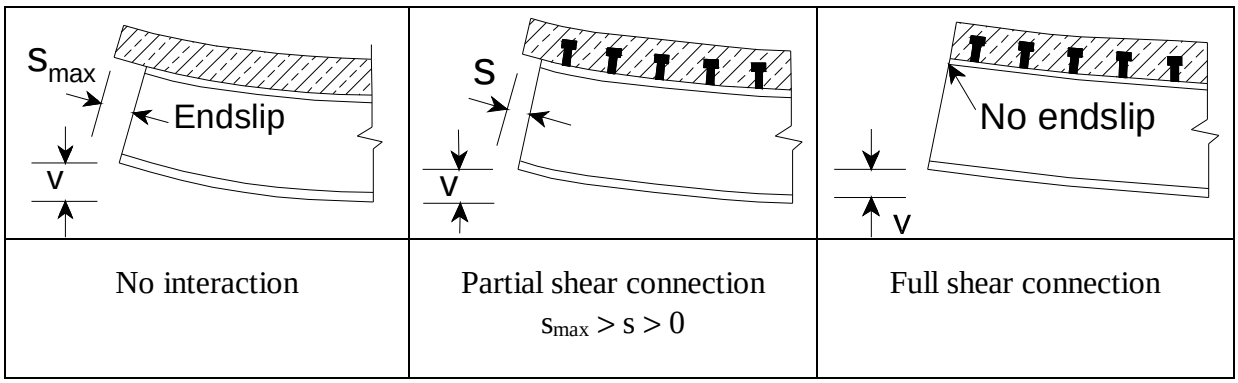


*Fig. 16. Partial and full shear connections.*

Eurocode 4 introduces the notion of so-called ductile connectors. Ductile connectors are those which have sufficient deformation capacity to justify the assumption of an ideal (elastic) plastic behaviour of the shear connection in the structure considered. Fig. 17 shows a comparison of the force-slip diagrams of ductile and non-ductile (rigid) connectors.

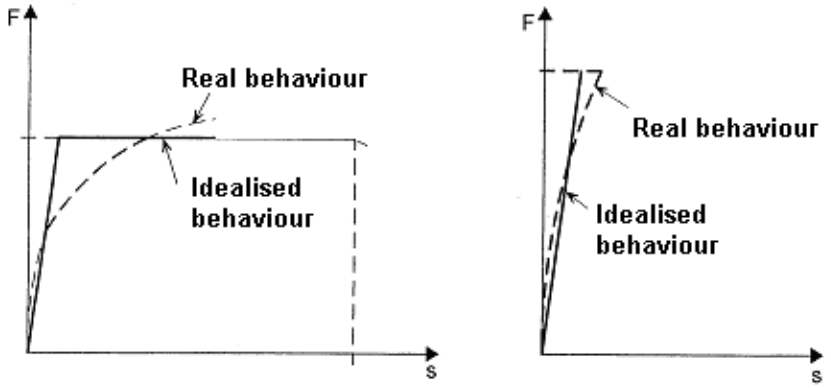


*a)* *b)*

*Fig. 17. Behaviours of a) ductile and b) non-ductile connectors according to Ref. [18].*

Ductile connectors are important because Eurocode 4 allows (and also recommends) the use of redistribution of the plastic moment of a cross-section and connectors. In general, headed studs with the appropriate length and shank diameter may be considered as ductile, when the ratio $h = n/n_f$ is within an interval prescribed in Eurocode 4. Here $h$ is the degree of shear connection. Furthermore, $n$ means the number of connectors with partial shear applied for the relevant length of the composite girder and $n_f$ means the number of connectors with full shear calculated for the relevant length of the same composite girder. Ratio $h$ is valid for steel I-sections with equal or asymmetrical flanges.

It has been a long tradition and still is to place the connectors so that their spacing follows the shear flow diagram. In such cases the elastic analysis is used. Nowadays another philosophy based on Eurocode 4 and the utilisation of plastic analysis is applied. As a consequence the connector spacing becomes more even and the total number of connectors is determined by the plastic normal force of the beam or slab. Plastic analysis can be applied only to cross-sections of class 1 and class 2 to Eurocode 3 [34]. Detailed information of connector spacing is given in Eurocode 4 as follows:

For full shear connection, on the one hand, the total design longitudinal shear force $V_l$ to be resisted by uniformly distributed shear connectors between the point of maximum sagging bending moment and a simple end support shall be

$$V_l = F_{cf} \tag{88}$$

where the normal force of beam or slab

$$F_{cf} = \min \begin{cases} A_a \cdot f_y / g_a \\ 0{,}85 \cdot A_c \cdot f_{ck} / g_c + A_{se} \cdot f_{sk} / g_s \end{cases} \tag{89}$$

and $A_a$ is the area of structural steel, $A_c$ is the effective area of concrete, and $A_{se}$ is the area of any longitudinal reinforcement in compression that is included in the calculation of the

bending resistance, and these areas relate to the cross-section at the point of sagging bending moment.

On the other hand, the total design longitudinal shear force $V_l$ to be resisted by shear connectors spaced in accordance with Eurocode 4 between the point of maximum sagging bending moment and an intermediate support or a restrained end support shall be

$$V_l = F_{cf} + A_s \, f_{sk} / g_s + A_{ap} \, f_{yp} / g_{ap} \tag{90}$$

Here $A_s$ is the effective area of longitudinal slab reinforcement and $A_{ap}$ is the effective area of any profiled steel sheeting. These areas relate to the cross-section at the support. Force $F_{cf}$ is obtained from Equation (89), but in case of a cantilever it is, according to Eurocode 4, taken as zero [35].

For the design of partial shear connections (with ductile connectors), the concept of a reduced ultimate moment ($M_u^{(r)}$) curve was introduced in Eurocode 4 (Fig. 18). In this procedure the slip along the steel-concrete interface does not need to be calculated. Since in this case the number of connectors is lower than the number of connectors used in full shear connection, the ultimate moment of the internal critical cross-section is reduced.

The global relationship between the reduced ultimate moment $M_u^{(r)}$ and the number of connectors $n$ can be represented by a quadratic, convex curve ABC, as shown qualitatively in Fig. 18. This relationship can also be considered in a non-dimensional form ($M_u^{(r)}/ M_u$, $h$). In this context $M_u$ is the ultimate moment and $M_{a,pl}$ is the bending moment acting in the beam causing plastic failure. In Fig. 18 plastic moments were determined by the so-called "stress-block method". Such a curve belongs to cross-section classes 1 and 2 only.

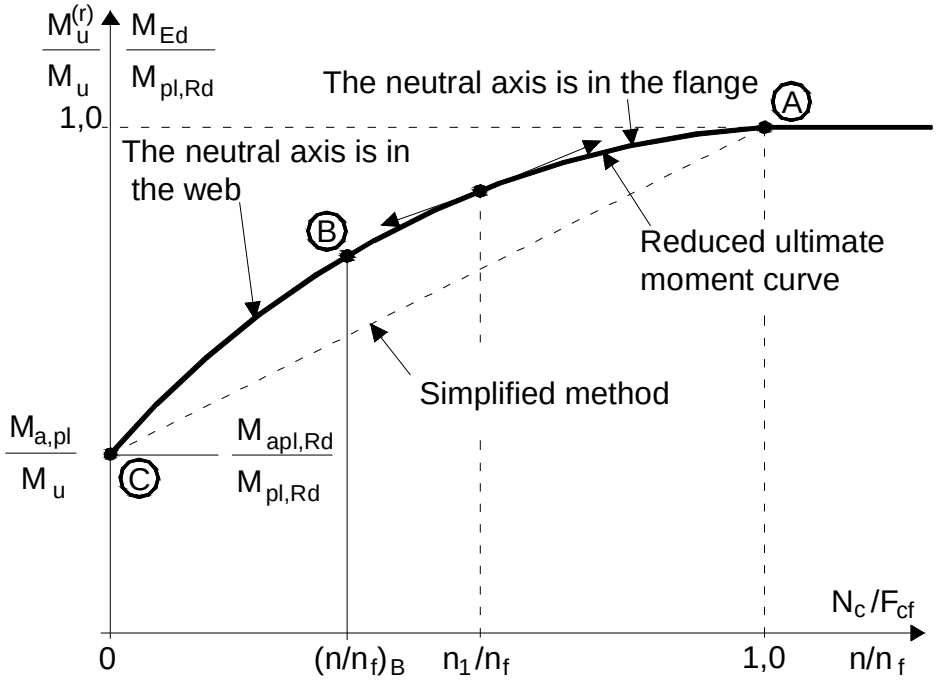


*Fig. 18. Reduced ultimate moment curve according to Refs. [18] and [35]. Ductile connectors.*

The convexity of curve ABC allows an alternative simplified approach that is always on the safe-side. This method defines the moment resistance $M_u^{(r)}$ in terms of a linear interaction with the degree of shear connection denoted by $h$, such that

$$M_u^{(r)} = M_{a,pl} + h\,(M_u - M_{a,pl}). \quad (91)$$

This "simplified method" is represented by the dashed line AC in Fig. 18. Line AC is only a linear interpolation between no-connection state and full connection state. Generally, a significant benefit may be obtained by using the stress block method in the range of $h$ = 0,5 to 0,7, but sometimes the greatest difference is obtained, when $h$ is less than 0,4.

In partial shear connections equation

$$N_c = \frac{M_{Ed} - M_{apl,Rd}}{M_{pl,Rd} - M_{apl,Rd}} F_{cf} \quad (92)$$

can be used in practical applications. This equation is based on the "simplified method" as shown in Fig. 18. Here $N_c$ is the compressive force in the concrete slab, $M_{Ed}$ is the design moment, $M_{apl,Rd}$ is the design plastic bending resistance of the steel beam section alone and $M_{pl,Rd}$ is the corresponding plastic resistance of the whole composite section, all in sagging. If normal force $F_{cf}$ is replaced by compressive force $N_c$ in Equations (88) and (90), the total design longitudinal shear forces $V_l$ can be calculated and used in partial shear connections.

If in a partial shear connection the connectors are not ductile, the longitudinal shear force $V_l$ can be determined from such a stress distribution, which is based on the assumption of full continuity at the interface between the steel beam and concrete slab. This shear force can be calculated at the critical cross-sections, which are defined in Eurocode 4 (Section 6.2.1.1). The compressive force in the concrete slab $N_c$ and the total design longitudinal shear forces $V_l$ can be calculated using the formulae of Eurocode 4 (Section 6.2.1.4) in the same way as in the case of partial shear connection with ductile connectors.

According to recent research [75], [76] there is a clear explanation for non-ductile behaviour of shallow beams without mechanical connectors. In this case the so-called "zip-flyer " effect of non-ductile connections is taken into account. It means that when on a force-displacement curve the maximum force is reached and the force begins to decrease, the connection gives after and the next point nearby in the concrete-steel connection begins to take the shear force. So it goes further as a wave and a zip-like effect is obtained. During this non-ductile redistribution of connection forces, the peak of the shear force diagram moves towards the centre of the beam while the load of the beam cannot be much increased. This effect becomes more obvious in short-span girders.

If the analysis is based on the elastic theory, the longitudinal shear per unit length shall be calculated on the basis of the widely used formula T = V·S/I. Generally this applies to bridge girders.

The merit of Eurocode 4 is that the notion of partial and full shear connection and ductile connectors and the method for considering such connections was introduced. In certain cases the uniform distribution of connectors is allowed along the critical lengths according to Eurocode 4 [35].

## 2.7 Behaviour of shear connectors in the concrete slab

### 2.7.1 Background

The present study deals with the behaviour of connectors and their influence on the stress and strain condition of a composite girder. Discussion on essential behaviour of shear connectors is therefore very important.

Mechanical connectors impose high load concentrations in the concrete slab. This is due to the so-called dowel action of the connectors [58]. The phenomenon of dowel action means basically a shear and bending transfer mechanism, which is illustrated in Fig. 19. All mechanical connectors (headed stud, bolt, HSFG bolt, angle, bar, T-section, channel-section, horseshoe, etc.) are simply steel dowels embedded in the slab.

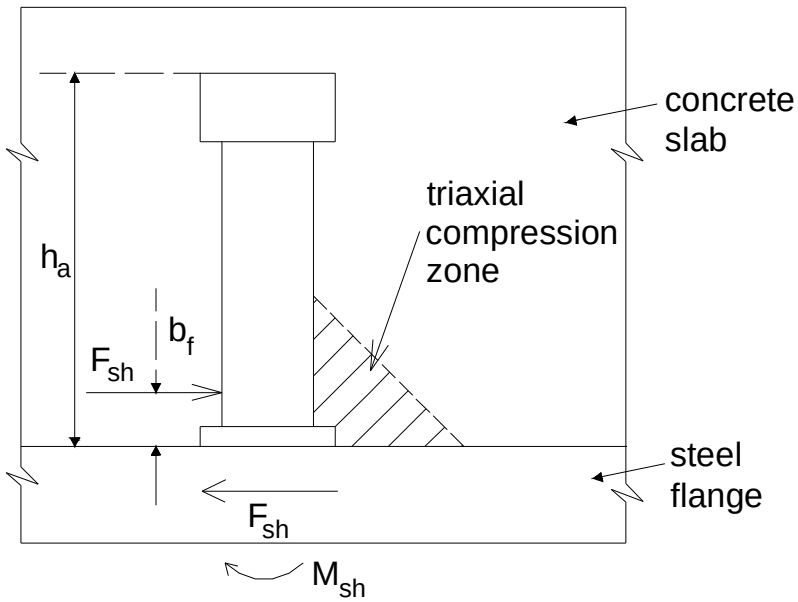


*Fig. 19. Dowel action [87].*

The resistance of a connector to this dowel action is referred to as the dowel strength, and this strength is often quoted in national standards. The dowel strength of mechanical shear connectors depends on the triaxial restraint of the concrete [78] in the bearing zone shown in Fig. 19. In this figure $F_{sh}$ is the shear force, $M_{sh}$ is the moment acting on the connector, $b_f$ is the distance between loading point of eccentric shear force $F_{sh}$ and interface of steel beam and concrete slab and $h_a$ is the height of connector. The dimensions of triaxial compression zone of concrete are dependent on the connector height.

The concentrated load induced by a connector is dispersed into the concrete slab and the action of this dispersal can induce tensile cracking, as shown in Fig. 20. These tensile cracks are induced by ripping, shear and splitting actions. Tensile cracking can also be induced by the dowel action particularly, when the connector is also resisting separation at the steel-concrete interface. These cracks are referred as embedment cracks. These four types of tensile failure of the slab can affect both the dowel strength and ductility of the shear connection. In order to differentiate the analyses that deal with splitting from those that deal with the longitudinal shear, splitting is concerned with lateral equilibrium, whereas shear is concerned with longitudinal equilibrium.

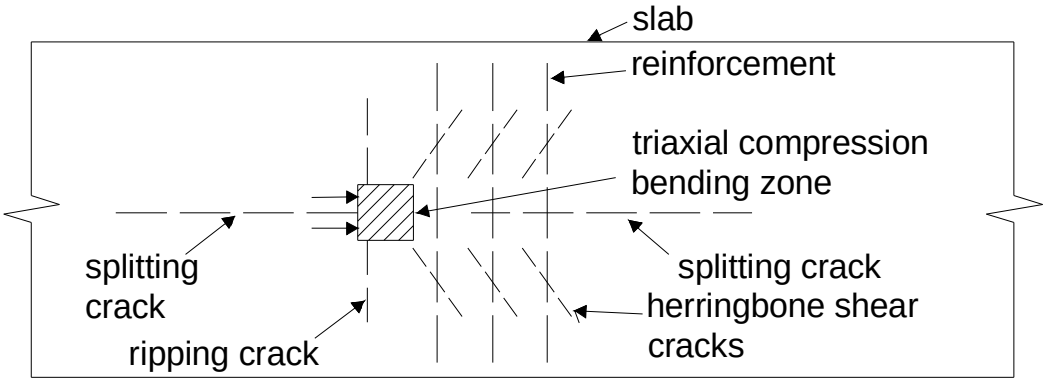


*Fig. 20. Tensile cracking induced by concentrated load [87].*

The herringbone formation of shear cracks due to excessive principal tensile stress [87] may affect the triaxial restraint of the concrete near the compressive zone of connectors and cause tension in the transverse reinforcement of the concrete slab.

Because of the large variety of mechanical shear connectors and because of the complexity of the dowel action, the strength and ductility of shear connectors are always determined experimentally.

In further parts of this Section the focus is on the splitting, embedment forces and interaction between the shear and axial forces.

### 2.7.2 Splitting

The shear connection causes local and global lateral stresses in the concrete slab. The ability of a slab to resist the concentrated forces imposed by individual connectors, groups of connectors and concentrations of connectors is referred to as local splitting. When the acting zones of individual connectors, groups of connectors, etc. overlap with the zones of other connectors, groups of connectors, etc., then this interaction affects the splitting loads. This form of splitting is referred to as global splitting.

A method is demonstrated here to predict the resistance of concrete splitting in the deck slab having bar connectors. The connector shear load is applied to the slab near its bottom surface (Fig. 21a). This load is dispersed two-dimensionally, both vertically and horizontally. Let us consider the horizontal direction first. In this case the concentrated load is assumed to act as a uniformly distributed load having width $b_a$. This load develops lateral (x-y plane) stresses as shown in Fig. 21a. In the figure $c$ means the longitudinal spacing, when connectors are placed in a single line, and $b_c$ is the effective width of the concrete slab.

The splitting problem in two-dimension was investigated by JOHNSON and OEHLERS [58] [87]. They studied first the influence of lateral stresses caused by bar connectors (or strip loads) placed either at the end (Figs. 22a and 22b) or at the intermediate section of the concrete prism. This study was based on finite element analysis. In case of an end bar-type connector, the length of the lateral zone was found to be $x_t \cong 1.75 b_c$ (Fig. 22a), while in the case of an intermediate connector $x_t \cong 1.4 b_c$ (Fig. 22d). The value of $x_t$ does not depend on

width $b_a$, but only on $b_c$. If value $x_t \cong 1.75 b_c$ is used, then the ratio of lateral force versus strip load is calculated either from finite element analysis [58] or from original elastic

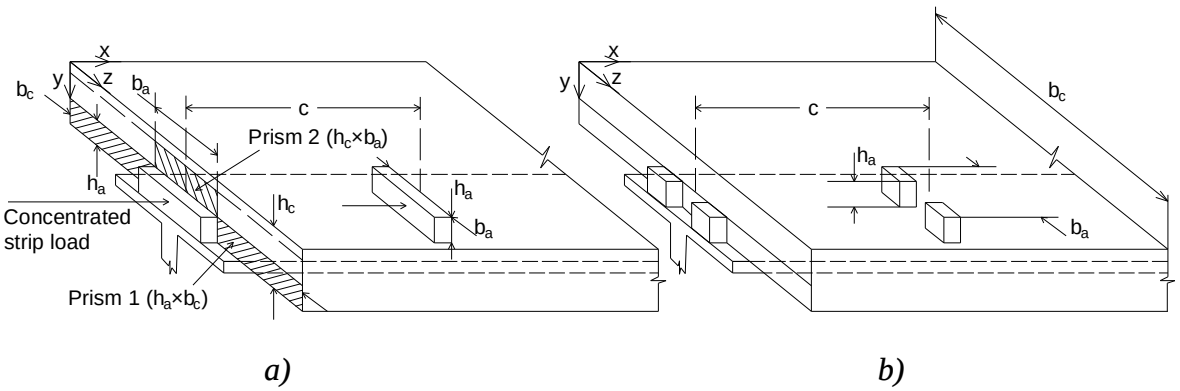


*Fig. 21. Composite T-beam [87], [90].*

method relating to the same problem [115]. The local splitting resistance of concrete is

$$F_{split} = \frac{0{,}6 \cdot b_c \cdot h_a \cdot f_{cb} \cdot p}{\left(1 - \frac{b_a}{b_c}\right)^2} \tag{93}$$

In Equation (93) $b_a$ is the effective breadth of concentrated patch load (or width of bar connector), $b_c$ is the width of concrete prism (or slab), $h_a$ is the depth of the strip load (or bar connector) and $f_{cb}$ is the indirect tensile strength of concrete.

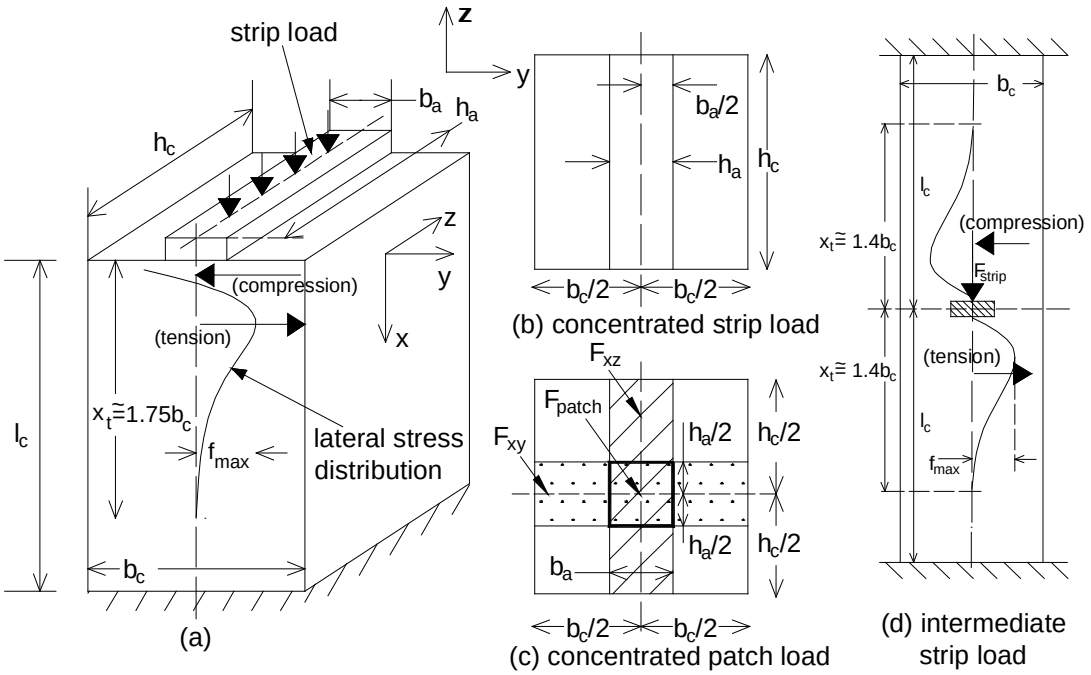


*Fig. 22. Strip and patch loads on prisms according to JOHNSON and OEHLERS [58],[90].*

When investigating the two-dimensional global splitting, a single line of connectors spacing with *c* is considered (Fig. 21a). The connectors apply a thrust on the concrete slab. Each connector induces a lateral tensile zone in front and a compressive zone behind (Fig. 22d),

or vice versa, depending on the thrust direction [58], [90]. In practical cases the lateral zones of individual connectors overlap with the zones of other connectors, which affects the splitting loads. This form of splitting is referred as global splitting, because lateral forces of all shear connectors can interact.

Fig. 23 shows, in case of a simply supported girder, the constant and variable components of the shear flow in general and at a design point Q. At a particular point four components of shear force flow can be distinguished (Fig. 23c). The two components on both sides of the point can be taken into consideration. The lateral tensile stresses, that induce splitting at a particular point, depend on the magnitude, variation, direction and the stepwise changes of the shear flow.

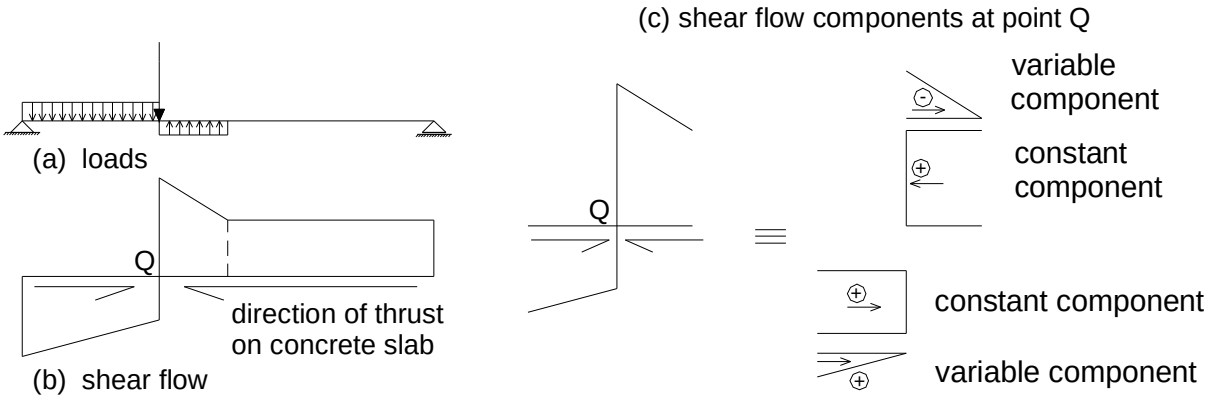


*Fig. 23. A simple example for shear flow components.*

It is necessary to define a different sign convention for the shear flow when dealing with splitting analyses in order to distinguish between lateral tensile and lateral compressive zones. The constant component of the shear flow is defined as positive when the connectors apply a thrust to the concrete slab that is directed towards the design point, that is the shear flow is directed towards the design point. The varying component of the shear flow is defined as positive when the shear flow acts towards the design point.

In Fig. 24 lateral stresses $f_d$ and $f_r$ are presented [87], [90]. They are caused by the constant and variable component of shear flow, respectively. In Fig. 24 $d_t$ means the length of splitting crack. Here the distance of connectors $c$ is equals to $d_t$. The value of $d_t$ is defined to be equal to $2b_c$. On Figs. 22a and 22d the maximum length of the lateral affected zone is $1{,}75b_c$. The connectors act independently, because the distance of the connectors $c$ is greater than $1{,}75b_c$. This means that the lateral stresses caused by the connectors do not overlap longitudinally. Fig. 24 shows that the positive shear flow induces lateral tensile stresses, while negative shear flow causes lateral compressive stresses at the design point. Formulae for the lateral stresses $f_d$ and $f_r$ were presented by OEHLERS [87].

The lateral stresses due to constant and variable components of the shear flow were determined separately by OEHLERS [87] using finite element method and elementary beam theory. It turned out [87] that global splitting is a function of the shear flow and not the ultimate resistance of the single connector unlike local splitting. This means that increasing of the number of connectors does not prevent global splitting. Splitting will occur when the sum of the four components (Fig. 23) of the lateral stresses reaches the tensile strength of concrete.

The two-dimensional splitting theory was developed for pair-wise bar-type connectors (Fig. 21b) and for headed stud connectors as well [90]. For the latter case, equivalent dimensions were determined [87], [88]. For composite girders with shallow haunches, equivalent prisms were developed for governing the two-dimensional splitting [89].

The two-dimensional splitting analysis underestimates the splitting resistance [90], which inspired JOHNSON and OEHLERS to develop formulae for the determination of the tree-dimensional splitting resistance [58], [87].

In 1981, JOHNSON and OEHLERS tested several concrete prisms subjected to patch loads [58]. They found an empirical formula

$$\frac{1}{F_{patch}} = \frac{1}{F_{xz}} + \frac{1}{F_{xy}} \tag{94}$$

for the determination of reciprocal value of splitting resistance of a concrete prism (Fig. 22c). Here $F_{xz}$ is the splitting load in x-z plane and $F_{xy}$ is the splitting load in x-y plane, acting on the detached and the dotted strips, respectively (Fig. 22c). $F_{xz}$ and $F_{xy}$ can be calculated by using Equation (93). Equation (94) is the so-called reciprocal relationship.

In 1989, using Equation (93) OEHLERS deduced a new formula

$$F_{patch} = \frac{0{,}6 \cdot b_c \cdot h_a \cdot f_{cb} \cdot p}{\left(1 - \frac{b_a}{b_c}\right)^2} + \frac{0{,}6 \cdot b_c \cdot h_a \cdot f_{cb} \cdot p}{\left(1 - \frac{h_a}{h_c}\right)\left(\frac{h_a}{h_c}\right)} \tag{95}$$

for the determination of splitting resistance of the concrete slab [87]. Here the first term is the splitting strength of Prism 1 in Fig. 21a (Equation (93)). Correspondingly, the second term represents the splitting strength of Prism 2 in the same figure. Equation (95) is the so-called additive relationship.

Unlike additive relationship, generally the reciprocal relationship gives larger strength values.

When the loaded concrete slab cracks in a point, but the transverse reinforcement prevents further crashing, is called post-splitting phenomenon. It is also discussed here. Splitting has been found to occur in composite T-girders subjected to monotonic loads [26], [17], in composite T-girders subjected to longitudinally moving loads [58], in composite L-girders [59], in composite haunched girders [114], in composite stub girder construction [71] and in composite hybrid beams with horizontal connectors [119].

The lateral stresses induced by the constant component of shear flow (Fig. 24a) are shown in Fig. 24b. If the slab is without reinforcement, the tensile stress zone around the maximum tensile stress $f_d$ moves with the crack tip. Therefore, the split propagates along the studs, parallel to the direction of thrust. Even though there was sufficient transverse reinforcement in the splitting zone, the splitting can occur. The transverse reinforcement resists not only the lateral tensile forces but also enables transferring of shear forces after splitting. As a consequence the variable component of shear flow may be assumed to be spread over the cracked zone and to

produce lateral tensile stresses (Fig. 24b). These stresses are of the same magnitude as those which initiate splitting. However, in this zone the tensile stress at the crack tip drops rapidly from $f_d$ to $f_r$ when the crack propagates. It means that lateral stress $f_r$ does not cause cracking, because it is smaller than the maximum tensile strength $f_d$. In other words, the transverse reinforcement does not prevent splitting [58], but does limit the propagation of the split, when only stationary loads are acting [87]. In Fig. 24 $d_t$ means the length of the splitting crack, $f_d$ is the lateral stress due to constant component of the shear flow, or maximum tensile strength, and $f_r$ is the lateral stress due to variable component of shear flow.

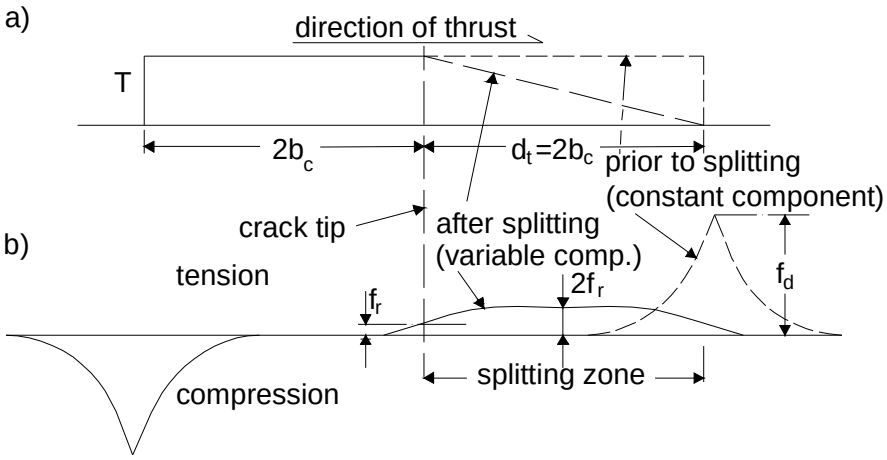


*Fig. 24. Propagation of splitting crack according to OEHLERS [87]. a) Shear flow. b) Lateral stress distribution.*

### 2.7.3 Embedment forces

In the analysis of composite girders discussed in Section 2.1.1, the assumption was made that the curvature of the concrete slab is always the same as the curvature of the steel beam. This assumption is justified, if no separation takes place in the steel - concrete interface. Therefore, the shear connection of a composite girder has to be constructed so that it resists both tensile and compressive forces normal to the interface surface. Mechanical shear connectors have such a shape that they efficiently resist axial tensile forces. These forces are not distributed along a line, but act more or less as concentrated “point” loads and are therefore likely to cause cracking at connectors. However, in general, the externally applied gravity loads cause compressive axial force in the interface of a T-shape composite girder [90], which does not cause cracking.

As presented by OEHLERS and BRADFORD [90], the global axial interface force distribution is analogous to the global lateral stress distribution induced by splitting forces described in Section 2.7.2. It was also shown, that the global lateral stress distribution curve envelopes the distribution curve of local stresses caused by the connectors (Figs. 22a and 22d). Hence, the global axial force distribution curve envelopes the local axial force distribution curves due to the vertical dispersal of the concentrated load from each connector. Local variations in the axial force distribution are also caused by web opening in the steel beam as well as local and lateral torsional buckling in the steel beam elements etc. The embedment forces of headed stud connectors are studied by McMACKIN et al., OLLGARD et al., and SLUTTER et al. [80], [91], [103].

Local embedment failure due to axial tensile load can be caused either by the cone surface failure or the shank neck failure of the stud. Using the surface area of the conical failure plane as the major parameter, McMACKIN et al. [80] developed formulae for determining the axial embedment force $X_{emb}$.

Apart from axial embedment failure, shear embedment failure can also occur [90]. In this case the shear force acting on a stud connector can produce a typical shear failure cone [90]. The corresponding shear embedment force $F_{emb}$ for different headed studs was determined by JOHNSON and OEHLERS [58] by using finite element analysis and by SLUTTER and DISCROLL [103] by using laboratory tests.

### 2.7.4 Interaction between shear and axial forces

The tensile loads acting on a composite girder can weaken the shear connection of a girder. Therefore, the interaction effect of an axial force $X_a$ and a shear force $F_{sh}$, that both can cause failure of a connector, is needed. Values for $X_{emb}$ and $F_{emb}$ forces can be obtained from pull and push-out tests.

The elliptical interaction curve, which originates from the laboratory tests of McMACKIN et al. [80], can be expressed in form

$$\left(\frac{F_{sh}}{F_{emb}}\right)^{\frac{5}{3}} + \left(\frac{X_a}{X_{emb}}\right)^{\frac{5}{3}} = 1 \tag{96}$$

This formula gives quite conservative results. Therefore, a more sophisticated formula was developed by OEHLERS et al. [90] by using finite element method. The validity of this formula was confirmed by laboratory tests. Notwithstanding the latter investigations, these types of design formulae need improvement.

As a conclusion of the discussion on the behaviour of shear connectors in the concrete slab it can be stated the following:

- Results of splitting analysis should be considered in standards.
- Interaction formulae between shear and axial forces of shear connectors need to be developed further.

# 3 COMPOSITE GIRDERS SUBJECTED TO DIFFERENTIAL STRAIN

## 3.1 Stresses caused by differential strain

In Chapter 2 analytical and numerical methods are summarised. Additionally, a new kind of method, the Author's Energy Method is introduced and used in the next chapters when evaluating the test results. In this chapter the problematic of differential strain acting on a composite girder is discussed. This is very important because the author's tests in Chapters 4 and 5 are mainly focused on this phenomenon (especially on the temperature difference).

Among stresses acting on a composite girder, stresses caused by differential strain (temperature difference, creep and shrinkage of slab) are of great importance. Concrete shrinkage and temperature difference between beam and slab lead to a restrained differential contraction or expansion between them. In reality, the temperature distribution may vary continuously through the depth and the length of the beam and the slab. In case of a simply supported beam, however, it is generally accepted to assume for calculations that the beam and the slab have constant but different temperatures. The value of temperature difference to be adopted is generally a constant (by most of the standards it is ± 10 $^{o}$C between concrete slab and steel beam). In case of continuous beam varying temperature function is considered (Fig. 25 as an example). The temperature difference effect is mostly observed and taken into account in bridges and similar structures.

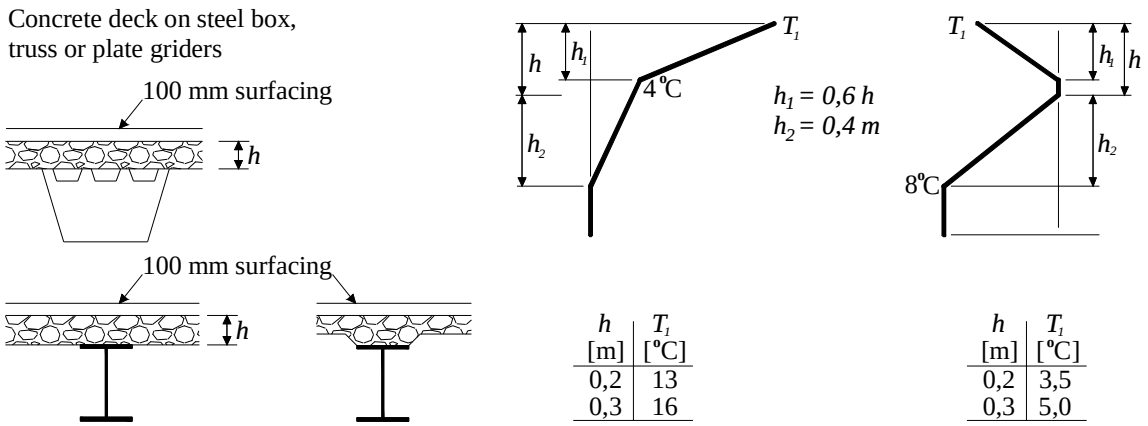


| h [m] | $T_1$ [°C] |
|---|---|
| 0,2 | 13 |
| 0,3 | 16 |

| h [m] | $T_1$ [°C] |
|---|---|
| 0,2 | 3,5 |
| 0,3 | 5,0 |

*Fig. 25. Temperature distribution for composite bridges by British Standard BS 5400 (Steel, Concrete and Composite Bridges. Part 5. Code of Practice for Design of Composite Bridges).*

Shrinkage strains occur over a period of months so that stresses resulting from them will be modified by creep.

In case of a simply supported beam the initial assumption is that the slab is disconnected from the beam and may expand or contract without restraint. The strain resulting from shrinkage or temperature difference is *e* which is to be considered as positive in extension. To maintain the initial length of the slab a force *N* shall be imposed at the center of gravity of the slab *($N = -e \times C_c$)*. It means that now the slab is reconnected to the beam. Force *N* is balanced by an equal opposite force *N* acting at the slab centroid (or by an equivalent force *N* relocated to the composite centroid and a couple $M = - N \times d_{ci}$. Using this elementary approach the moment due to differential strain is constant along the span. As a function of moment *M* and normal force *N* the normal stresses can be calculated. This simplified calculation method is generally accepted in practice.

Calculation of shear stresses particularly in the interface of beam and slab are also important. Shear stresses cannot be directly calculated on the basis of the previous simplified calculation method. Using the most conservative approach the shear caused by concrete shrinkage and temperature difference are confined to the ends of the composite girder. In case of an absolutely rigid shear connection theoretically an infinitely large interface shear appears at the girder ends. In reality, even with very rigid shear connectors, this phenomenon cannot be developed because of the plastic behaviour of the composite girder.

Calculation of shear flow due to differential strain as function of shear connector stiffness can be carried out using the differential equation of NEWMARK [85] or HAWRANEK-STEINHARDT [52]. Some standards are based on the ”exact” [52] solution but also simplify the distribution of shear along the girder by replacing the exponential curve of shear flow by a straight line. Other standards adopt triangular or rectangular shear diagram whose length is a function of the effective width or span. Some codes prescribe shear connector stiffness values.

In statically determinate structures the shrinkage of concrete does not alter the vertical shear and the effect of shrinkage is represented as additional deflection. In statically indeterminate girder shrinkage leads to redistribution of vertical shear which results in the rise of total shear force at intermediate supports and in the fall of total shear force at the end supports. Accordingly, bond failures are first expected in the hogging moment regions.

Creep of concrete is a complex phenomenon. It can be modelled by a linear or non-linear viscoelastic material model. The non-linear viscoelastic structure is influenced by the effect of age of concrete at loading, the effect of load duration and the deferred action of response in unloading. The principle of superposition is valid for both cases. The creep phenomenon is also dependant on a lot of conditions.

Methods encountered in the literature are:

Effective Modulus Method (FABER 1927) [37].
Rate of Creep Method (DISCHINGER 1937) [31], [32].
Creep Fibre Method (BUSENANN 1950) [13].
Approximate and Exact Method due to SATTLER (1959) [99].
Effective Modulus Method for Composite Girders (FRITZ 1961) [47].
Rate of Flow Method (ENGLAND and ILLSTON 1965) [33].
Improved Dischinger Method (NIELSEN 1970, TROST 1968-1973, RÜSCH, JUNGWIRTH and HILSDORF 1973) [84], [120]-[123], [97].
CEB-FIP Model Code Method (1978, 1990) [14], [15], [16].

The so-called Rate of Creep Method is used and developed further by many researchers. This method does not take into count the effect of age of concrete in loading and deferred action of response in unloading. The Improved Dischinger Method corrected the last problem. The CEB-FIP Model Code Method, which is the basis of Eurocode 2, eliminates all disadvantages of the Dischinger Method and introduces an additional term for initial creep as well.

## 3.2 Temperature influence on simply supported composite bridges

One of the main goals of the experimental investigations carried out by the present author is to study composite girders subjected to temperature difference. This is the reason to discuss this topic here.

Although the thermal expansion coefficient is approximately identical for steel and concrete, temperature influence may cause considerable internal stresses in composite bridges due to the significant difference in heat conduction (steel has a heat conductivity approximately 50 times as big as than that of concrete). This phenomenon is especially important when air temperature changes abruptly or the steel girder is exposed to intensive sunshine.

Measurements of temperature differences between the particular elements of composite bridges were already conducted by a rather large number of researchers even in the 1950's. One of the earliest and most elaborate measurement series was carried out in the Strength Analysis Laboratory of the Karlsruhe University [64]. During the measurement process temperature was recorded at certain locations of the steel beam and the concrete slab, at different times and under various weather conditions (rain, sunshine, etc.). The characteristic results of this work are shown in Fig. 26. It turned out that the ratio of shaded areas to areas exposed to sunshine also had a significant influence on the vertical temperature distribution in the examined girder. The greatest temperature difference between concrete and steel members was approximately 15 °C.

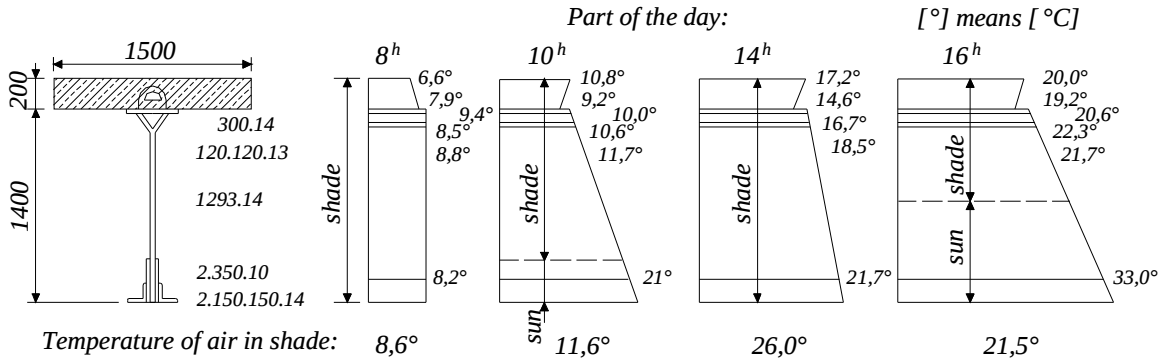


*Fig. 26. Experimental research of Karlsruhe University on composite girders investigating the influence of temperature difference.*

Similar results were obtained by other researchers as well. In the summer of 1978 and in the winter of 1979 temperature measurements were carried out on the Ostrova-Kolbova bridge in the Czech Republic [101]. The cross-section of this composite girder bridge and the location of measuring points can be seen in Fig. 27. The measured temperature distributions at mid-span

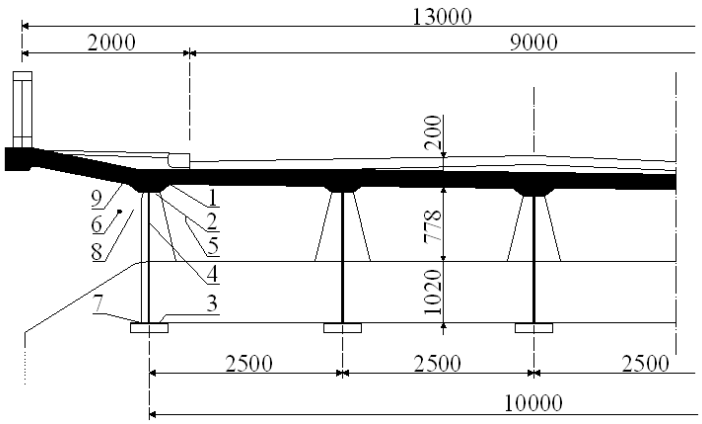


*Fig. 27. Cross-section of the Ostrava-Koblova composite bridge and location of the measuring points. Measures in millimetres.*

cross-section are shown in Figs. 28 and 29. The greatest temperature difference between concrete and steel members was approximately 7 °C.

Temperature measurements were also conducted on the Praha-Brandys composite bridge in the same country in the summer of 1981 [101]. Figs. 30 and 31 present the location of the measuring points and the measured temperature distributions at mid-span cross-section in this

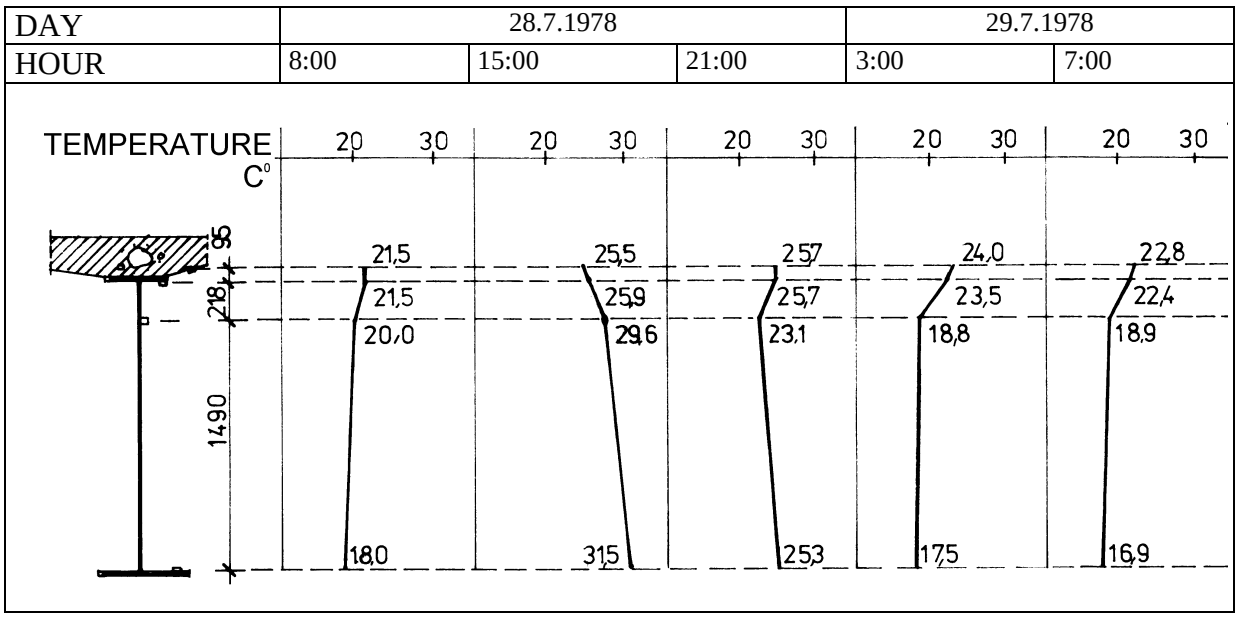


*Fig. 28. Temperature distribution across the mid-span cross-section of the Ostrava-Koblova composite bridge in summer 1978. The measures are in millimetres and temperatures in Celsius.*

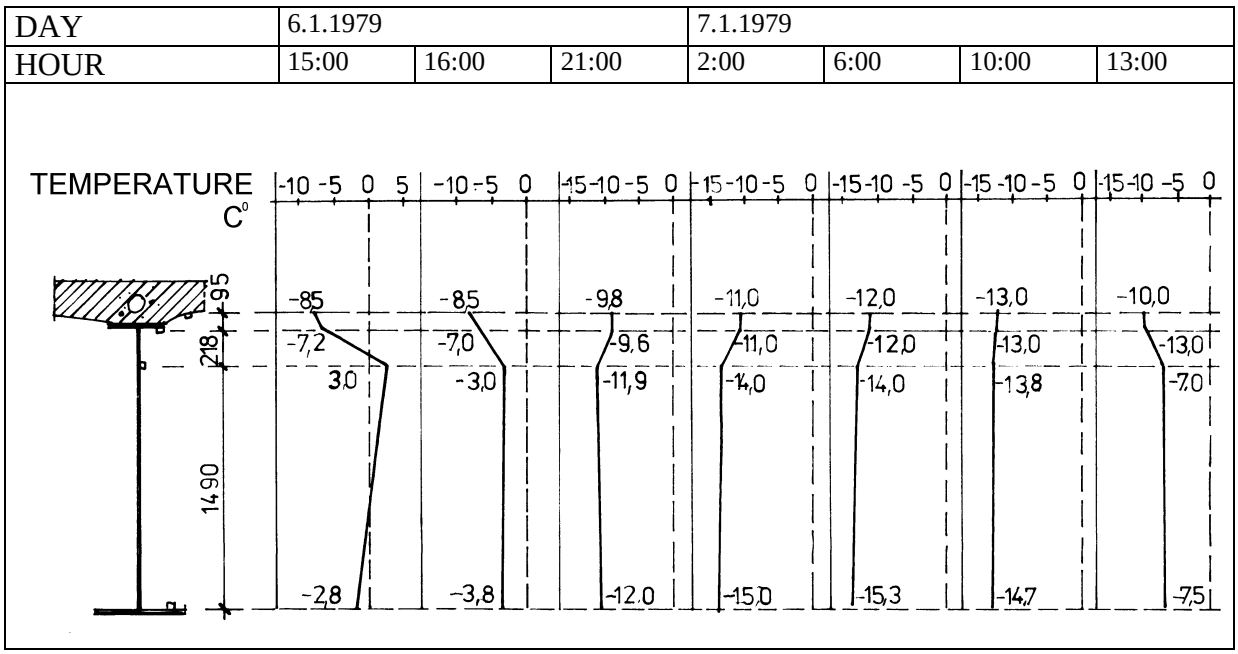


*Fig. 29. Temperature distribution across the mid-span cross-section of the Ostrava-Koblova composite bridge in winter 1979. The measures are in millimetres and temperatures in Celsius.*

case. Fig. 32 summarizes the temperature distribution in an envelope curve as function of time. From Figs. 30, 31 and 32 it can be concluded that the temperature difference between the extreme fibres of concrete and steel was approximately 10 °C.

| DAY | 11.7.1981 | | | | | |
|---|---|---|---|---|---|---|
| HOUR | 1:00 | 6:00 | 12:00 | 17:00 | 20:00 | 24:00 |
| OUTER TEMP. °C | 20,0 | 15,5 | 28,0 | 31,5 | 27,5 | 22,0 |
| INNER TEMP. °C | 20,0 | 18,0 | 25,5 | 27,5 | 26,0 | 23,0 |

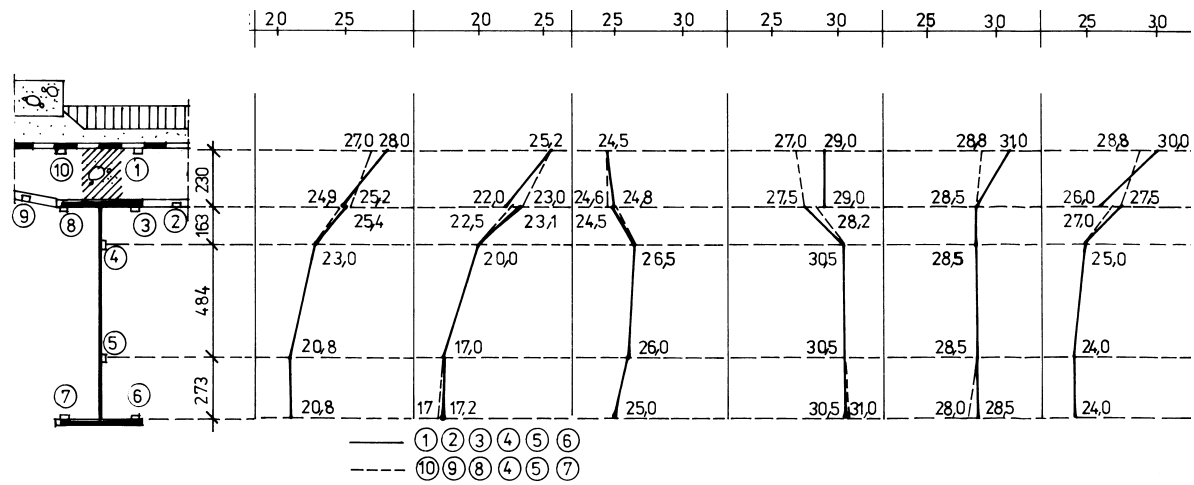


*Fig. 30. Temperature distribution across the mid-span cross-section of the Praha-Brandys composite bridge in summer 1981. The measures are in millimetres and temperatures in Celsius.*

| DAY | 11.8.1981 | | | | | |
|---|---|---|---|---|---|---|
| HOUR | 1:00 | 7:00 | 10:00 | 14:00 | 18:00 | 23:00 |
| OUTER TEMP. °C | 20,0 | 15,0 | 20,5 | 28,5 | 30,0 | 20,5 |
| INNER TEMP. °C | 21,0 | 15,0 | 20,2 | 26,5 | 29,5 | 22,5 |

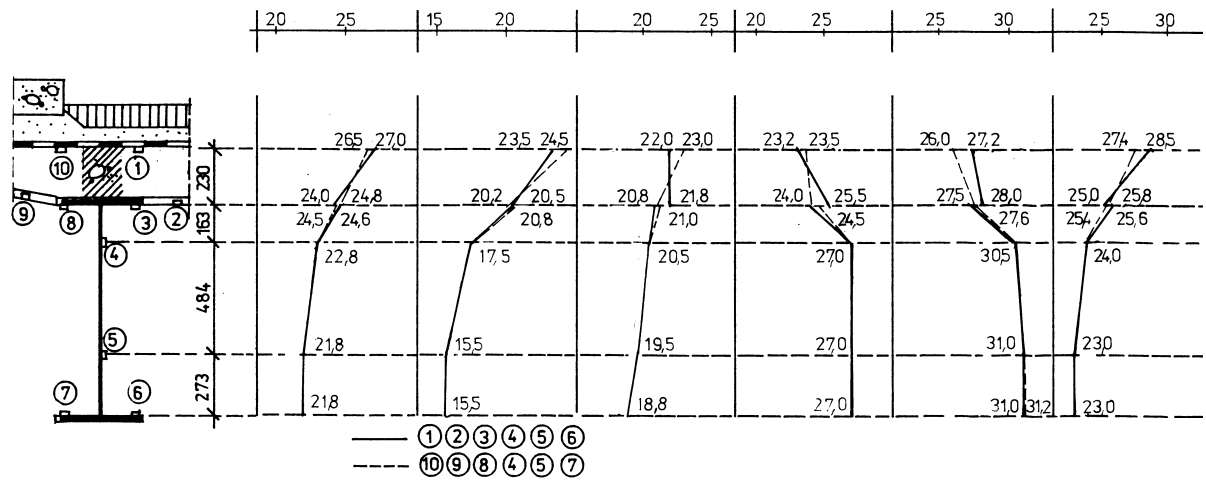


*Fig. 31. Temperature distribution across the mid-span cross-section of the Praha-Brandys composite bridge in summer 1981. The measures are in millimetres and temperatures in Celsius.*

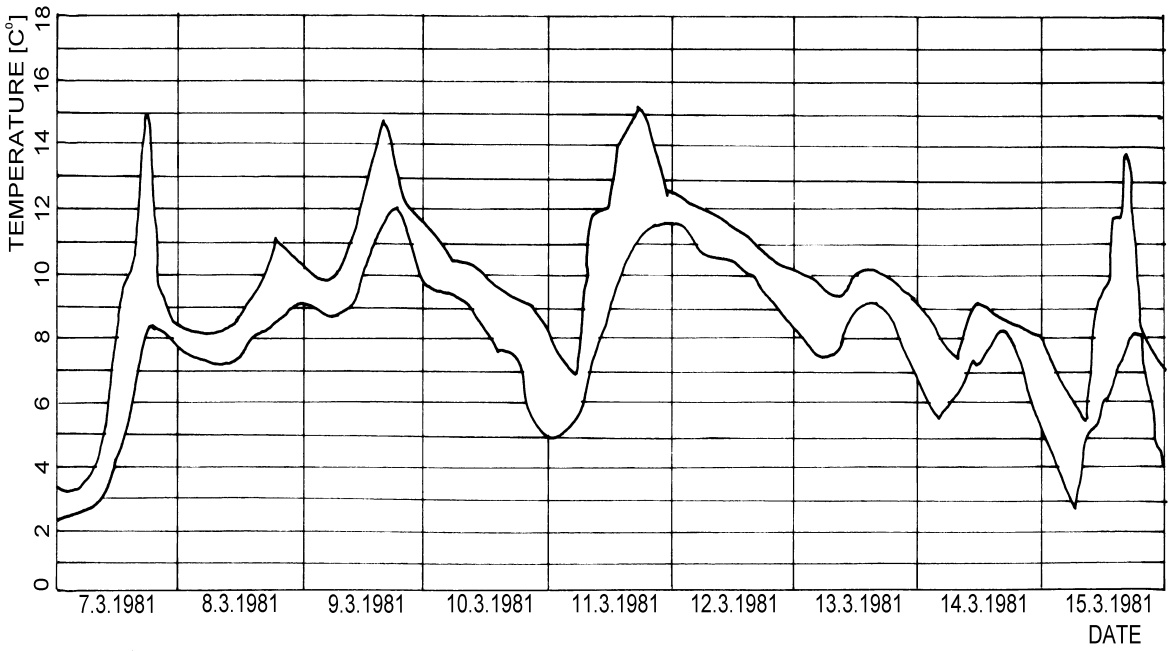


*Fig. 32. Typical maximal and minimal temperature distribution in March 1981 on the Praha-Brandys composite bridge in the Czech Republic.*

# 4 EXPERIMENTAL INVESTIGATIONS OF STEEL-CONCRETE COMPOSITE GIRDERS

## 4.1 Antecedents of the present author's investigations on steel-concrete composite girders

Research work on the vibro-creep phenomenon (i.e. long-term deformation caused by vehicle load) of steel-concrete composite structures was carried out in 1977 at the Department of Structural Engineering (formerly Department of Steel and Reinforced Concrete Structures) of Budapest University of Technology and Economics (formerly Technical University of Budapest). Five beam-type steel-concrete composite girder specimens with span 1500 mm were tested (Table 2). The girders and test arrangement are shown in Fig. 33.

*Table 2. Dimensions and ultimate loads of the steel-concrete composite girders tested by DAO [25].*

| Speci-men | Span L [mm] | Steel beam | Slab dimensions [mm] | | Angle connector | Connector spacing [mm] | Static ultimate load [kN] |
|---|---|---|---|---|---|---|---|
| | | | Width | Height | | | |
| P1 | 1500 | Welded I beam | 300 | 80 | L 40x40x4 | 100 | - |
| P2-1 | | Hot-rolled I 160 beam | 250 | 85 | L 40x40x4 | 125 | 296 |
| P2-2 | | | 250 | 85 | L 40x40x4 | 125 | 312 |
| P3-1 | | | 250 | 80 | L 40x40x4 | 125 | 245 |
| P3-2 | | | 250 | 80 | L 40x40x4 | 125 | 250 |

The material of the employed steel belonged to steel grade 37 (ultimate tensile strength 370 $N/mm^2$) and the grade of concrete was C20. Pretests were conducted with the first specimen to check the proper connector type and the longitudinal spacing of the connectors. First the specimens were subjected to repeated loading and then loaded statically up to failure. Finally – using these experimental results [25] – a method for considering the vibro-creep phenomenon of composite structures was developed.

## 4.2 Experiments conducted by the author

The author carried out similar tests as described in Section 4.1 because of two reasons (Fig. 33). Firstly, in civil engineering generally limited number of test results are available for experiments opposed to other fields of engineering, especially to mechanical and aviation engineering, and secondly, in this way comparison of the results of DAO [25] and the author was possible.

The main purpose of the tests carried out by the author was to investigate steel-concrete composite girders subjected to temperature difference. These girders were investigated for various types of connectors.

The testing procedure and the test arrangements of the experimental investigations conducted by the present author in the early 1990's are summarized below. Later on they were evaluated by numerical methods based on finite element models that were calibrated so that they fit to the test results. So a more comprehensive overview of the whole problem field was obtained. As a consequence, a uniform system was created to introduce the conducted experiments. Altogether two series of tests were carried out. In the first test series three specimens,

Specimens S1, S2 and S3, were tested. The second test series consisted of two specimens, Specimens S4 and S5. Details on these tests and specimens are given bellow.

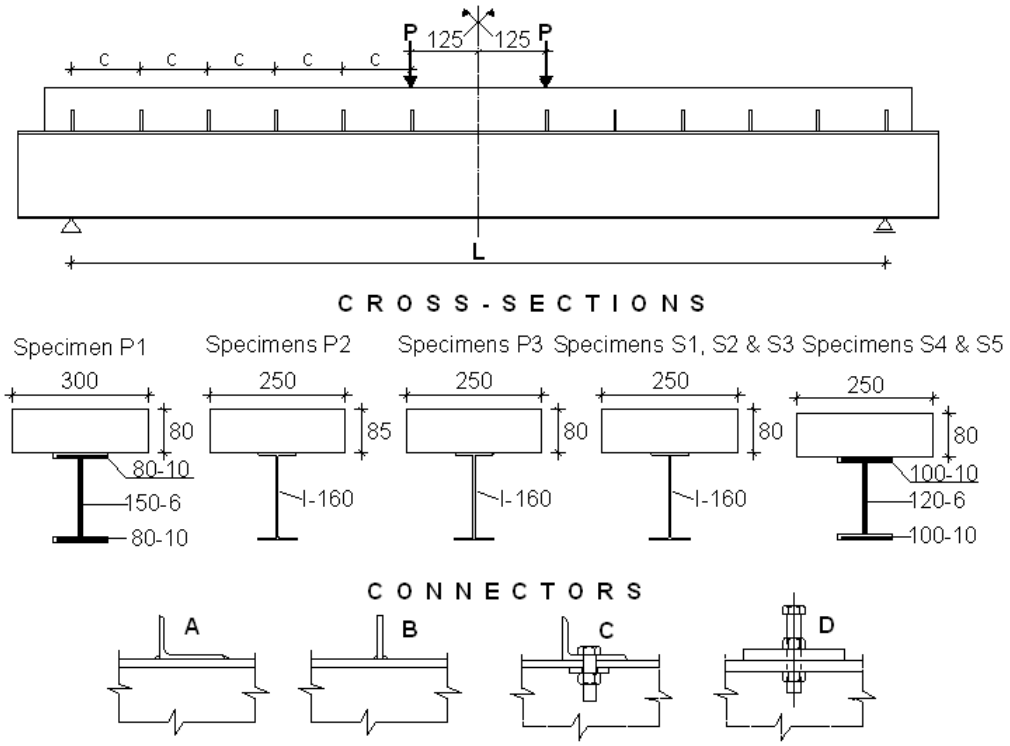


*Fig. 33. Main dimensions and load arrangements of the investigated steel-concrete composite girders. Measures in millimetres.*

For the first test series (Table 3, Fig. 34, Fig. 35 and Fig. 36) three composite girders with 1500 mm span consisting of I 160 steel beams and 250 mm wide and 80 mm deep reinforced concrete slabs were manufactured. Angle connectors of size L 40x60x6 $mm^3$ at a longitudinal spacing of 125 mm were used in the first and third specimens. In the second specimen flat steel 40x6 $mm^2$ connectors were employed.

*Table 3. Investigations on steel-concrete girders conducted by the present author.*

| Test se-ries | Speci-men num-ber | Ref. num-ber. Year | Span L [mm] | Steel beam type | Connector Type | Con-nector spacing [mm] | Gravi-ty loading | Tem-pera-ture loading | Static ultima-te load [kN] |
|---|---|---|---|---|---|---|---|---|---|
| 1 | S1 | [105], [106] 1990 | 1500 | Hot-rolled | Angle L 40x60x5 $mm^3$ | 125 | Two patch loads | Direct (heating the steel beam) | 256 |
| | S2 | | 1500 | Hot-rolled | Steel plate 40x60x6 $mm^3$ | 125 | | | 264 |
| | S3 | [105], [106] 1991 | 1500 | Hot-rolled | Angle L 40x60x5 $mm^3$ and HSFG bolt M16-8.8 | 125 | | | 209 |
| 2 | S4 | [93], [107] 1992 | 2000 | Welded | HSFG bolt M16-8.8 | 130 | | Indirect (pre-stressing the steel beam) | Not mea-sured |
| | S5 | | 2000 | Welded | HSFG bolt M16-8.8 | 130 | | | 187 |

The grade of steel was S 235 (according to the present Eurocode 3 [34]). In the third composite girder the angle connectors were not welded on the upper flange of the I 160 beam, but fixed to it by means of M16-10.9 high-strength friction grip bolts (with pretension force of 100 kN), nuts and special washers, so that the hardening process of concrete slab could occur freely. Thus the free shrinkage of the concrete slab caused no stresses in the steel beam.

In the second test series (Table 3, Fig. 37) two 2200 mm long composite girder specimens were fabricated in order to investigate the influence of temperature difference by a simulation process. In this series the steel beams were made of welded members with steel grade S235. The slab of the girders was a precast concrete element of size 250 x 80 $mm^2$. In the both specimens the connectors were 80 mm long full threaded HSFG M16 bolts with grade 8.8 at a spacing of 130 mm. These bolts had dual role. On the one hand they functioned as headed shear-connector studs, on the other hand they ensured the composite behaviour of the specimen connecting the concrete slab to the prestressed steel beam. The 50 mm headed part of the bolt (Fig. 37) served as a shear connector (Fig. 33), while the top nut, the steel plate element of size 80x100x6 $mm^3$, the top flange of the welded steel beam and the bottom nut composed the friction grip connection part. Both the steel plate and the top flange of the beam were sand-blasted elements. The bolt hole diameters in the top flange were 19 mm. This way a slight relative displacement (approximately 1,0-1,5 mm) between the concrete slab and steel beam, necessary for prestressing the latter member, was provided.

The composition of concrete used for the first and second test series is shown in Table 4.

*Table 4. Composition of concrete used in the first and second test series girders.*

| Material | | ρ [$kg/m^3$] | Material content | |
|---|---|---|---|---|
| | | | $m_{rel}$ [%] | $m_{abs}$ [$kg/m^3$] |
| 350 Portland cement | | 3100 | 10,8 | 335 |
| Sand-gravel | 0,1-5 mm | 2620 | 42,8 | 1122 |
| | 4 – 8 mm | | 14,3 | 374 |
| | 8 – 16 mm | | 14,3 | 374 |
| Water | | 1000 | 17,5 | 175 |
| Air | | 0 | 0,3 | - |
| Total | | - | 100 | 2380 |

The strength of concrete was determined from test data obtained from six 150 mm cube tests and six cylinder tests (150 mm diameter, 300 mm height). All test samples were made at the same time and under the same conditions as the test specimens. Out of the above mentioned test data the grade of concrete was C25. For the purpose of numerical analysis the initial modulus of elasticity was also measured (Table 5).

*Table 5. Initial modulae of elasticity of concrete used in the first and second test series girders.*

| Series No. | $E_c$ [$N/mm^2$] |
|---|---|
| 1 | 31920 |
| 2 | 29550 |

At each connector 6 mm stirrups were used. For a simplified formwork assembly every composite girder was placed on the floor in upside-down position during the concrete casting process. The dimensions, loading arrangements, measuring points and instrumentation of the test girders are shown in Fig. 34, Fig. 35, and Fig. 36, respectively.

Parallel to the composite girder manufacturing, push-out specimens (Fig. 38) for checking the load bearing capacity of the individual connectors were fabricated using materials of the same grade as in the test specimens.

The program of the first test series was divided into four stages. In the first stage of the first test series, one day after starting concrete casting, deformations – caused by concrete shrinkage – were measured using a mechanical Pfender Strain gauge instrument. The size of the Pfender balls was 1/16 inch and their base distance was 100 mm.

In the second stage of the experiment (first test series), Specimen S1 was tested under long-term effective concentrated load of 20 kN applied at mid-span, when the concrete age was between 14 and 28 days.

In the third stage of the experimental program of the first test series – which formed the main portion of first test series – the three composite girders were subjected to temperature difference, then later on a combination of temperature difference and long-term effective load. In this program the heating of the specimen was provided by four plate heaters of 600 Watts each, which were fixed on the lower flange of the beam. In this process it took approximately one hour to raise the temperature of the lower flange of the steel beam to the appropriate level to obtain uniform temperature throughout the composite girder and to reach the planned temperature difference at the beam-slab interface during cooling-down.

In the fourth stage of the experimental program of the first test series, the three specimens were statically loaded to failure. The statical load was provided by LUCAS hydraulic jack of 500 kN capacity, acting at the mid-span. The load was distributed into two patch loads by thick steel plates of 250 mm spacing.

The following parameters were measured in the framework of the first test series:

- Temperature by 25 nickel-to-chrome-nickel thermocouple in case of Specimens S1 and S2 and by touching sensor-tipped thermometer type GANZ 1 PT-385.
- Slip values between reinforced concrete slab and steel beam by inductive transducers of measuring length of 10 mm (control measurements were simultaneously taken by Pfender instrument).
- Elongation at mid-span and deflection of the beam. Japanese (KYOWA) strain gauges and inductive transducers having measuring length of 50 mm were used.
- Load was supplied by a 500 kN (LUCAS) hydraulic jack.

In case of Specimen S3 the tightening force of the high-strength M16-10.9 bolts was applied by a calibrated torque wrench. The specified value of pretension force was 100 kN. Readings of measurement data were electronically taken and recorded by DATCON data-logging system governed by a computer. The system developed at Budapest University of Technology and Economics [63] consisted of 300 data logging channels and graphic mode. For example, in case of Specimen S3 only, 25 logging channels were required, out of which 17 pieces for strain gauges, 7 pieces for monitoring slip and deflection, and the rest for monitoring pressure in the hydraulic jack.

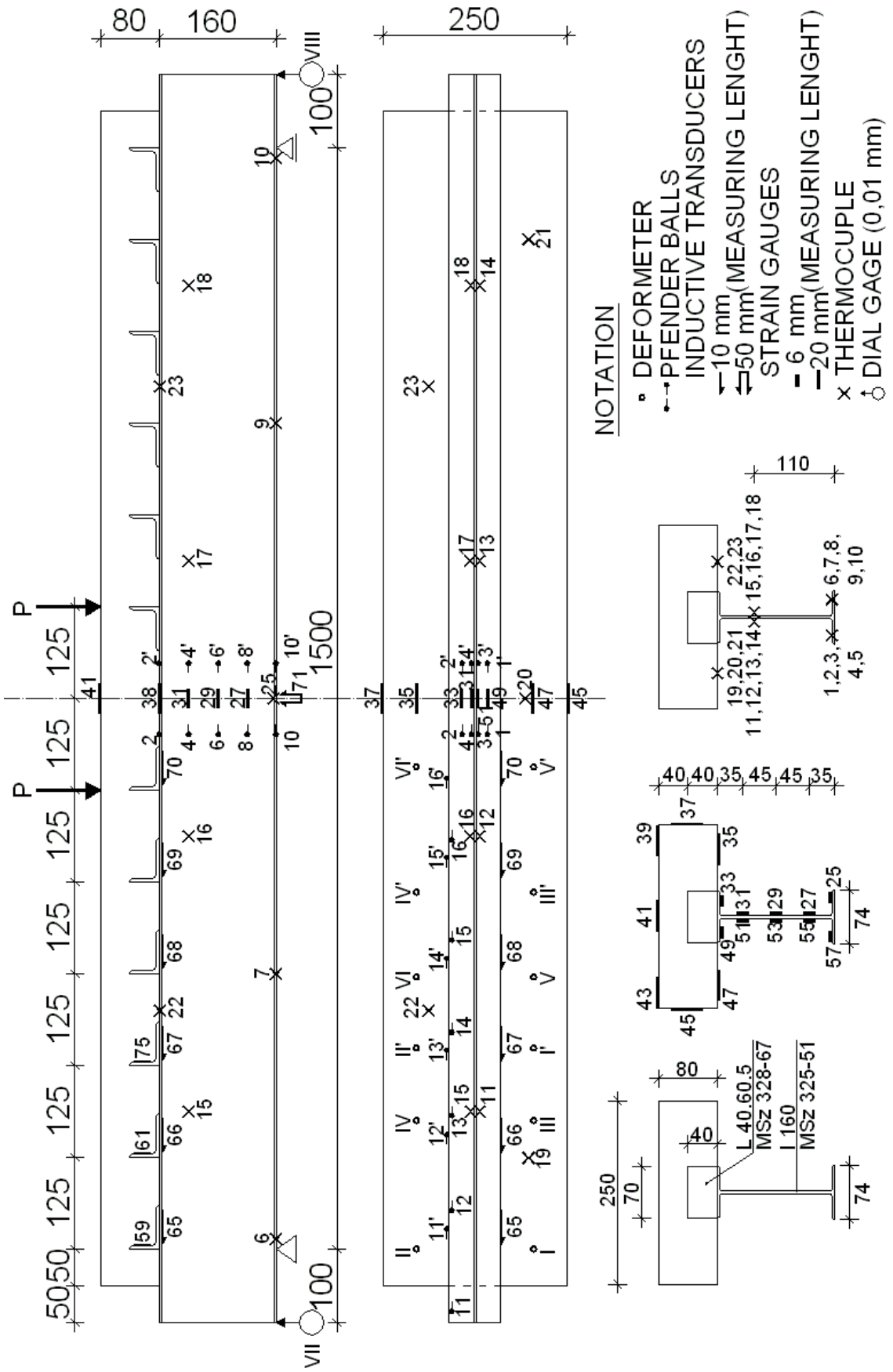


*Fig. 34. The dimensions, measuring points and instrumentation of Specimen S1. Measures in millimetres.*

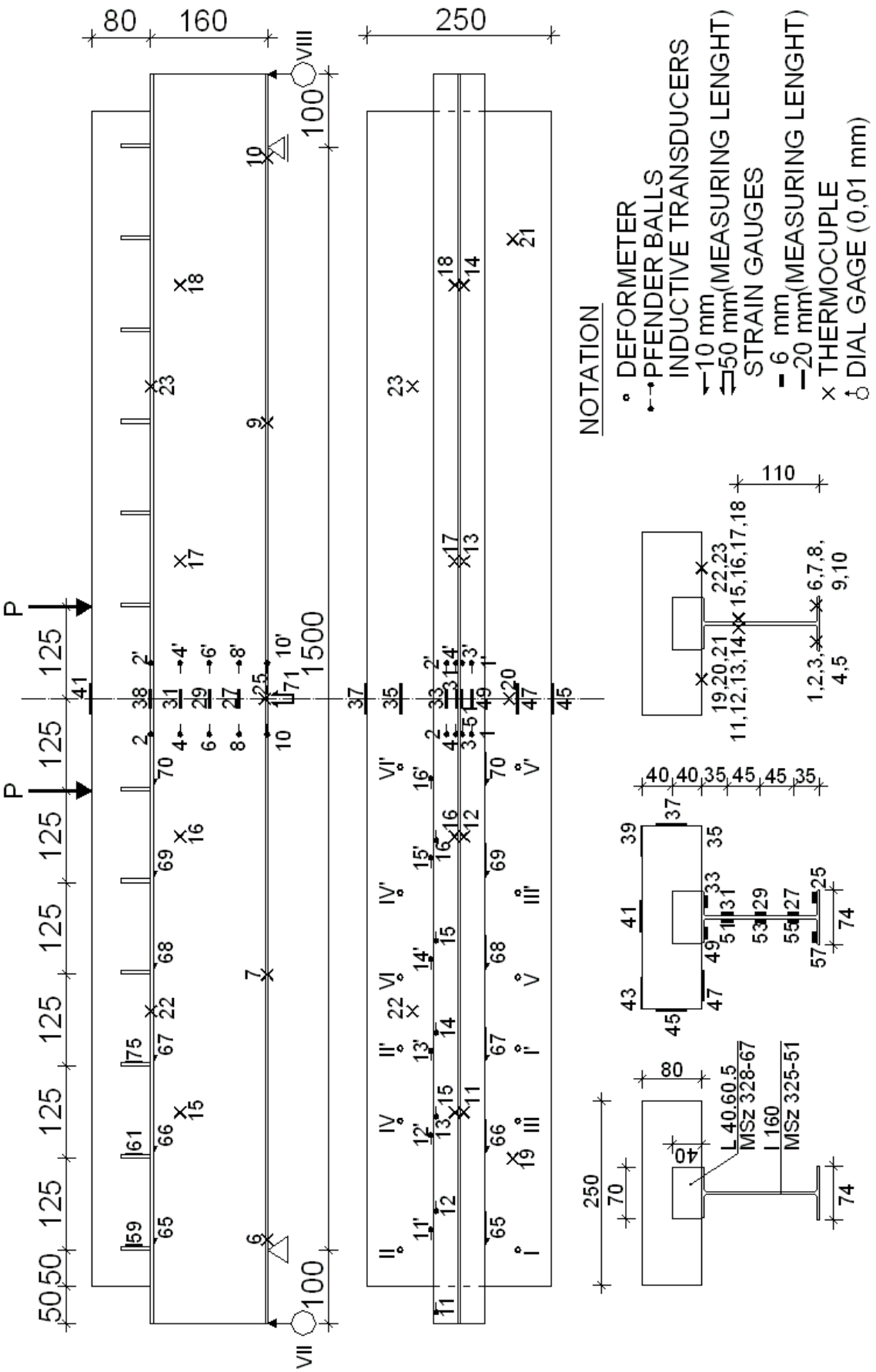


*Fig. 35. The dimensions, measuring points and instrumentation of Specimen S2. Measures in millimetres.*

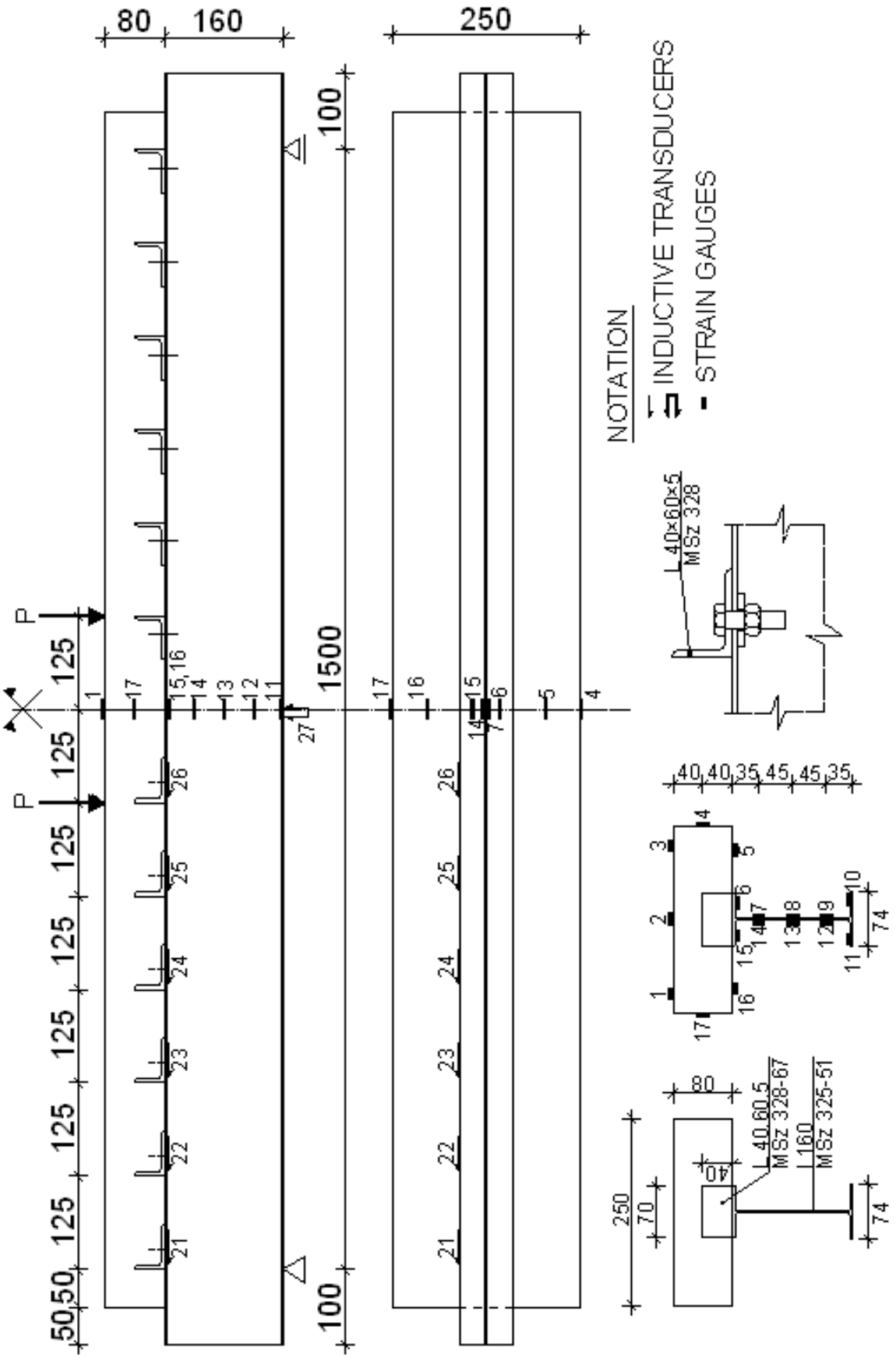


*Fig. 36. The dimensions, measuring points and instrumentation of Specimen S3. Measures in millimetres.*

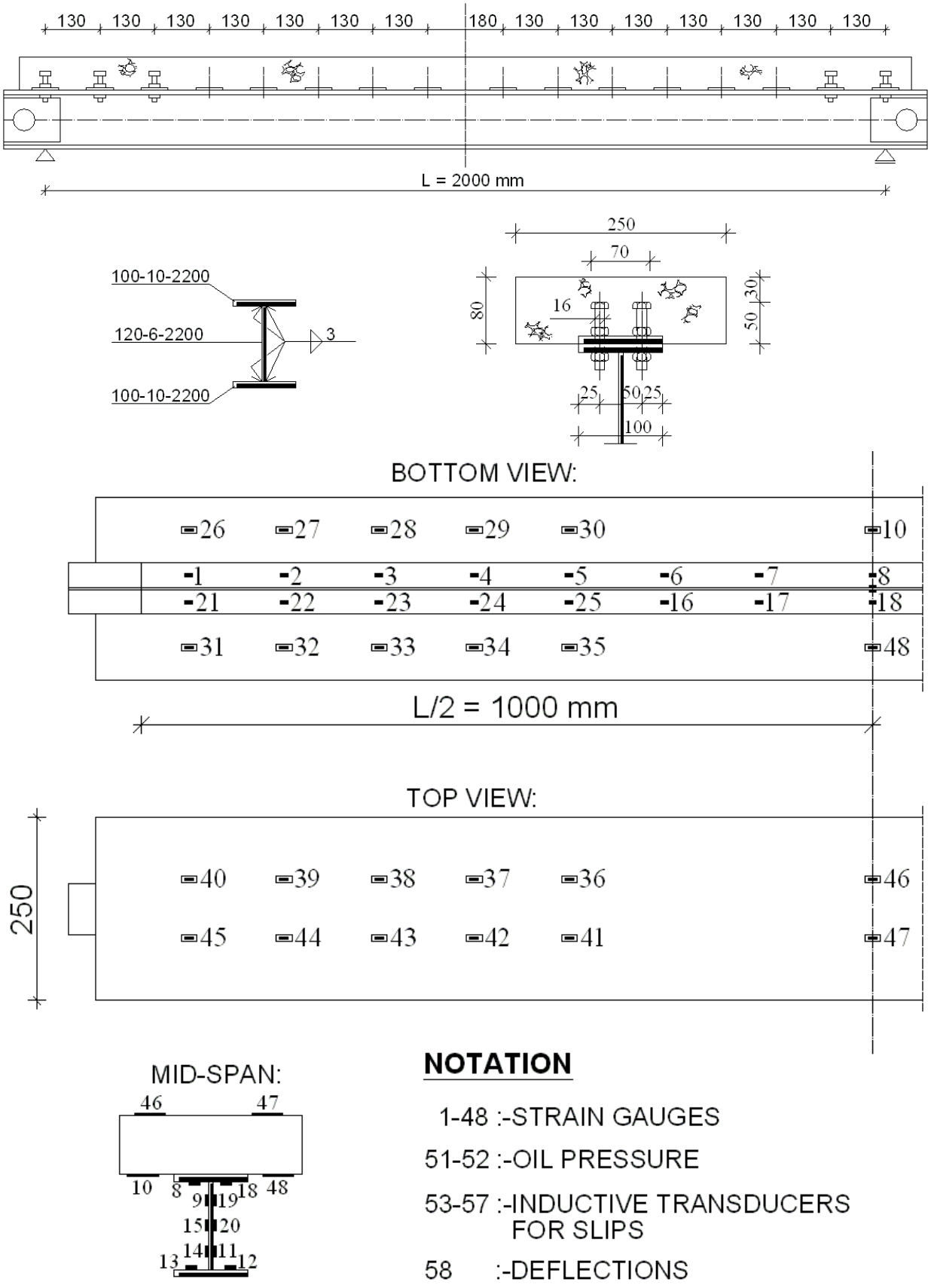


*Fig. 37. The dimensions, measuring points and instrumentation of Specimens S4 and S5. Measures in millimetres.*

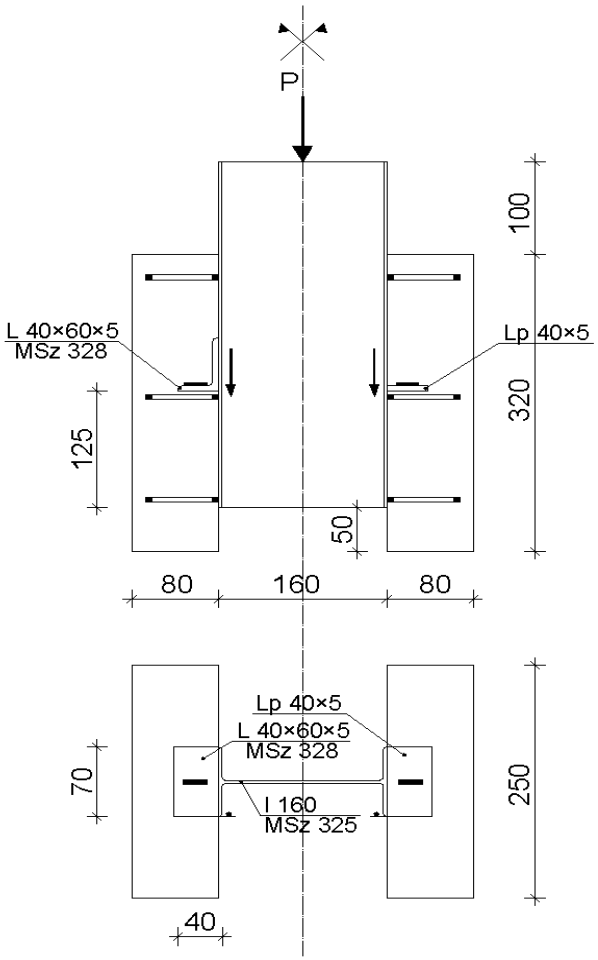


*Fig. 38. Push-out tests of Specimens S1 and S2, respectively. Measures in millimetres.*

The program of the second test series was divided into two stages (Table 3, Fig. 37). In the first stage Specimens S4 and S5 were subjected to simulated temperature difference, when the composite girders were in upside-down position, i.e. the concrete slab was at the bottom and the steel member at the top so that the connectors (bolts) could be easily and correctly tightened. The axial prestressing of the steel beam (simulating temperature difference) was carried out using a hydraulic jack. Tensile forces 287 kN and 278 kN were applied to the steel beams of Specimens S4 and S5, respectively, causing longitudinal normal stresses of 106 N/mm$^2$ and 102 N/mm$^2$ in the steel beams of respective girders. Prestressing was ensured by bolt-tightening (the specified value of pretension force was 100 kN) and then removal of the hydraulic jack. Using strain-gauges the normal stress distribution on the whole cross-section (concrete and steel) was measured only at the mid-span of the composite girder, in other cross-sections only the top flange stresses of the steel beam were checked. Nevertheless, in the support region the stress-state was evaluated by photoelastic stress analysis. During this test the surface of the web was covered by a 120 mm x 400 mm photoelastic layer, which was bonded on reflecting paint. A video camera recorded, double-refracted and analysed the lights for assessing the principal normal and shear stresses along the web part (Figs. 39 and 40).

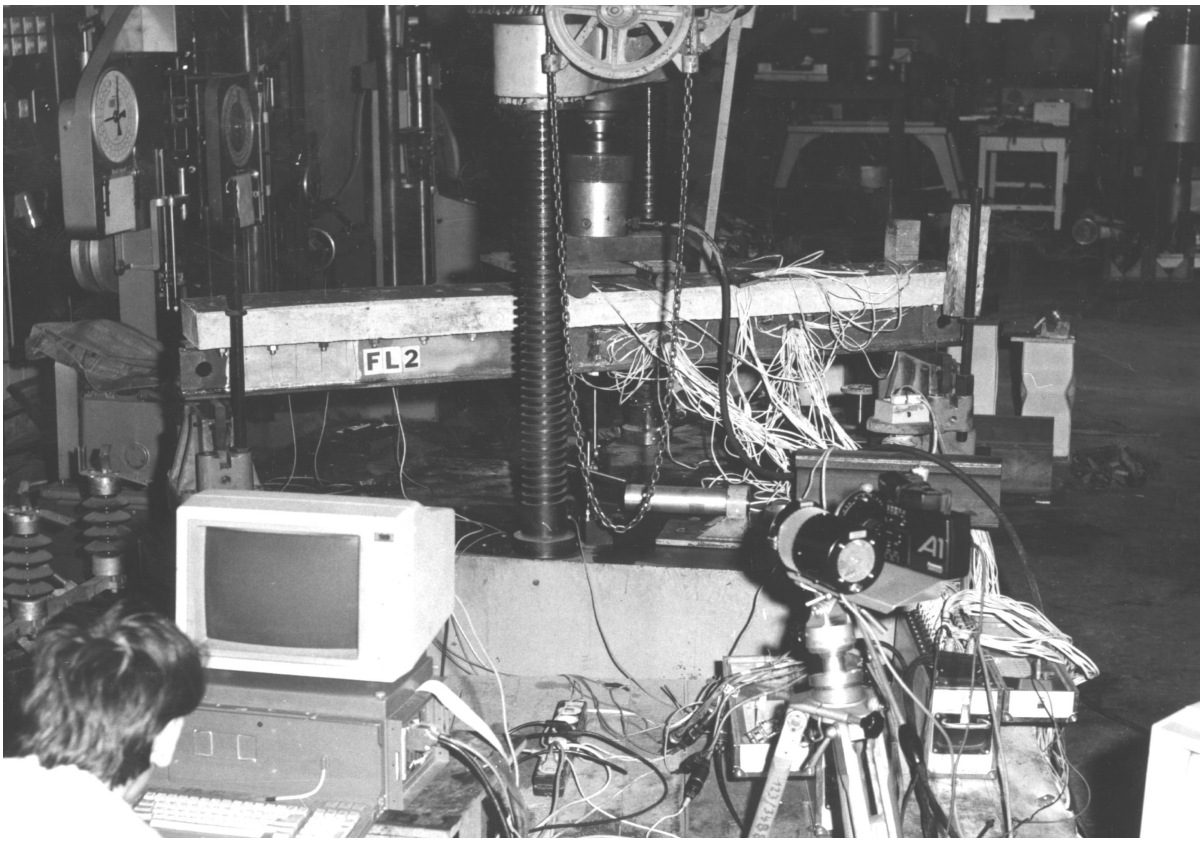


*Fig. 39. Test arrangement of the second experimental series.*

In the second stage of the second test series, after simulation of temperature difference, the beams were also examined in their normal position (concrete plate at the top) by applying two concentrated forces symmetrically to the mid-span and with a spacing of 250 mm.

*Fig. 40. Photoelastic layer in the support region. Specimen S5.*

During the second stage of the second test series, in addition to the increase of the applied load the following parameters were measured:

- Slip between reinforced concrete slab and steel beam using inductive transducers and measuring length of 10 mm.
- Strains at mid-span using Japanese (KYOWA) strain-gauges.
- Deflections of the composite girder using inductive transducers with a measuring length of 50 mm.
- Tightening force of the high-strength M16-8.8 bolts applied by a calibrated torque wrench (the specified value of pretension force was 80 kN).
- Stresses by photoelastic stress analysis in the support region.

The failure of Specimen S4 can be seen in Fig. 41.

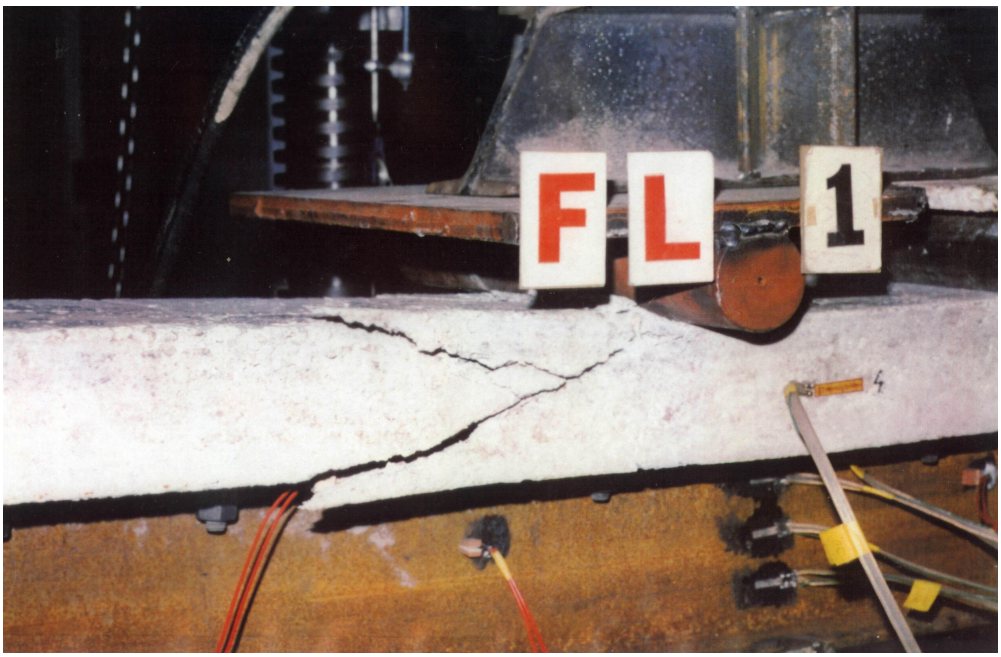


*Fig. 41. Failure of Specimen S4.*

# 5 VERIFICATION OF THE EXPERIMENTAL RESULTS PRESENTED IN SECTION 4.2

## 5.1 Finite element models used in the verification

For verification of the test results described in Chapter 4 two kinds of finite element models, Model 1 (for each specimen) and Model 2 (only for Specimens S4 and S5) are built up. The analysis is carried out using LUSAS software program package developed for civil engineering purposes [42], [108], [109] and [110]. Every model is based on three-dimensional idealisation of the specimens tested. Linear material properties are used so that the behaviour of the structure can be followed and the measured test results compared.

In Model 1, the steel beam and concrete slab are modelled with three-dimensional solid continua (HX8M element) and the connectors by so-called joint (JNT4) elements. These elements contain three linear springs, which model the shear behaviour of the connectors and the restrained uplift between the slab and the beam. Using joint elements the connector stiffness values can be changed providing a possibility to carry out a parametric study. The model and the mesh are shown in Fig. 42.

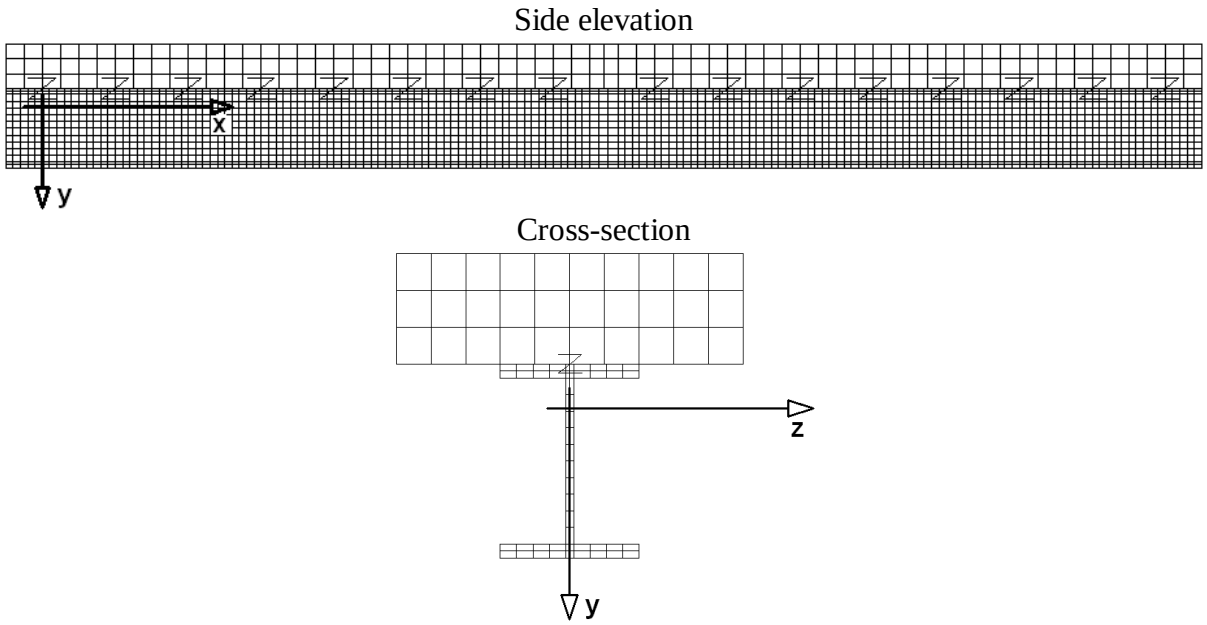


*Fig. 42. Three-dimensional finite element model (Model 1) with solid continua and spring (joint) elements. Letters Z symbolise the joint elements.*

In Model 2, the steel beam, concrete slab and connectors are modelled with three-dimensional solid continua elements. To avoid a large number of nodes only half of the composite cross-section is modelled along the entire span. This is possible, because the displacements perpendicular to the symmetry surface of the beam are restrained. The mesh is built up using three-dimensional solid continua with HX8M and PN6 LUSAS type elements with 8 and 6 nodes, respectively. These solid continua have 3 degrees of freedom at each node (u, v, w). The model and the mesh are shown in Fig. 43. The modelled structure of the reinforced concrete slab is subjected to 40 $^{o}$C temperature loading. Additionally, two patch loads are applied at the top of the composite girder symmetrically to the mid-span (Fig. 33). This modelling method facilitates to examine the entire structure and the connector type D (Fig. 33). The whole model comprised of 34537 nodes and 7796 elements, respectively.

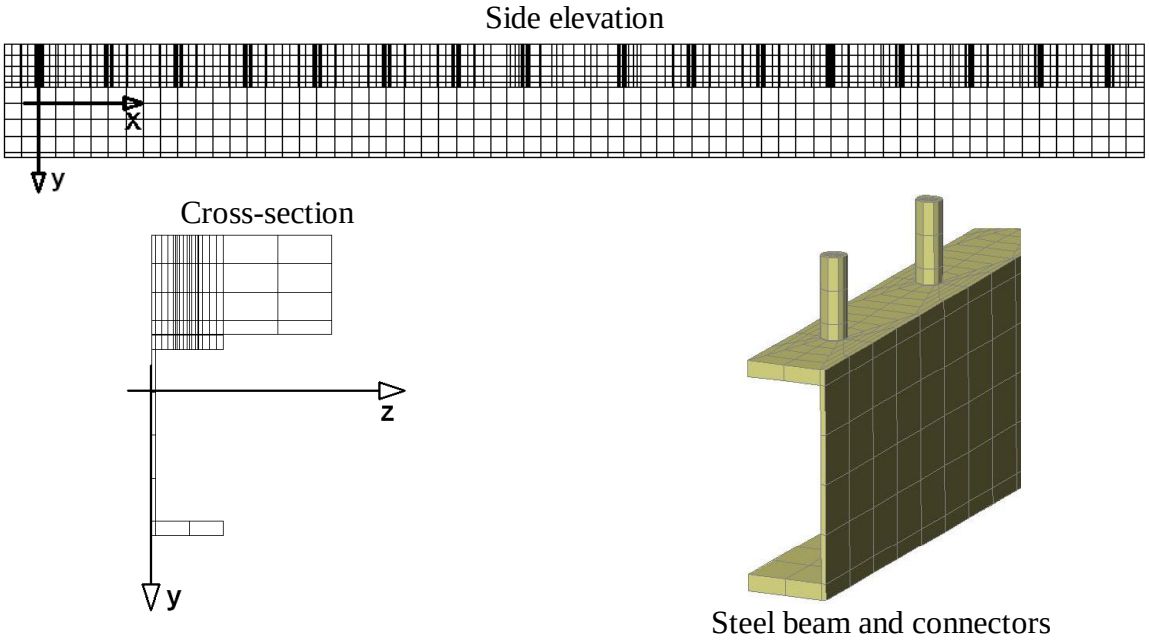


*Fig. 43. Three-dimensional model (Model 2) with three-dimensional elements.*

## 5.2 Results obtained by experimental methods and comparison with other results

### 5.2.1 Longitudinal slip at connectors due to shrinkage as function of time

Fig. 44 shows a comparison of longitudinal slip values at connectors due to shrinkage as function of time in case of Specimen S1. The origin of the co-ordinate system is at the first connector in the vicinity of the support. From these results it can be concluded that on the first and second day the majority of deformations due to shrinkage are completed. The envelope curves of experimental results contain two waves, the maximum slip is 0,018 mm.

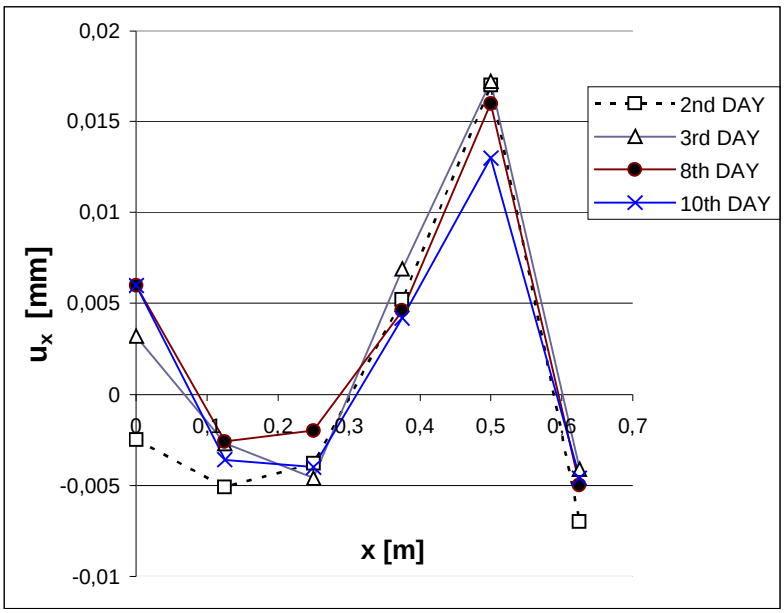


*Fig. 44. Comparison of longitudinal slip values at connectors due to shrinkage as function of time (Specimen S1) according to the experiments. The origin of the co-ordinate system is at the first connector.*

### 5.2.2 Longitudinal slip at connectors due to long-term loading as function of time

Fig. 45 shows a distribution of longitudinal slip values at connectors due to long-term loading as function of time in case of Specimen S1. The applied load was 20 kN at mid-span acting from day 14 of concrete age (this is day 0 on push-out specimens (Fig. 38)) to day 28. The results are demonstrated only for one half of the girder. The origin of the co-ordinate system is at the first connector in the vicinity of the support. The maximum slip is 0,024 mm.

The results of the comprehensive processes can be seen in Fig. 45. When the long-term load is applied, the creep and shrinkage of concrete commences, the concrete starts to strengthen and the bond stresses to develop. However, as a consequence of long-term loading, significant slip values can occur when the bond between beam and slab is interrupted and at the same time friction is developed at the interface.

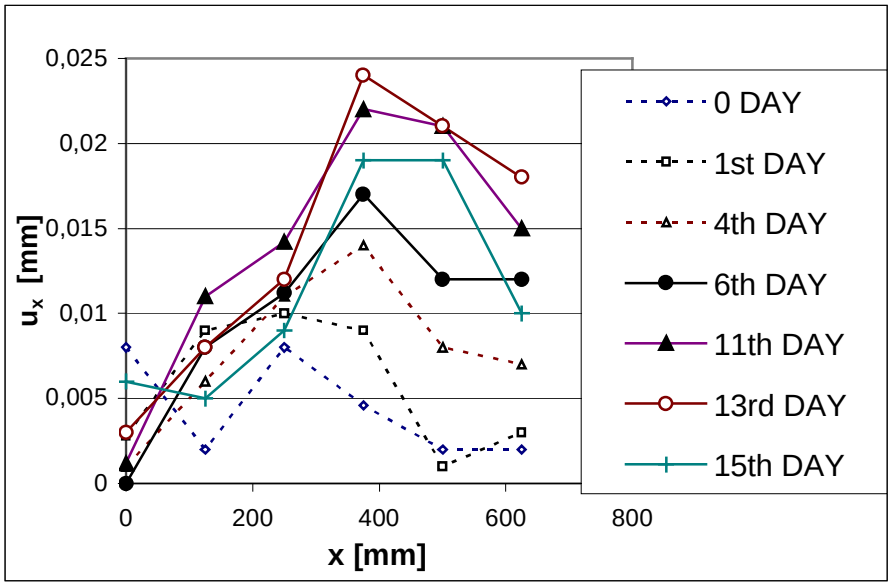


*Fig. 45. Distribution of longitudinal slip (Specimen S1) as function of connector distance x from the first connector (support section) – to mid-span cross-section of the girder. The curves are valid for applied external long-term load of 20 kN acting at mid-span.*

### 5.2.3 Longitudinal slip at connectors due to two-patch loads

The purpose of this section is to determine the connector stiffness values only for Model 1 applied to Specimens S1, S2 and S3 using test results and FEM analysis. It can be done indirectly so that the connector stiffness values in the LUSAS Joint model are varied so far that the best fitting between the calculated and measured slip values are reached.

Fig. 46 shows the distribution of longitudinal slip values at the connectors of Specimen S3 due to two patch loads (Fig. 36). The data are obtained from the tests. The origin of the co-ordinate system is at the first connector in the vicinity of the support. Longitudinal slip values at each connector due to various loads for Specimen S3 are shown. The curves are determined for applied external loads of 49,6, 59,8, 73,4, 96,6, 112,6, 128,6, 139,6, 159,6, 165,4, 175,2, 196,4, 198,8, 202,8, 205,2 and 206 kN, respectively. Here small slip reduction can be seen at the first connector. These results are similar to those presented by BODE and SCHANZENBACH [11] (Fig. 3).

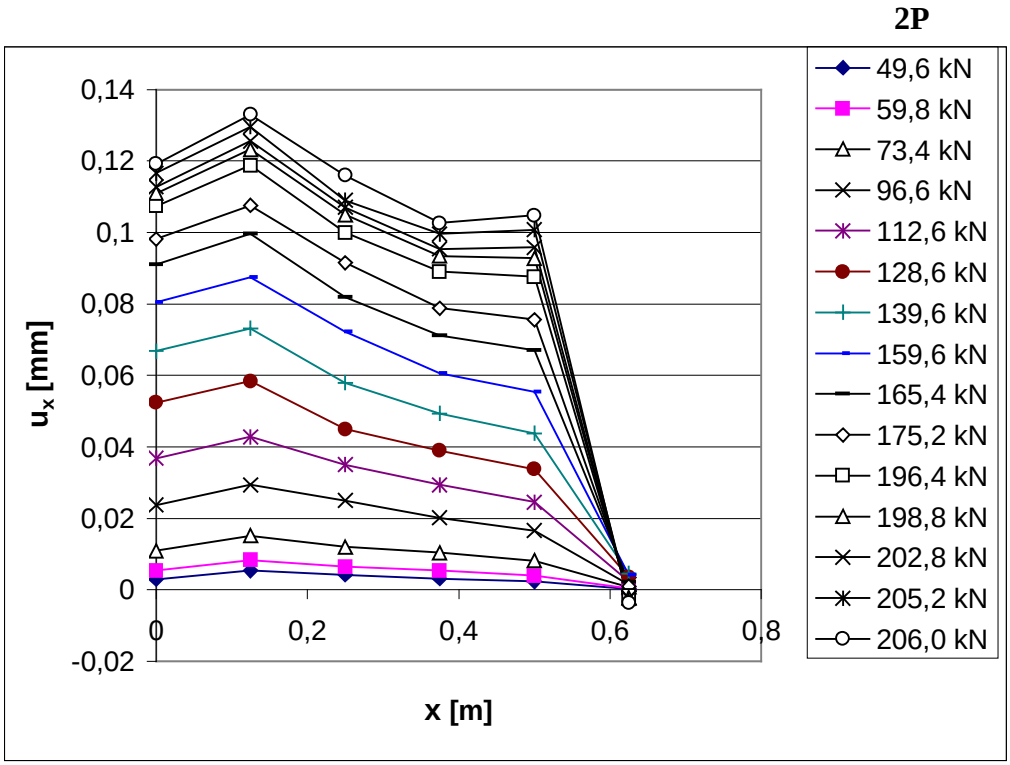


*Fig. 46. Distribution of longitudinal slip (test results of Specimen S3) as function of connector distance x from the first connector (support section) – to mid-span cross-section of the girder. The curves are valid for various applied external loads (2P).*

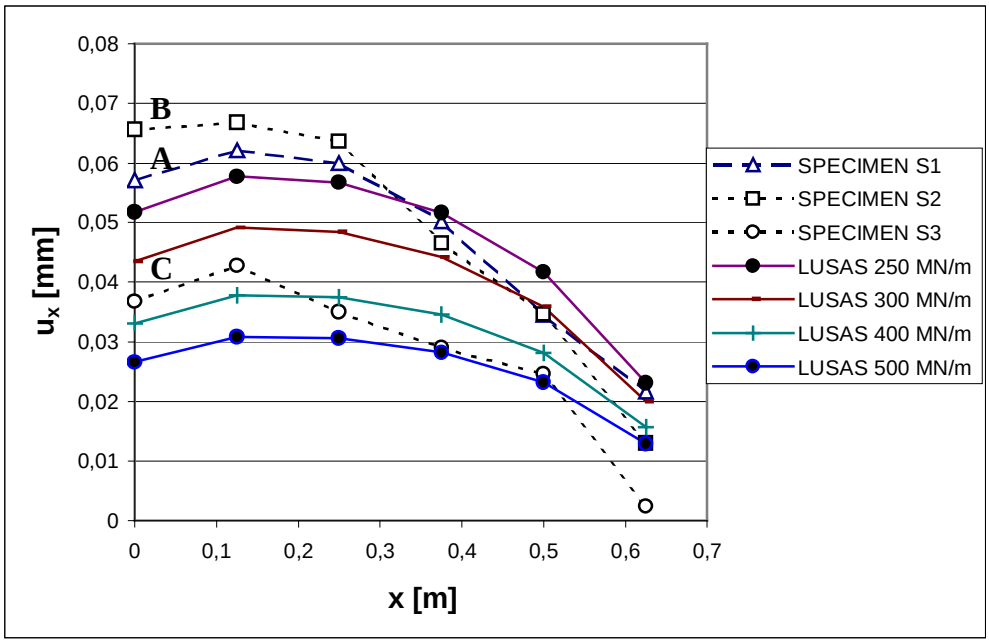


*Fig. 47. Measured and calculated slip at different connectors in Specimens S1, S2 and S3, spring stiffness $k_y$ = 250, 300, 400, 500 MN/m. Distances x measured from the support (first connector).*

Fig. 47 demonstrates that the slip values due to concentrated load of 100 kN are equivalent to a stiffness range of $k_y$ = 250–500 MN/m as calculated in the LUSAS analysis. Here the dashed lines represent the test results obtained, when different connector types, i.e. A, B, and C (Fig. 33), were used.

### 5.2.4 Longitudinal connector forces due to temperature difference

The purpose of this section is to determine the connector stiffness values only for Model 2 applied to Specimens S4 and S5. Connector stiffness values are determined from the test results, in order to calculate the shear flow at the interface of slab and beam. As a function of shear force per unit length the internal forces and stresses can be calculated using the numerical and analytical models of the composite girder.

For test series 2, where temperature difference of 40 $^{o}$C is simulated by prestressing the steel beam, the connector forces can be determined indirectly. This process is outlined below. Stresses measured in the slab of Specimen S4 can be found in Table 5. Similar relationship can be observed for Specimen S5 as well. In Fig. 48 normal forces N(x) due to test and due to the Hawranek-Steinhardt method are depicted.

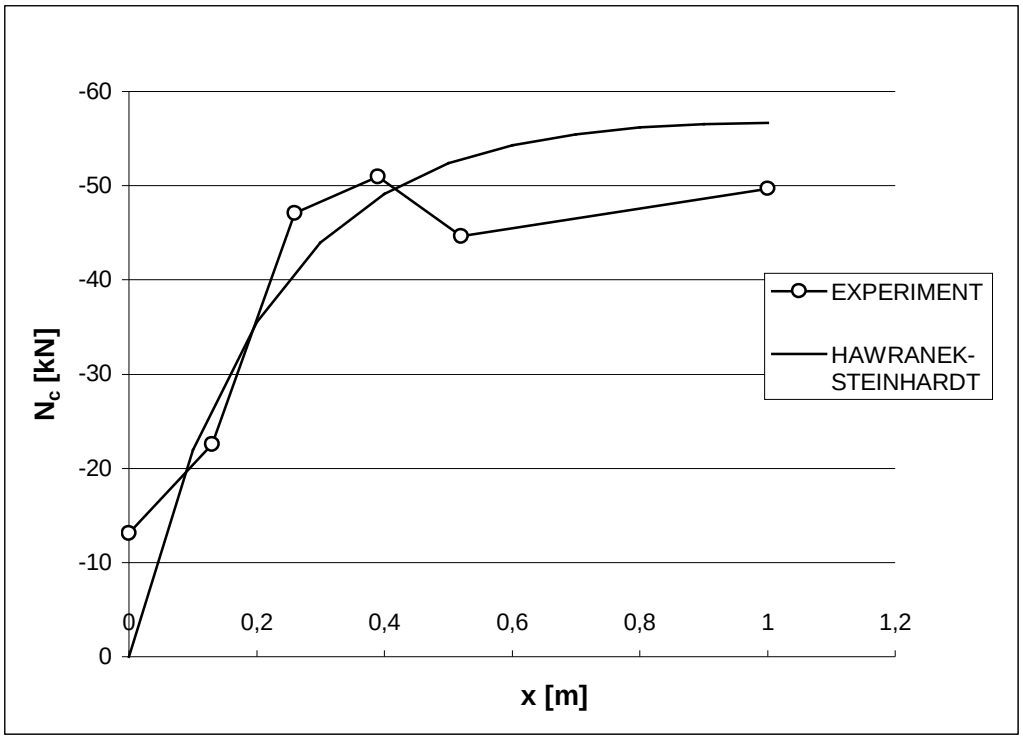


*Fig. 48. Axial (normal) forces $N_c$ in the slab due to temperature difference 40 $^{o}$C and according to the calculation based on the Hawranek-Steinhardt method (Specimen S4).*

In order to calculate the spring constant value, a measured datum is needed. A point of the experimental curve shown on Fig. 48 (depicted using data in Table 5) is selected so that the resulting curve determined by the Hawranek-Steinhardt method would provide the best approximation of the experimental curve. In this point the axial force in the concrete slab at x = 195 mm from the support is $N_c$ = -36 kN. This way the value of 2600 N/mm$^2$ for spring constant of elastic layer could be calculated. Using this value and the notation used previously, the elastic parameter $\omega^2$ gets the value 0,0023 m$^{-2}$.

Using Hawranek-Steinhardt and the Author's Energy methods the normal force *N(x)* and shear force per unit length *T(x)* can be calculated as function of the spring stiffness.

According to Hawranek-Steinhardt method

$$N(x) = N_o \left\{ 1 - \frac{\cosh\left[ w \cdot \left( \frac{l}{2} - x \right) \right]}{\cosh w \frac{l}{2}} \right\} \tag{97}$$

and

$$T(x) = \frac{dN(x)}{dx} = N_o \left\{ \frac{w \cdot \sinh\left[ w \cdot \left( \frac{l}{2} - x \right) \right]}{\cosh w \frac{l}{2}} \right\} \tag{98}$$

where $N_0$ is the axial force obtained with infinitely rigid joint. In this experiment (Specimen S4) the normal force $N_0$ is 57,61 kN for prestressing force is 287 kN.

*Table 5. Normal force $N_c$ on the slab due to temperature difference 40 $^oC$. Arrangement of strain gauges can be seen in Fig. 37. $s_{x,c}$ is the average normal stress in the slab.*

| x [m] | Number of strain gauge | $\sigma_{measured}$ [N/mm$^2$] | $\sigma_{x,c}$ [N/mm$^2$] | $N_c$ [kN] |
|---|---|---|---|---|
| 0 | 26 | -1,54 | [(0,48+0,41)/2+ (-1,54-1,98)/2]/2= -0,658 | $\sigma_{x,c} \cdot A_c$ = -0,658·2·10$^4$·10$^{-3}$= -13,15 |
| | 31 | -1,98 | | |
| | 40 | +0,48 | | |
| | 45 | +0,41 | | |
| 0,13 | 27 | -2,34 | -1,130 | -22,60 |
| | 32 | -4,22 | | |
| | 39 | +1,33 | | |
| | 44 | +0,71 | | |
| 0,26 | 28 | -4,08 | -2,355 | -47,10 |
| | 33 | -6,20 | | |
| | 38 | +0,74 | | |
| | 43 | +0,12 | | |
| 0,39 | 29 | -5,54 | -2,547 | -50,95 |
| | 34 | -5,80 | | |
| | 37 | +0,68 | | |
| | 42 | +0,47 | | |
| 0,52 | 30 | -4,84 | -2,232 | -44,65 |
| | 35 | - | | |
| | 36 | +0,24 | | |
| | 41 | +0,54 | | |
| 1,0 | 10 | -5,38 | -2,485 | -49,7 |
| | 48 | -5,50 | | |
| | 46 | +0,47 | | |
| | 47 | - | | |

With the help of the shear force per unit length shown in Fig.49 the connector forces can be determined by multiplying the shear flow by the connector spacing. Thus the connector forces can be indirectly calculated. (In the experiment uniform spacing was used for the connectors.)

In order to verify the distribution of the shear force per unit length, calculations are carried out using the Author's Energy Method, as well as the LUSAS Joint and LUSAS Solid FEM models presented in Section 5.1. Using the LUSAS Joint model both stresses and forces can be calculated. The LUSAS Solid model ensures calculation of stresses but not forces. Therefore, in order to be able to compare the distribution of shear flow (results calculated using the Hawranek-Steinhardt and the Author's Energy Method in Fig.49) with the shear stresses calculated using LUSAS Solid model (Fig. 50), the LUSAS Joint model needs to be invoked. In both LUSAS Solid and LUSAS Joint model, shear stresses $\tau_{xy}$ were calculated along the girder in the steel beam fibre being infinitely close to the connector.

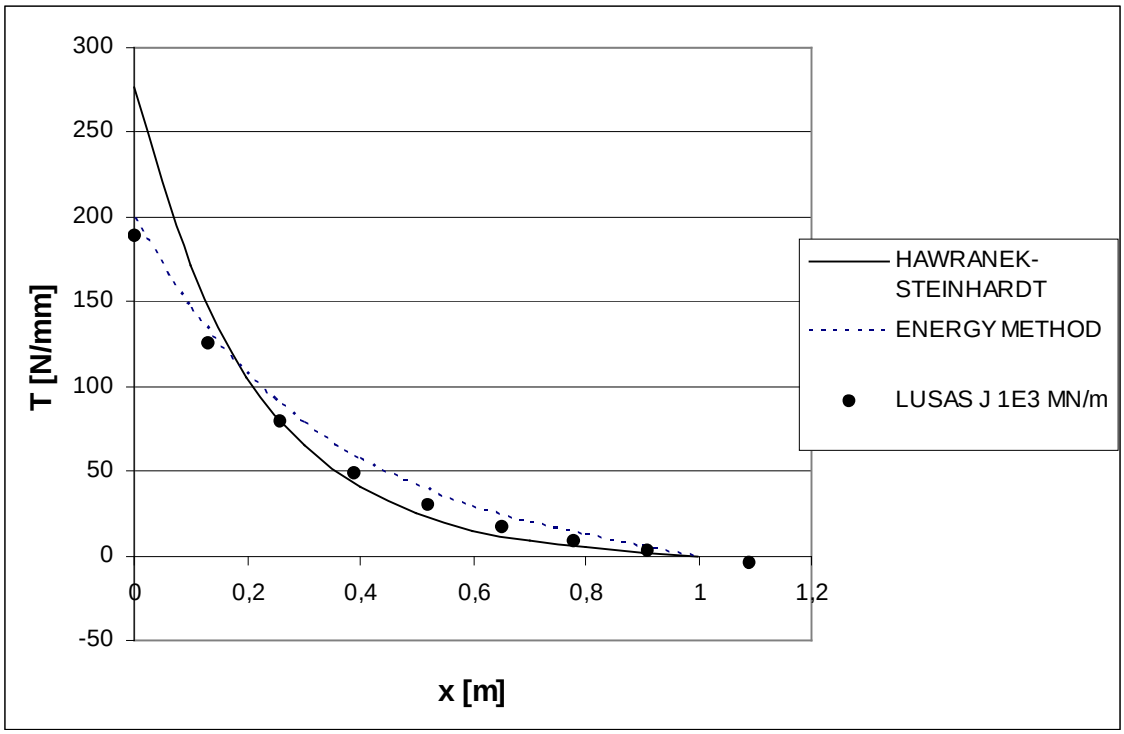


*Fig. 49. Shear forces per unit length T(x) due to a simulated temperature difference of 40 $^{o}$C from test and based on the Hawranek-Steinhardt and the Author's Energy methods along the half girder (Specimen S4).*

The primary conclusion drawn from Figs. 49 and 50 is that the closest results are provided by the Author's Energy Method and the LUSAS Joint model (connector stiffness $k_y$ value is $10^3$ MN/m). The Hawranek-Steinhardt method provides the highest value at the end of the girder, while the stress calculated using the LUSAS Solid model is approximately half of this value. This shows that modelling the temperature difference phenomenon of composite girder by using so-called joint element or elastic layer leads to results that are on the safe side. In comparison with the Hawranek-Steinhardt method, which provides rather high values at the supports, the use of the Author's Energy Method is recommended.

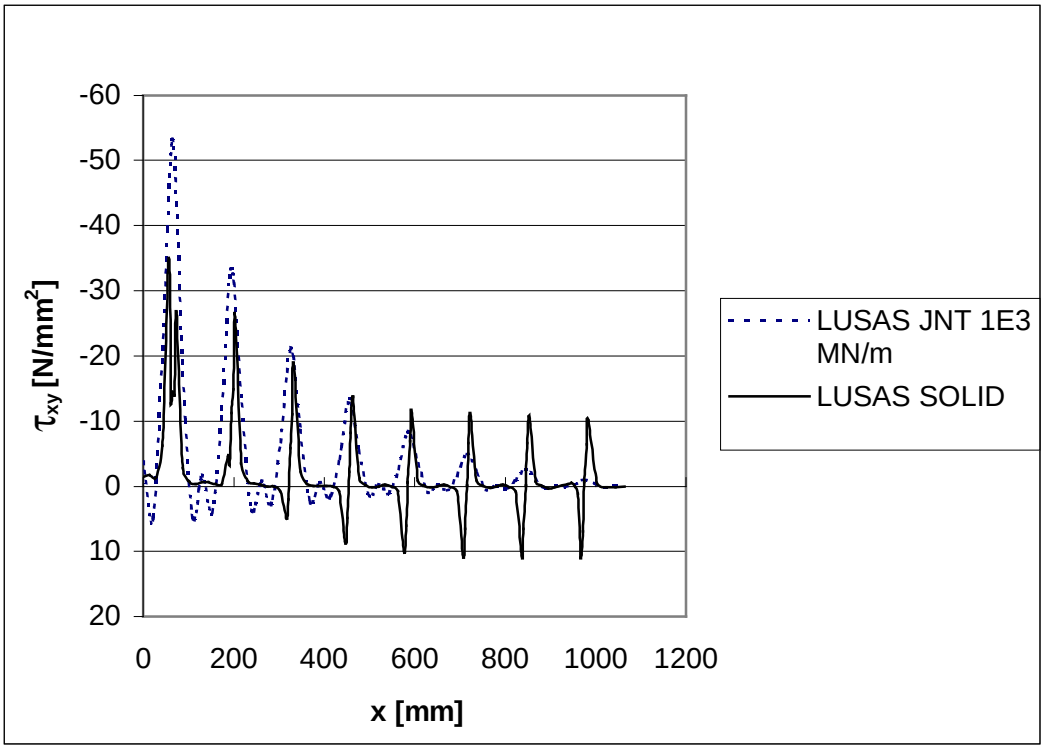


*Fig. 50. Comparison of shear stresses $t_{xy}(x)$ at the connectors due to temperature difference of 40 $^{o}C$ (Specimen S4). The dashed line results are obtained by using LUSAS Joint model and the solid line results by using LUSAS Solid model.*

### 5.2.5 Normal stresses

The purpose of this section is to present the measured normal stresses $s_x$ due to temperature difference of 40 $^{o}$C and two patch loads (Fig. 33). These stresses are then compared to the calculated values, which originate from a finite element analysis and the Author's Energy Method and other methods. In the calculations spring stiffness values presented in Sections 5.2.3 and 5.2.4 are used.

Fig. 51 shows normal stresses $s_x$ at mid-span due to temperature difference as function of the vertical distances $e$ from the lower edge of the beam. These stresses are obtained from numerical analyses and the tests conducted by the author. It can be seen that both the results obtained by LUSAS and the Author's Energy Method are in conformity with the experimental ones.

Fig. 52 shows the distribution of normal stresses $s_x$ at mid-span when Specimen S1 is subjected to 100 kN concentrated load. Fig. 53 shows the corresponding stresses in Specimen S5 when it is loaded with 64 kN and temperature difference of 40 $^{o}$C. The results obtained by LUSAS and the Author's Energy Method are in conformity with the experimental ones.

Fig. 54 shows the calculated (LUSAS Solid and the Author's Energy Method) and measured normal stresses $\sigma_x$ in the lower fibre of the upper steel flange due to combination of simulated temperature difference and concentrated load of 100 kN in case of Specimen S5. The measured results are in accordance with the calculated stresses.

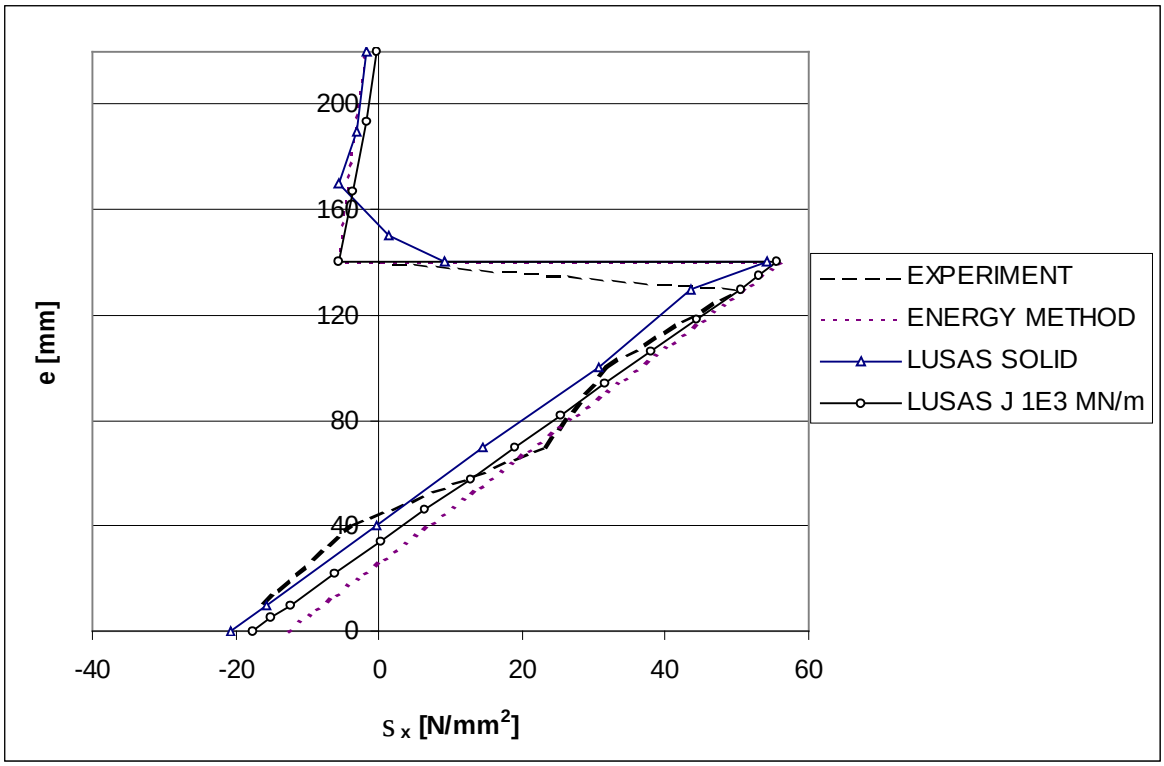


*Fig. 51. Comparison of normal stresses $s_x$ at mid-span at different heights **e** due to temperature difference 40 $^oC$ (Specimen S4).*

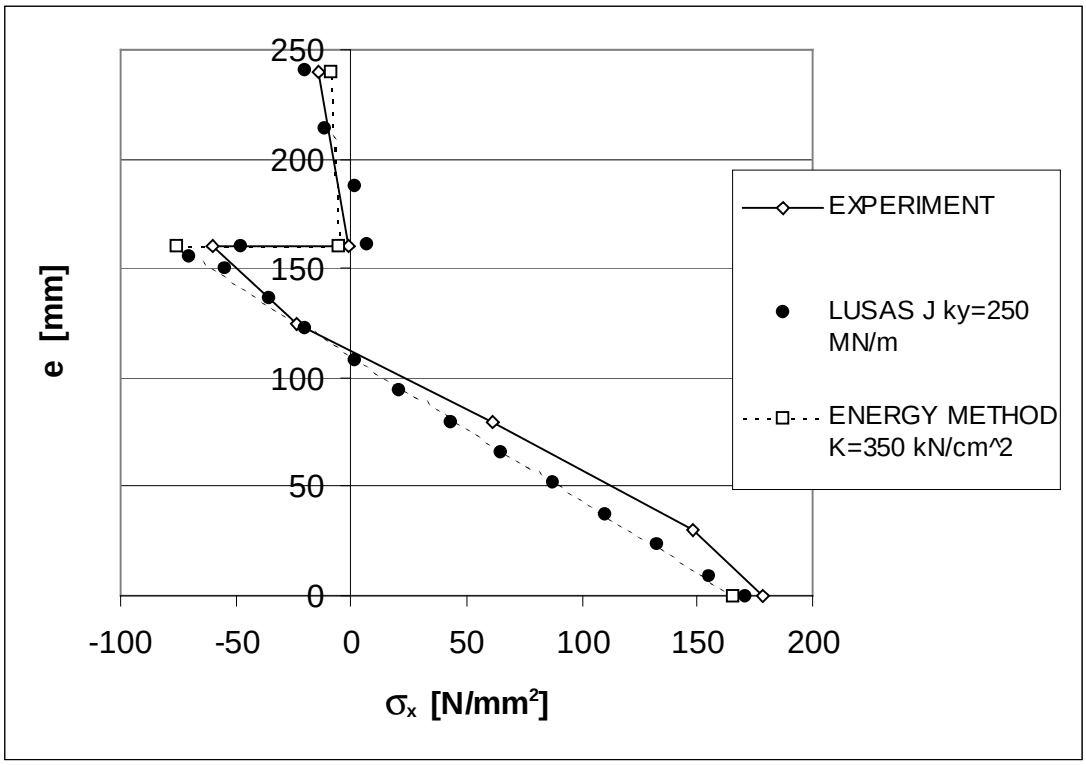


*Fig. 52. Comparison of normal stresses $s_x$ at mid-span at different heights **e** due to 100 kN concentrated load (Specimen S1).*

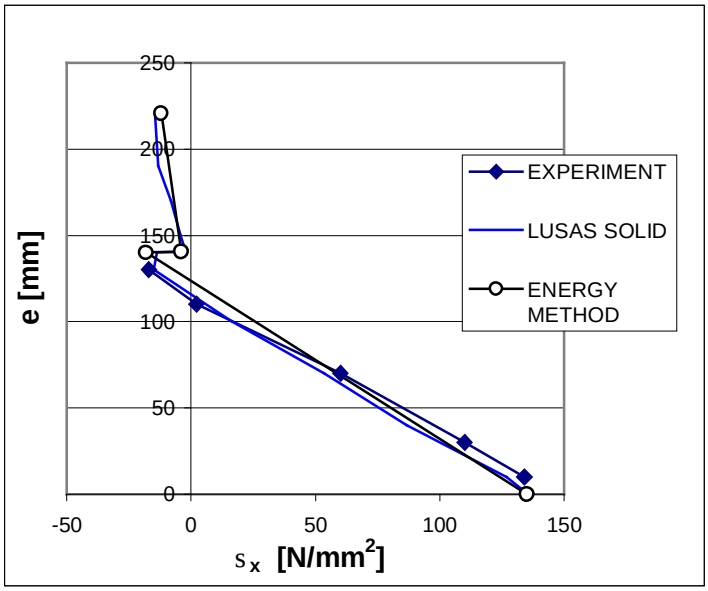


*Fig. 53. Comparison of normal stresses $s_x$ at mid-span at different heights **e** due to combination of temperature difference 40 $^oC$ and concentrated load 64 kN (Specimen S5).*

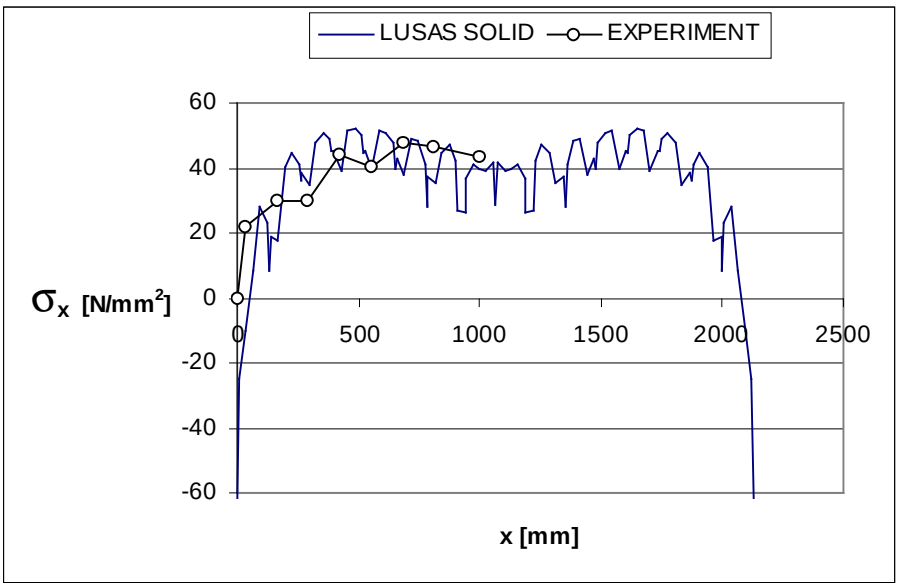


*Fig. 54. Comparison of normal stresses $s_x$ at the lower fibre level of the upper steel flange due to combination of temperature difference 40 $^oC$ and concentrated load 100 kN along the length of Specimen S5.*

### 5.2.6 Deflections

The purpose of this section is to show the influence of connector types presented in Fig. 33 on the mid-span deflection.

Fig. 55 shows the relationship between the vertical deflection and the calculated bending moment at mid-span of 8 different specimens (Tables 2 and 3). Table 6 summarises the main data in connection with Fig. 55. This demonstration method allows the comparison of specimens with different spans, but almost the same bending stiffness. It can be noticed that the ultimate moment *M* is almost the same for all specimens excluding Specimen S3. Unlike

Series Specimens S, the scattering of measured results of the Series P beams is quite small. This is because of practically similar dimensions (Table 2) and same type of connectors. Out of Series Specimens S, Specimens S1 (connector type A), S2 (connector type B) and S5 (connector type D) have almost the same ultimate moment, while Specimen S3 (connector type C) provides a lower value because of the high slipping capability of the connection.

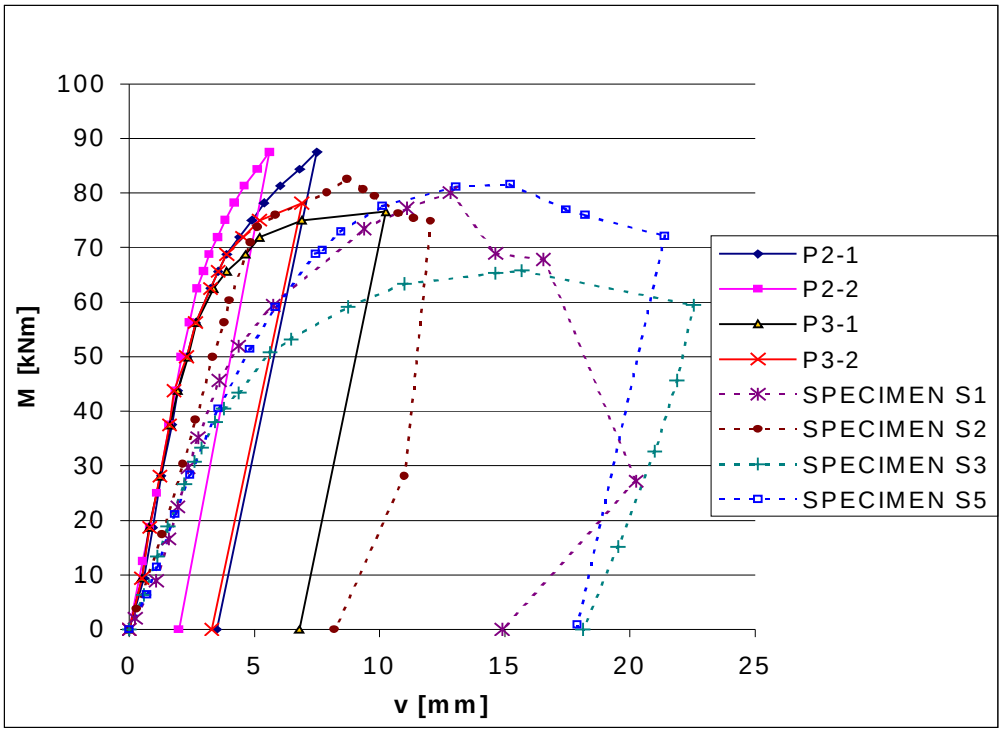


*Fig. 55. Comparison of deflections due to concentrated load at mid-span containing data of DAO [25] (Series P2 and P3) and Specimens S1, S2, S3 and S5.*

Fig. 56 comprises results of the experiments of DAO [25] as well as the results obtained by the author and values calculated by the elementary strength theory and LUSAS results. It can be seen that beams of Series P are generally more rigid than the composite girders of Series Specimens S. The results of the Elementary Theory and LUSAS Solid model are in the rigid zone.

*Table 6. Comparison of the mid-span deflections of the specimens described in Chapter 4.*

| Conductor of the test | Specimen | Span [m] | $M_{max}$ [kNm] | $v_{max}$ [mm] |
|---|---|---|---|---|
| PLATTHY & DAO | P2-1 | 1,5 | 87,5 | 3,5 |
| | P2-2 | 1,5 | 87,5 | 2,0 |
| | P3-1 | 1,5 | 76,5 | 6,8 |
| | P3-2 | 1,5 | 78,1 | 3,2 |
| SZABÓ | Specimen S1 | 1,5 | 80,0 | 14,9 |
| | Specimen S2 | 1,5 | 82,5 | 8,2 |
| | Specimen S3 | 1,5 | 65,8 | 18,1 |
| | Specimen S5 | 2,0 | 81,1 | 19,9 |

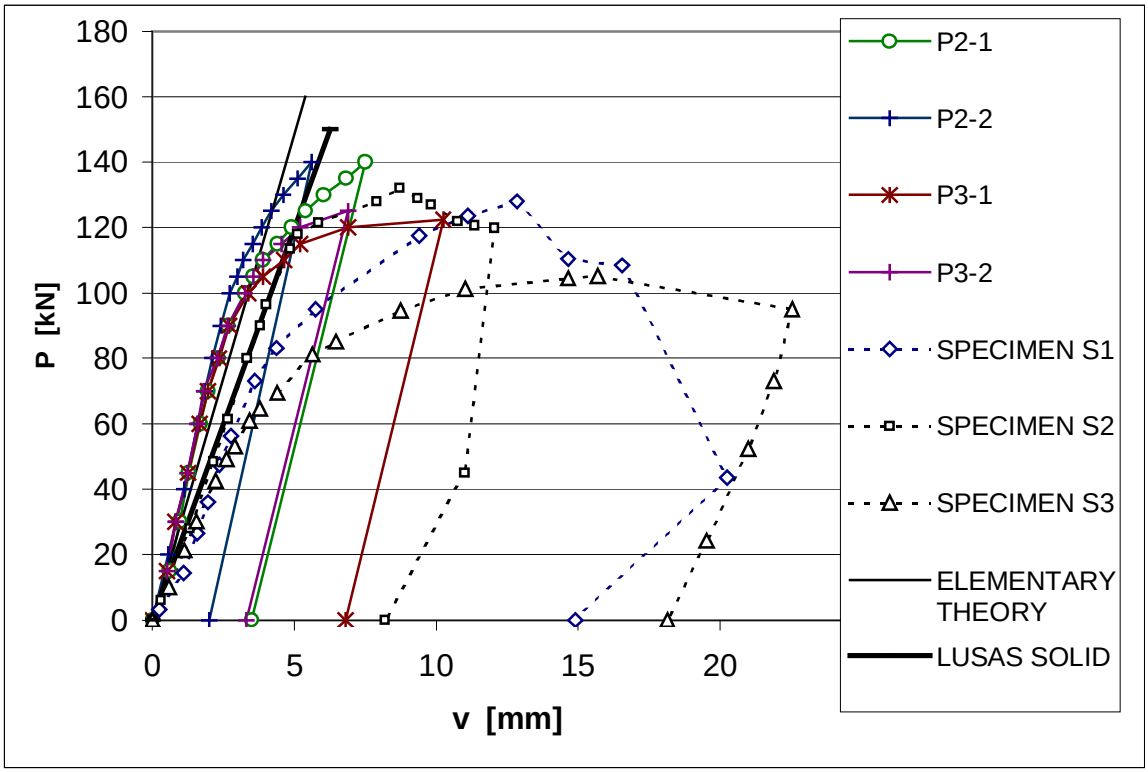


*Fig. 56. Comparison of deflections at mid-span due to concentrated load.*

Fig. 57 shows the temperature difference versus vertical deflection relationship in the first test series (Specimens S1, S2 and S3) containing loading and unloading phase. In case of Specimen S4 and S5 the temperature difference was only simulated by prestressing and that is why the heating process could not be investigated. The experimental results are fairly different because of different connector stiffness values.

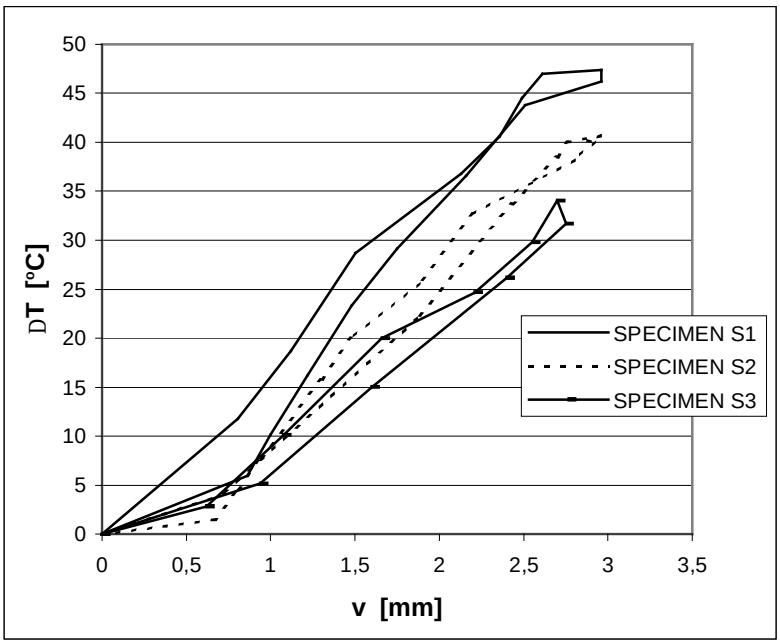


*Fig. 57. Comparison of deflections at mid-span due to temperature difference. Specimens S1, S2 and S3.*

## 5.3 Evaluation of results obtained by photoelastic method

### 5.3.1 Evaluation process

The purpose of this section is to present the measured shear stresses $t_{xy}$ in the steel beam web at the support region due to temperature difference of 40 $^{o}$C and compare those with the calculated values which originate from the finite element analysis and the Author's Energy Method. The influence of connectors on the principal stress distribution is shown here as well. The photoelastic analysis is an alternative method to determine the normal and shear stresses.

Since only few results are available on the stress condition of the beam end due to temperature difference, this method, although not quite accurate, is also discussed below [12] [107] [127].

During the measurement process a video recording was made of the test series 2 and slides were copied relating to certain states of the composite girders. The evaluation was carried out in the following load cases:

- State after prestressing (Specimens S4 and S5, Fig. 58).
- 2P = 92, 6 kN static load (Specimen S5).

Residual stresses caused by temperature effects were simulated by prestressing the steel beam with an axial force of 290 kN that is equivalent to 40 °C temperature difference. (More precisely the tensile forces 287 kN and 278 kN were applied to the steel beams of Specimens S4 and S5, respectively).

For the purpose of photoelastic analysis a kind of glasses and various plastics are applied, which become double refracted materials only when subjected to loading. The extent of double refraction is proportional to the difference of principal stresses (HOLISTER [54]). A double refracted layer subjected to light (electromagnetic vibration) produces phase-difference in the light-components. This phenomenon can be recognised by the polariser and analyser, which are the main elements of the reflection polariscope (Figs. 39 and 40). The polariser comprises special filter, which can transmit only one component of light-waves, i.e. the component vibrating in a particular plane. The plain polarised light occurring after the polariser is split into two ortogonally polarised components. These components propagate though the photoelastic layer at different velocities, while the frequency of the vibration remains costant. The second polariser is called analyser. When examining a lighted area of photo-elastic layer through a polariser and an analyser, two different patterns can be seen namely isocromatic and isoclinatic patterns. In front of the double refracted layer isocromatic and isoclinatic curves can be obtained from different rotated positions of the polariser and the analyser. In all points of the isochromats the phase-difference of the two light-components is zero or has the fractional value (Table 7) of the wavelength and at the same time the extent of principal stress difference is constant within a particular curve in all points of the isochromats. The principal stress directions in the points of isoclines are parallel with the polarisation planes and the principal stress direction is the same within each curve.

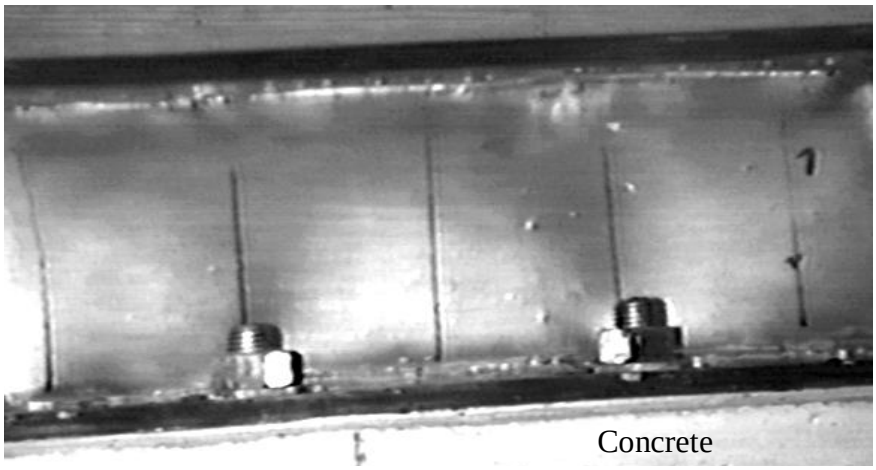


*Fig. 58. Isocromatic fringe pattern after prestressing of Specimen S4. The specimen is in upside position.*

### 5.3.2 The calibration process

The fringe order of isochromats can be determined by compensation process using white light source. This means that the compensation bar (Fig. 59) made of the same material as the photaelastic layer has to be examined by using reflective polariscope, then the analyser has to be rotated to such an extent that the original colored isochromat is replaced by a black isocromat in the examined point. The fringe order of the isochromat crossing this particular point can be determined from the angle of rotation.

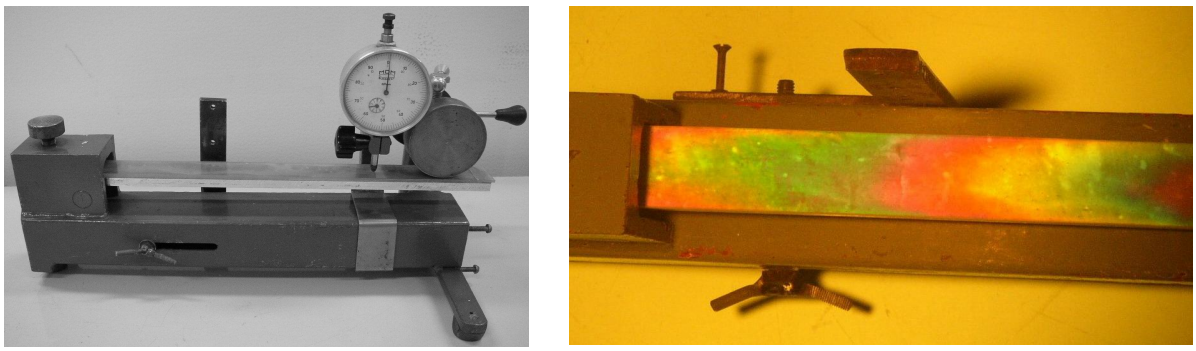

*Fig. 59. Calibration process.*

Based on this method the colours and the fractional isocromatic fringe orders belonging to the particular colours are shown in Table 7 (crossed polarisers).

*Table 7. Colours and the fractional isocromatic fringe orders.*

| **Colours** | **Number** |
|---|---|
| Black | 0,00 |
| White | 0,15 |
| Light yellow | 0,25 |
| Yellow | 0,50 |
| Yellow-purple | 0,75 |
| Purple | 1,00 |

### 5.3.3 Evaluation of test results and comparison of experimental and numerical data

If

$$e_1\text{-}e_2 = f_e \cdot m \tag{99}$$

where $e_1$ and $e_2$ are the principal strains, $f_e$ is the photoelastic constant of the layer (established by calibration: $1090 \cdot 10^{-6}$) and $m$ is the fringe order of the isochromat and

$$s_1 - s_2 = \frac{E_a}{1+m}(e_1 - e_2) \tag{100}$$

where $s_1$ and $s_2$ are the principal stresses and $E_a$ and $m$ are the modulus of elasticity and Poisson's ratio of the web material, respectively, then the difference of principal stresses is

$$s_1 - s_2 = \frac{E_a}{1+m} f_e \cdot m \tag{101}$$

The shear stress $t_{xy}$ as function of this difference is

$$t_{xy} = \frac{s_1 - s_2}{2} \sin 2j \tag{102}$$

where $j$ is the angle of principal tensile stress $s_1$.

The trajectory network can be developed by drawing short straight lines parallel with the principal stress directions in the points of isoclines as tangents of trajectory lines.

Isocromatic and isoclinatic patterns of the web of Specimen S4 in the prestressing state can be seen in Fig. 60. On the basis of Equations (101) and (102) and the isocromatic and isoclinatic patterns the test results can be assessed. As an example, the verification of a measured shear stress value is demonstrated here. This value, which is the maximum one ($t_{xy,max}$), is developed in the web of the steel beam at 65 mm distance from the support line (Fig. 61). The measured values used for verification are shown as framed numbers in Fig. 60. Using these values the maximum shear stress $t_{xy,max}$ can be calculated as follows:

$$t_{xy,max} = \frac{E_a}{2(1+m)} f_e \cdot m \sin 2j = \frac{210000}{2(1+0{,}3)} 1090 \cdot 10^{-6} \cdot 0{,}3 \cdot \sin(2 \cdot 9^0) = 8{,}16 \text{ N/mm}^2$$

The results obtained by LUSAS Solid model and the Author's Energy Method are in conformity with the photoelasic experimental ones (Figs. 61 and 62). It can be seen that the results from the Author's Energy Method fit the experimental curve better than those obtained by the Finite Element method, in which not continuous elastic layer, but discrete connectors are used.

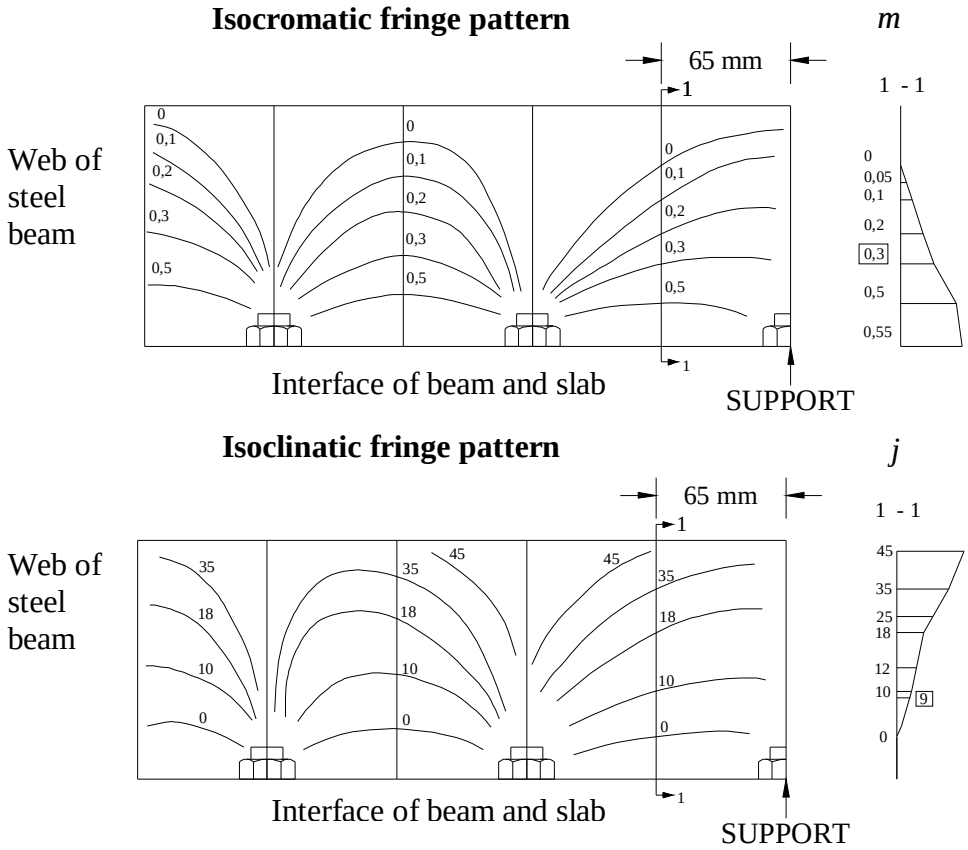


*Fig. 60. Isocromatic and isoclinatic fringe patterns of the web of Specimen S4 in the prestressing state.*

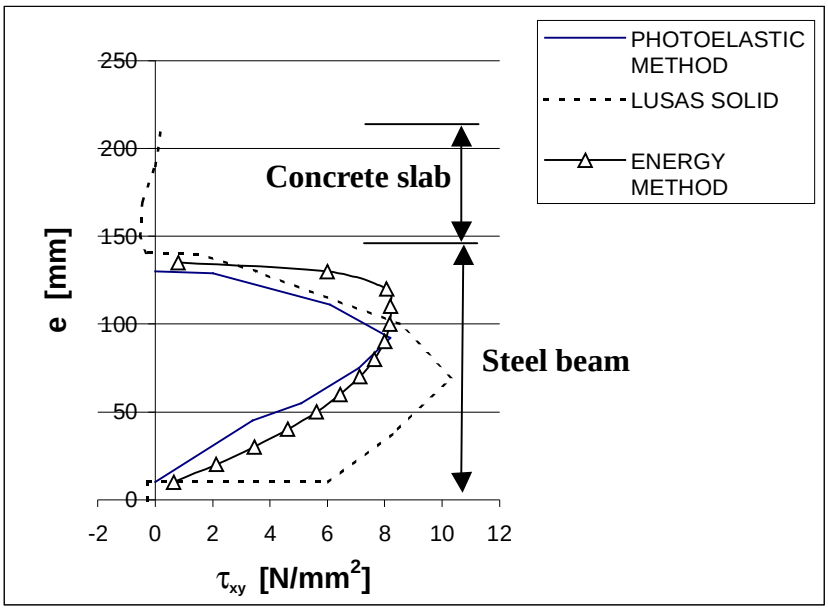


*Fig. 61. Prestressing state of Specimen S4. Shear stresses $t_{xy}$ in the beam web 65 mm apart from the support line.*

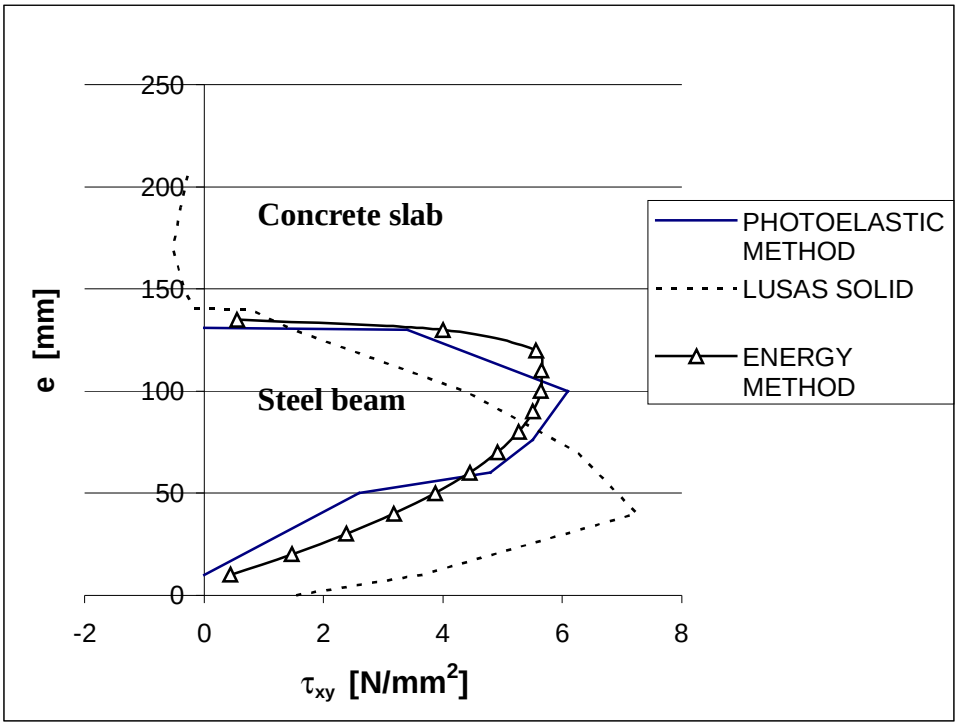


*Fig. 62. Prestressing state of Specimen S4. Shear stresses $t_{xy}$ in the beam web 195 mm apart from the support line.*

As it is demonstrated by this simple example, the photoelastic method is an excellent additional tool to examine structural details for which the elementary beam theory cannot be applied. The photoelastic measurement provides a global overview and facilitates finding of deficiencies and stress peaks in the structure [66].

# 6 PARAMETRIC STUDIES OF STEEL-CONCRETE COMPOSITE GIRDERS

## 6.1 Background

In Chapter 5 some parametric studies are already carried out by using LUSAS finite element program to determine connector spring stiffness values for Model 1 (Fig. 42). These studies allow the author to suggest his energy method for the determination of shear flow at interface due to temperature difference. Notwithstanding the earlier parametric studies, the present chapter contains additional numerical and analytical studies in order to find out the influence of varying shear connector stiffnesses on the longitudinal normal stresses $s_x$ and shear flow *T(x)*. Based on the analytical parametric studies new equations are deduced to take into consideration the elastic behaviour of shear connectors.

## 6.2 Parametric studies concerning longitudinal normal stresses

In Fig. 63 the curve obtained from LUSAS Joint model results (connector spring stiffness value $k_y$ = 1000 MN/m) shows good compliance with the results originated from LUSAS Solid model at mid-span. This agreement between the two sets of results is used as a calibration method for the connection stiffness in case of Specimen S5 (Table 3, Fig. 37). The reason is that to carry out a comparison between the results of the so-called "exact" methods and the present study is difficult, as the dimensions of the spring constants have different units (in the first case it is MN/m$^2$, while now it is MN/m).

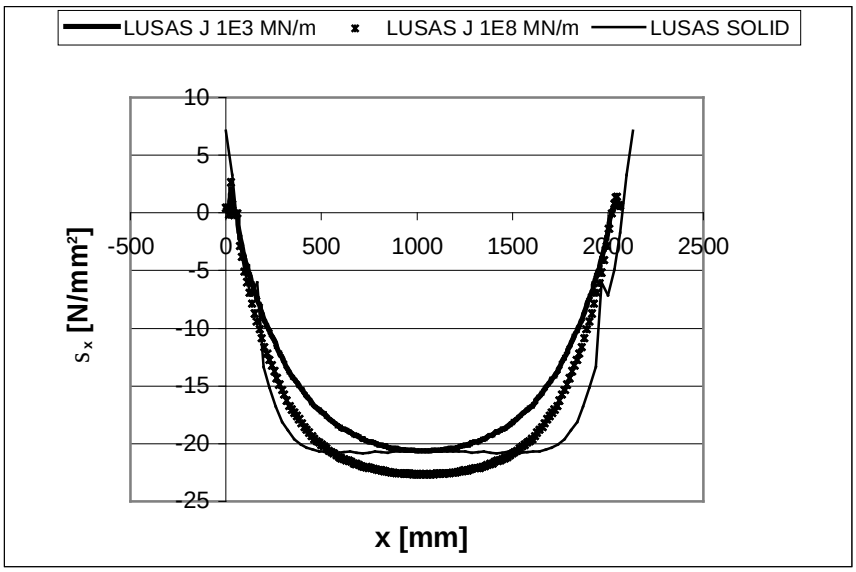


*Fig. 63. Comparison of normal stresses $s_x$ at extreme fibre of lower flange of the steel beam due to 40 $^oC$ temperature difference of Specimen S5 (values from LUSAS Joint and LUSAS Solid model).*

Fig. 64 shows normal stresses $s_x$ at mid-span at different heights *e* of Specimen S1 (Table 3, Fig. 34) due to 100 kN concentrated load. These values are obtained by LUSAS FEM analysis using variable connector stiffness values. On the tension side of the steel beam and in the concrete slab the calculated values are practically independent of the connector stiffness, but in the compression flange these values are fairly different. These differences represent a problem analogous to the effect of long-term loading, which is explained bellow. To handle

the creep effect, in practice generally the well-known Effective Modulus Method (FRITZ [47]) is used. The LUSAS program package is capable to model the creep phenomenon of concrete using constitutive laws and directly the CEB-FIP creep model [16] but for beam elements only. Since in this study solid elements are used, the latter model cannot be applied.

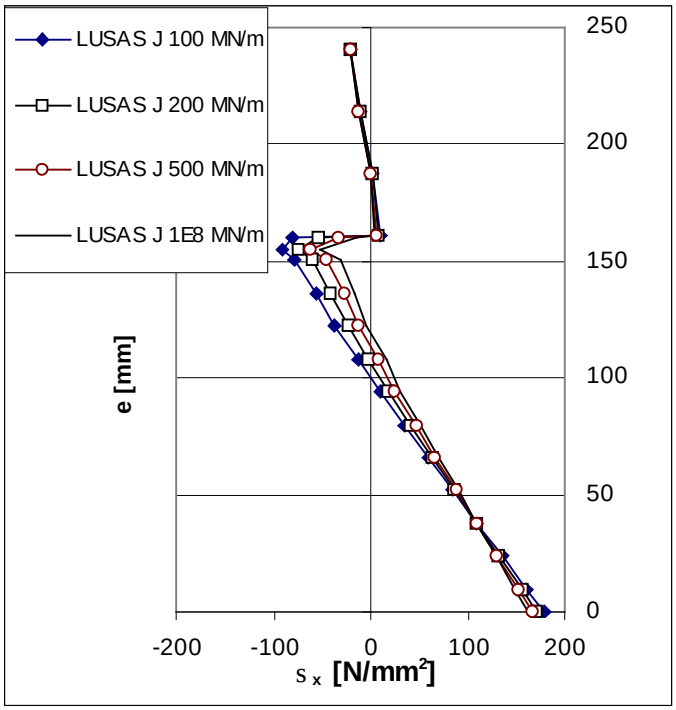


*Fig. 64. Comparison of normal stresses $s_x$ at mid-span at different heights **e** of Specimen S1 due to 100 kN concentrated load. The results are obtained by FEM analysis using different connector stiffness values ($k_y$ = 100…$10^8$ MN/m).*

Fig. 65 shows normal stresses $\sigma_x$ at mid-span and different heights ***e*** of Specimen S1 (Fig. 34), when 100 kN concentrated load is applied and creep is considered (short-term (t = 0)

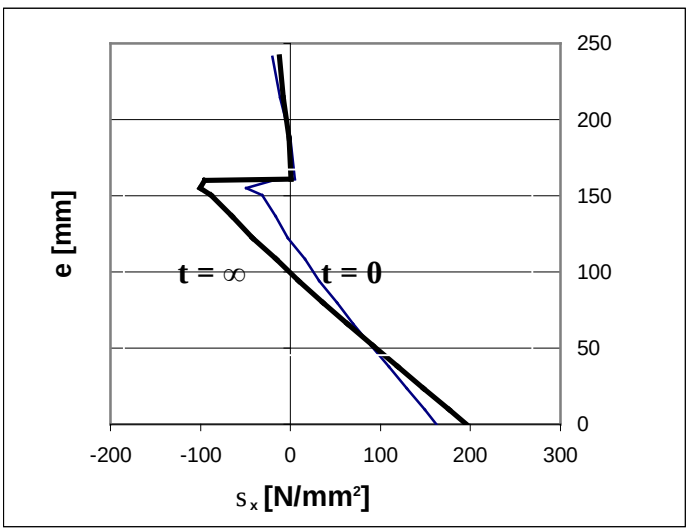


*Fig. 65. Comparison of normal stresses $s_x$ at mid-span at different heights **e** of Specimen S1 due to 100 kN concentrated load and creep. The results are obtained by FEM analysis applying short-term (t = 0) and long-term effects (t = ¥).*

and long-term effect (t = ∞)). The normal stresses $s_x$ in the compression flange are fairly different, which is similar to the results shown in Fig. 64.

### 6.3 Parametric studies concerning shear flow in the support regions

For the basis of the parametric study concerning shear flow, two types of girders are chosen, Specimen S4 (Chapter 4, Section 4.2) and a sample girder with 6 m span. The sample composite girder consists of a beam with an IPE 750 profile and a concrete slab of 1200 x 200 $mm^2$. Both girders are subjected to uniformly distributed load. The aim of this parametric study is to estimate the effect of the elastic behaviour of connectors in the support region.

In the support region (Figs. 66 and 67) the shear flow obtained by the Hawranek-Steinhardt method and the Author's Energy Method are fairly different. Because of that, two independent methods are invoked, the LUSAS FEM and the method of redundant forces [74]. The straight lines in the figures represent the results obtained by elementary beam theory. The maximum values obtained by LUSAS are in good correlation with those obtained by using the Author's Energy Method, while the results of the Redundant Force method are close to those obtained by the Hawranek–Steinhardt method. Since there are discrepancies especially in the support region due to the different approximation functions used for calculations in the studied and discussed methods, the well-accepted Hawranek–Steinhardt method is considered as the basis of the parametric study in this section.

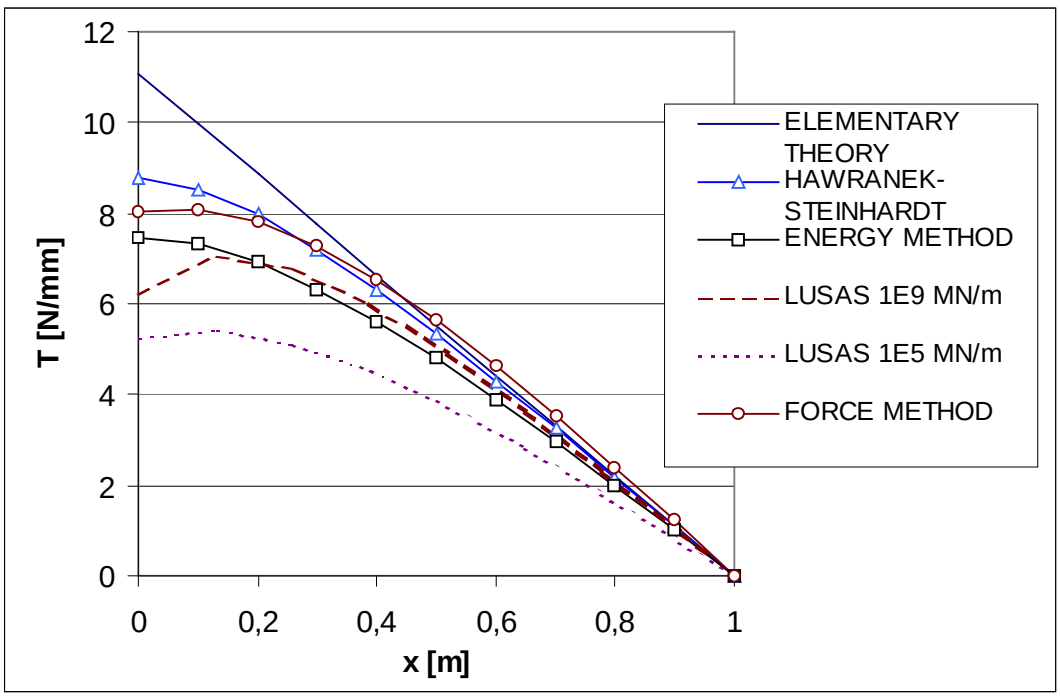


*Fig. 66. Comparison of shear flows obtained by using different methods in the case of Specimens S4 and S5 when subjected to 2 kN/m uniformly distributed load.*

The normal force due to uniformly distributed load can be obtained directly from differential Equation (22) that yields to equation

$$N(x)=\frac{q}{w^2\cdot d}\left(1-\frac{D_{abs}}{D_{full}}\right)\left[\frac{1-\cosh(wL)}{\sinh(wL)}\sinh(wx)+\cosh(wx)+\frac{w^2\cdot x}{2}(L-x)-1\right] \tag{103}$$

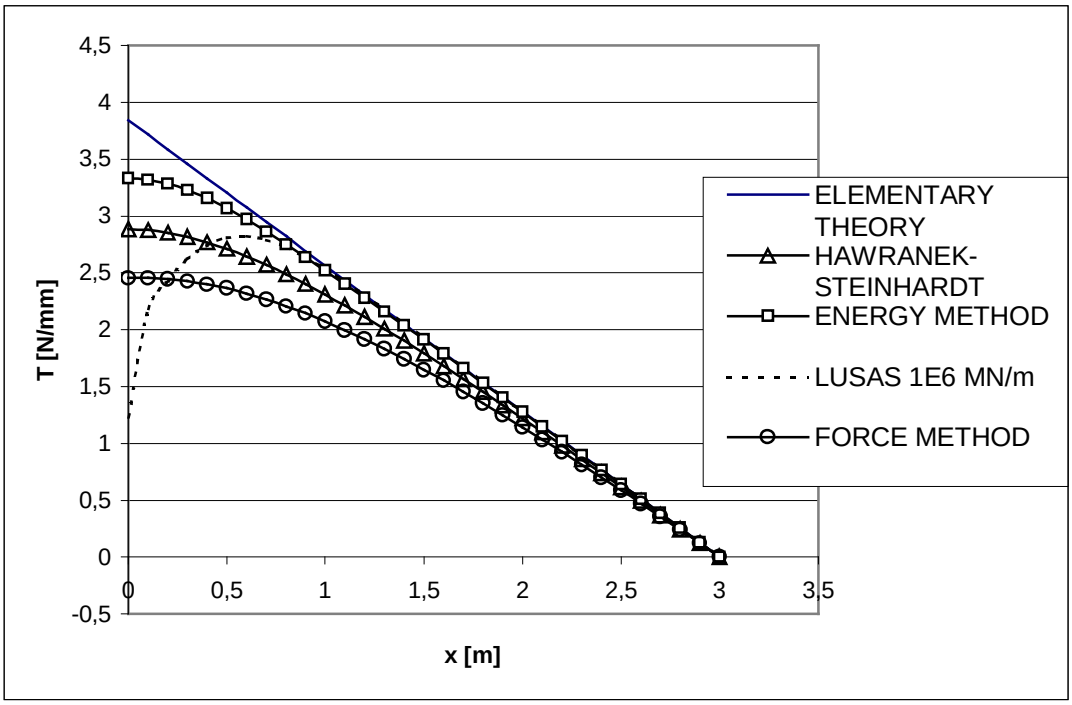


*Fig. 67. Comparison of shear flow obtained by different methods in case of a composite girder with 6 m span subjected to 1 N/mm uniformly distributed load.*

At mid-span

$$N(L/2)=\frac{q}{w^2\cdot d}\left(1-\frac{D_{abs}}{D_{full}}\right)\left[\frac{1}{\cosh(wL/2)}+\frac{w^2\cdot L^2}{8}-1\right] \tag{104}$$

Introducing expression

$$N_{full}=\lim_{w\to\infty}N\left(\frac{L}{2}\right)=\frac{qL^2}{8d}\left(1-\frac{D_{abs}}{D_{full}}\right) \tag{105}$$

Equation (104) can be transformed to

$$N(x)=\frac{8\cdot N_{full}}{(wL)^2}\left[\frac{1-\cosh(wL)}{\sinh(wL)}\sinh(wx)+\cosh(wx)+\frac{w^2\cdot x}{2}(L-x)-1\right] \tag{106}$$

Finally, by considering Equations (18) and (106), the total longitudinal shear force per unit length

$$T(x) = \frac{8 \cdot N_{full}}{wL^2}\left[\frac{1-\cosh(wL)}{\sinh(wL)}\cosh(wx) + \sinh(wx) + w\left(\frac{L}{2} - x\right)\right] \tag{107}$$

is obtained. At the support

$$T(0) = \frac{8 \cdot N_{full}}{wL^2}\left[\frac{1-\cosh(wL)}{\sinh(wL)} + \frac{wL}{2}\right] \tag{108}$$

Introducing expression

$$T_{full} = \lim_{w\to\infty} T(0) = \frac{4 \cdot N_{full}}{L} \tag{109}$$

Equation (107) can be transformed to

$$T(x) = \frac{2 \cdot T_{full}}{wL^2}\left[\frac{1-\cosh(wL)}{\sinh(wL)}\cosh(wx) + \sinh(wx) + w\left(\frac{L}{2} - x\right)\right] \tag{110}$$

Entities $N_{full}$ (Equation (105)) and $T_{full}$ (Equation (109)) express how big the extreme axial force $N$ (at mid-span) and the extreme shear flow $T$ (at the support), respectively, in case of the simply supported and uniformly loaded single-span composite girder are, when the connectors have no flexibility. When they are known, all other cases having any connector flexibility can be covered by using Equations (106) and (110).

By virtue of Equations (108) and (109) the ratio

$$V = \frac{T(0)}{T_{full}} = 1 - 2\frac{\cosh(wL) - 1}{wL \cdot \sinh(wL)} \tag{111}$$

can be introduced and a parametric study can be carried out to estimate the difference between the behaviour of elastic and rigid connections at support line of a simply supported and uniformly loaded composite girder. The result is graphically shown in Fig. 68.

A similar calculation process can be carried out for other load cases as well. In case of a single point load in the middle, it leads to expression

$$V = 1 - \frac{1}{\cosh\left(\frac{wL}{2}\right)} \tag{112}$$

Also this result is shown in graphical form in Fig. 68.

The examined cases cover all practical spring constants $K$ of usual headed-stud connections as well [68], [70] ($K = 0{,}5 \cdot 10^2$ to $3 \cdot 10^{-3}$ mm$^2$/N).

If the $K$ value is estimated, then $w{\cdot}L$ can be calculated for a given cross-section and a given span $L$. Using the curves presented in Fig.68 ratio $z$ can easily be determined. If the shear

flow is calculated using elementary beam theory, then based on the determined $z$ value the elastic shear force per unit length at support line can be calculated.

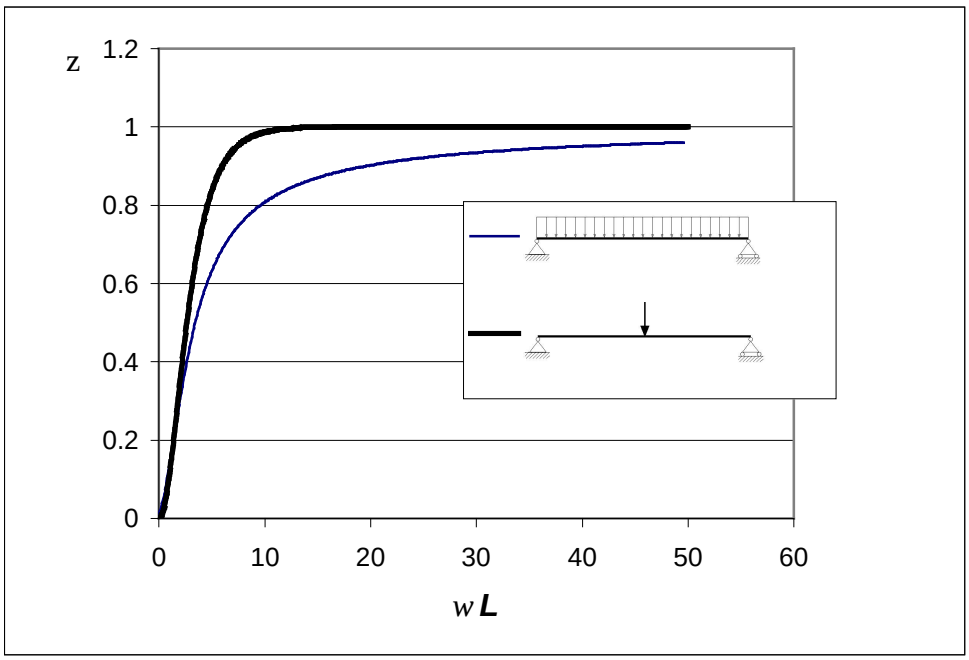


*Fig. 68. Relationship between* $z$ *and* $w \cdot L = L\sqrt{\frac{K}{C^*}\frac{D_{full}}{D_{abs}}}$ *in two different cases.*

# 7 EXPERIMENTAL AND NUMERICAL ANALYSES OF WOOD-BASED COMPOSITE GIRDERS

## 7.1 Introduction

In Chapter 2 calculation methods for multi-material composite cross-sections are discussed, which are valid for wood-concrete composite girders as well. Tests, numerical analyses and parametric studies on steel-concrete composite girders are presented in Chapters 4, 5 and 6 considering the behaviour of connectors and their influence on the stress and strain condition of a composite girder. The aim of the present chapter is the same. Since wood is an orthotropic material, it can be taken into consideration in a finite element model.

Wood-concrete composite structure concept was for the first time applied to bridges already in the 1930's. In the 1960's, some remarkable wood-concrete composite bridges were built, like the Keystone Wye bridge in the USA [65]. In comparison with conventional wood bridges, the composite bridges, built recently for instance in Finland, seem to be the most economical ones. Besides that the concrete deck gives good protection against weather and abrasion caused by traffic. So wood-concrete composite structures seem to be a potential alternative for bridge superstructure.

So far the development of connections of wood-concrete composite girders was carried out only by few researchers. The solutions, which meet the requirements of effectivity, durability and easy and cheap manufacturing, still remain unsolved, but several investigations have been carried out for instance in the frame of the Nordic Timber Bridge Projects [77], [116], [117]. These projects covered wood-concrete composite bridges, tests on shear connectors of wood-concrete composite bridges, design of wooden arch bridges and arch bridges for road traffic, rules concerning the design of Nordic timber bridges, construction costs of timber and wood-concrete composite bridges in comparison with concrete, prestressed precast concrete and steel bridges in Finland, measurements and follow-up tests of timber and wood-concrete composite bridges, arch bridges for pedestrian traffic, life cycle assessment of timber bridges, analysing methods of a composite girder containing wood, monitoring of timber bridges, fatigue of timber bridges and fatigue of joints in timber structures, and chemical wood protection. These projects report about 50 completed new bridges in the Nordic countries.

Long-term behaviour of wood-concrete girders is also investigated. In references [45] and [46] all phenomena affecting the long-term behaviour of timber, concrete and connectors, such as creep, mechanosorptive creep, shrinkage/swelling and temperature variations, are fully considered. These influences should be considered and addressed in the standards as well in case of wood-concrete girders.

From calculation point of view, due to the large number of connectors, even a simply supported composite girder is internally statically indeterminate. Additionally, the regions beyond the support lines are of special interest, because they, according to the beam theory, do not contribute to the connector forces, although the situation in reality is different. These facts gave reason to the present section and tests carried out by the author and other researchers.

## 7.2 Tests with wood-plywood composite girders

In 1999, an experimental study on wood-plywood composite structures subjected to gravity loads was carried out by the author to find out the real connector force distribution of composite girders [112], [113]. Two similar specimens of length 2070 mm were tested; only

the spacing of the connectors was different being 100 mm in one case and 140 mm in the other. The geometry and measuring system of the T-shape girders are shown in Fig. 69 and Fig. 70.

The flanges of the beams tested consisted of 210 mm wide and 20 mm thick plywood plates and the webs of 68 mm wide and 176 mm high pine planks. Because the study was concentrated on the regions beyond the support lines, 335 mm long cantilevers were used thus giving a span of 1400 mm. The loading comprised two knife-edge forces originated by a hydraulic jack. The forces were located symmetrically with respect to the mid-span and had a spacing of 200 mm.

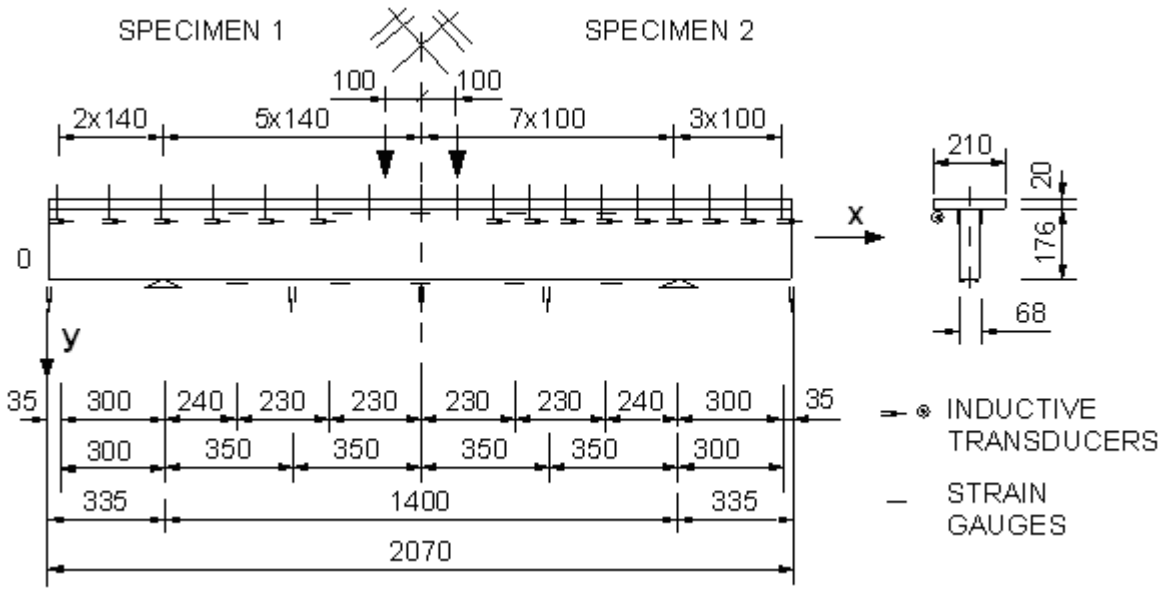


*Fig. 69. Measurements, connector spacing, loading arrangements and location of inductive transducers and strain gauges in the two specimens tested. All measures in millimetres.*

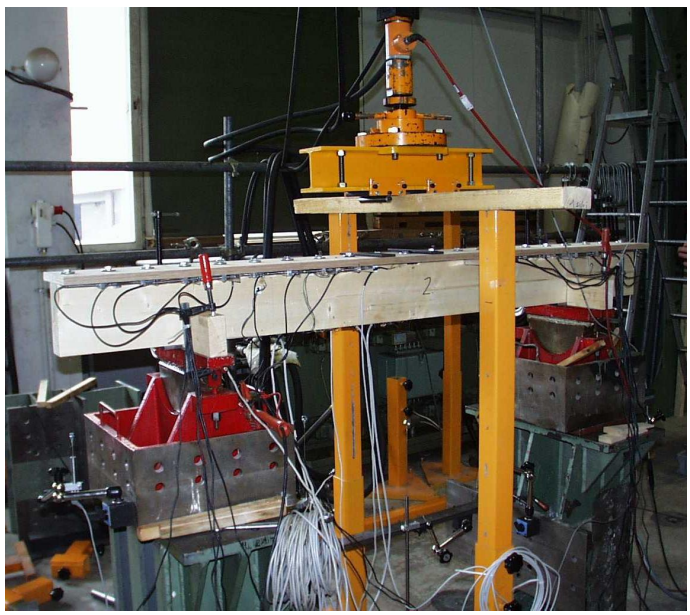

*Fig. 70. Specimen 2. Photo: L. Salokangas.*

Each connector comprised the following six elements (Fig. 71); one 9,42 mm diameter screw (total length 76 mm, head high 7 mm, cylindrical length 25 mm, threaded length 48 mm) with a 17,13 mm diameter head, one circular hollow washer with 12 mm diameter, another washer with 37 mm diameter, a 14 mm long and 32 mm thick rubber cylinder having a centric hole of 12 mm in diameter and, finally, two plywood washers. This arrangement made only longitudinal relative displacement between the flange and web possible.

*Fig. 71. Connector elements used in the tests described. Photo: L. Salokangas.*

The experimental tests were carried out according to ISO Standard 68691. During the tests, the applied load, deflection of the girder and the slip between the wooden beam and plywood plate were measured. For both specimens, the value of 30 kN was chosen as the estimated total ultimate load. The loading sequence was the following (Fig. 72):

- Load increase from 0 to 12 kN in two minutes (speed 6 kN/min).
- Constant load 12 kN for 30 seconds.
- Unloading from 12 kN to 3 kN in 90 seconds (speed 6 kN/min).
- Constant load 3 kN for 30 seconds.
- Load increase from 3 kN up to failure (speed 0,5¨2,0 mm/min measured from deflection).

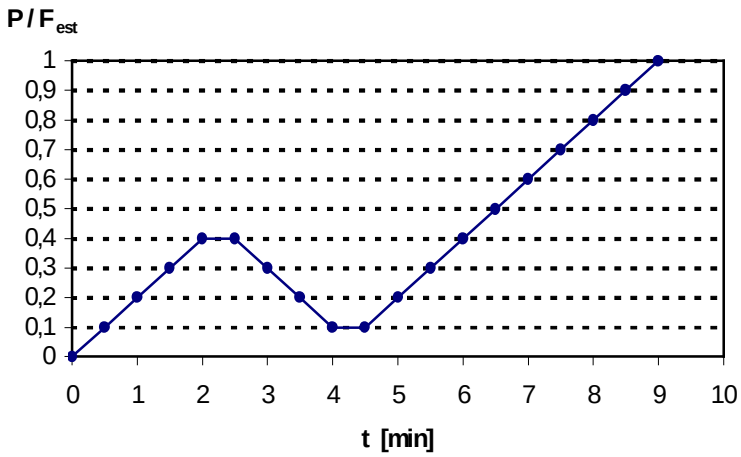


*Fig. 72. Applied test load P related to the estimated maximum load $F_{est}$ as function of time t.*

In both cases, the failure took place at the mid-section of the girder because of bending stresses in the wooden part. Before that, the joint to plywood was destroyed by shear at the beam-ends. The failure loads were 37,65 kN and 64,038 kN, respectively. The failure pattern of Specimen 2 can be seen in Fig. 73.

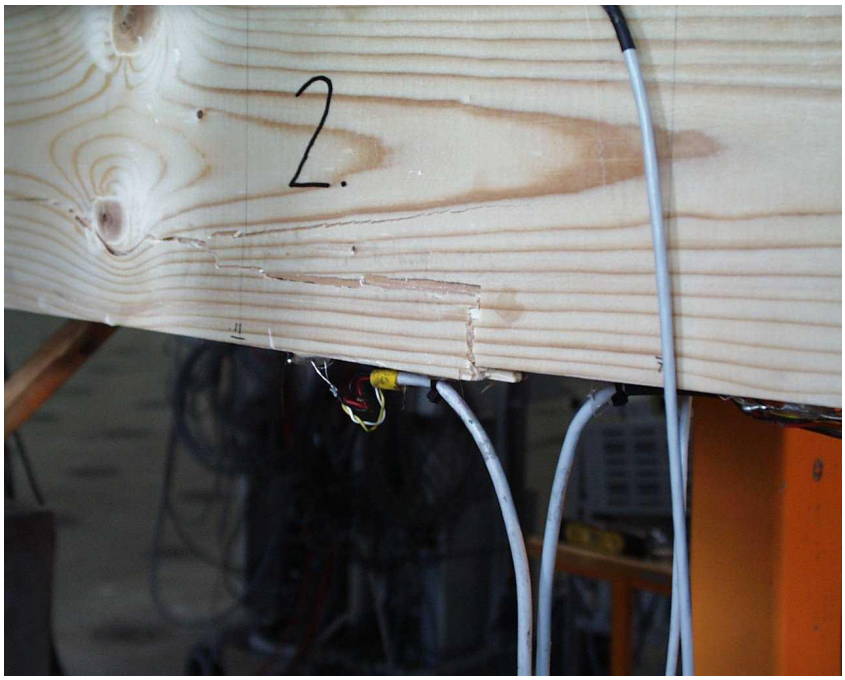


*Fig. 73. Failure pattern of Specimen 2. Photo: L. Salokangas.*

## 7.3 Numerical analysis

### 7.3.1 Overall analysis

The experimental tests were followed by numerical analyses. The main goal of this investigation was to carry out a parametric study – based on the tests – varying connector stiffness. Both specimens were modelled with a three-dimensional idealisation of the structures and three-dimensional elements.

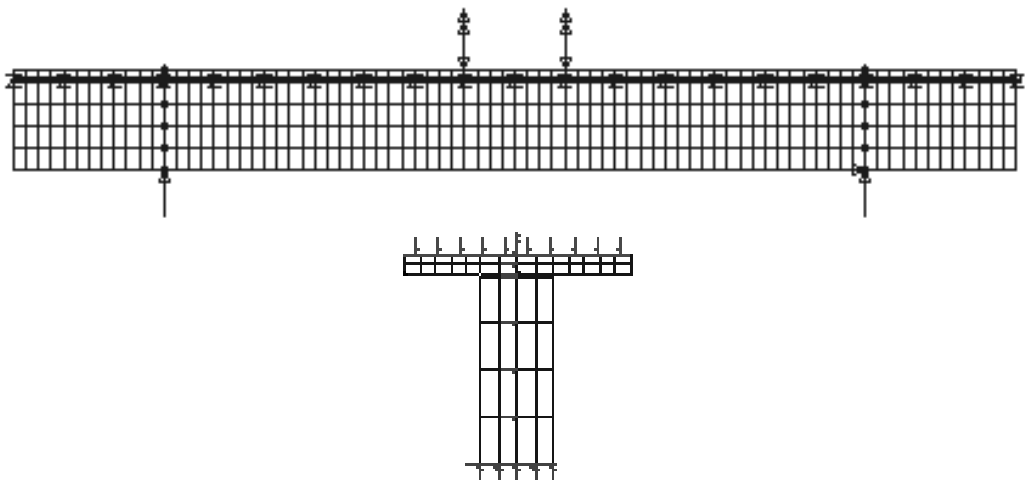

*Fig. 74. The mesh used for Specimen 2 in the FEM analysis, elevation and cross-section.*

LUSAS finite element software was applied. The mesh was developed by means of the graphical pre- and post-processing system of LUSAS. The 3-dimensional solid continua HX8M with 8 points for the wood web and plywood slab and appropriate joint elements JNT4 for the connectors, respectively, were used. The finite element mesh of the model of Specimen 2 (Model 2*) is shown in Fig. 74. Global coordinate system presented in Fig. 69 was created for the solid elements and a local one for the joints. The number of elements and nodes in Specimen 1 was 2778 and 4675, respectively. The corresponding figures in Specimen 2 were 3541 and 5712, respectively.

The material properties obtained from the experimental part of the study are presented in Table 8. The connector elements, i.e. the JNT4 joint elements, included three linear springs whose stiffnesses are denoted by $k_x$, $k_y$ and $k_z$. Stiffnesses $k_x$ and $k_z$ were given approximately infinite values. Spring stiffness $k_y$ was varied, thus giving an opportunity to incorporate slip and redistribution of connector forces in the analysis. By this means, a tool also is obtained to adjust such values in the FEM analysis so that the experimentally measured connector forces could be analytically followed.

For comparison, the experimentally and analytically obtained slip values, respectively, are presented in Fig. 75.

*Table 8. Material properties for wood and plywood used in the FEM analysis.*

| Symbol | $E_x$ | $E_y$ | $E_z$ | $G_{xy}$ | $G_{yz}$ | $m_{xy}$ | $m_{yz}$ | $m_{xz}$ |
|---|---|---|---|---|---|---|---|---|
| | [N/mm$^2$] | | | | | | | |
| Wood | 11000 | 370 | 370 | 690 | 690 | 690 | 0,16 | 0,16 |
| Plywood | 15200 | 507 | 507 | 550 | 550 | 550 | 0,2 | 0,2 |

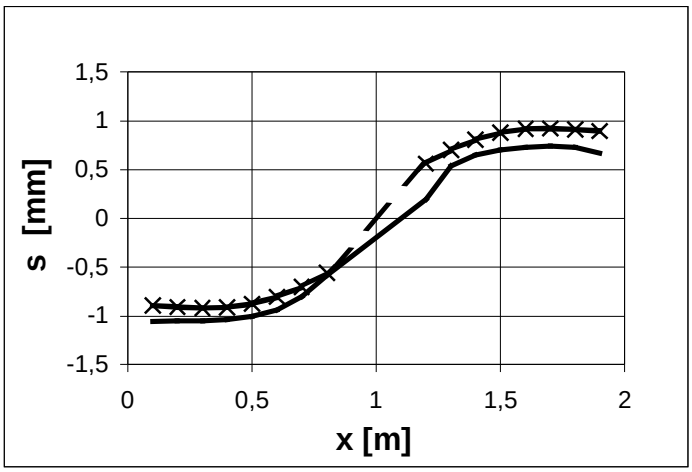


*Fig. 75. Comparison of the experimental (full line) and analytical (dashed line) slip values of Specimen 2 with 30 kN total load and spring stiffness $k_y$ = 0,5 MN/m at various distances x from the beam end.*

### 7.3.2 Parametric study

Because of good agreement between the experimental and analytical values, the FEM analysis can be considered reliable to describe the phenomenon under discussion more generally. That is why a parametric study is carried out to see, how the connector forces depend on the horizontal spring stiffness $k_y$, i.e. the connector flexibility. Again, Specimen 2 is used as the

base structure with the experimental test-loading set-up. The result is shown in Fig. 76. It can be seen, that for deformable connectors, i.e. with small $k_y$-values, the connector force distribution is relatively even and differs from that obtained by the traditional bending theory based on stiff connectors. It is also seen, that the stiffer the connectors are, the more the location of the maximum connector force deviates from the beam end, which is another contradiction. This result, however, is in accordance with the result obtained by BODE and SCHANZENBACH [11] discussed in the introduction.

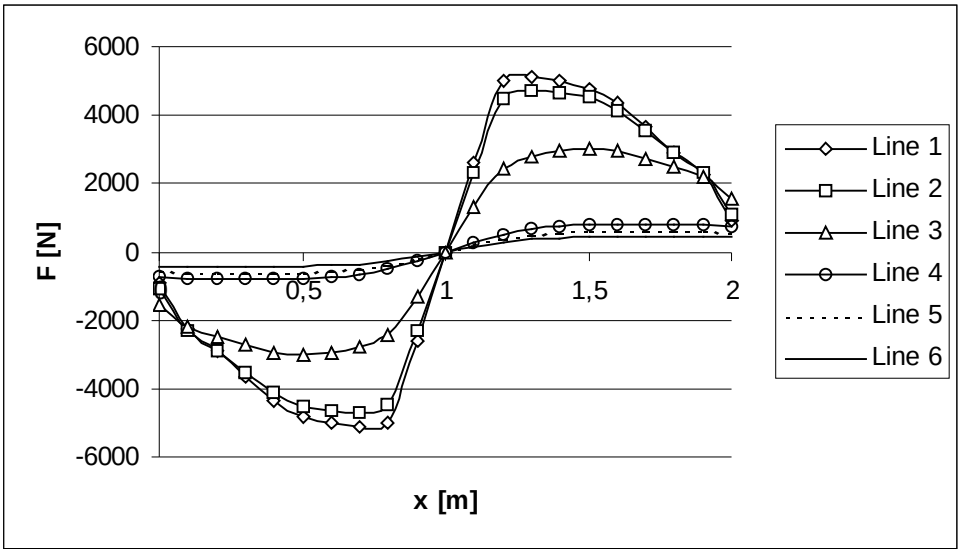


*Fig. 76. Distribution of connector force F as function of spring stiffness $k_y$ according to the parametric study with Specimen 2. The curves from 1 to 6 are valid for $k_y$ equal to $10^{15}$, 100, 10, 1, 0,7 and 0,5 MN/m, respectively. The applied load is 30 kN.*

Distribution of the longitudinal stress $\sigma_x$ along the beam and through the depth was also recorded. The result is shown in Figs. 77 and 78. The distribution of the normal stress $s_x$ at the bottom extreme fibre of Specimen 2 according to the parametric study as function of spring stiffness $k_y$ is shown in Fig. 77. From this figure it can be concluded that significant stress peaks occur in the support regions violating the traditional bending theory**.** Additionally, due to rigid connection normal stresses are decreased in the mid-span cross-section by approximately 25 %.

Fig. 78 presents the vertical distribution of the normal stress $s_x$ at different cross-sections near the support region. At the interface of wood and plywood in every examined cross-section an abrupt change of horizontal stresses can be experienced. At cross-sections with x equalling to 433 and 533 mm the curves tend to follow linear stress distribution.

Fig. 79 shows normal stresses $s_x$ at mid-span due to 30 kN concentrated load as function of the vertical distances *e* from the lower edge of the beam. These stresses are obtained from numerical analyses and the tests conducted by the author. It can be seen that the results obtained both by LUSAS and the Author's Energy Method are in good conformity with the experimental ones. In the author's method, isotropic material properties are considered in contrast with the finite element method, where orthotropic material properties are taken into account. The good agreement between numerical results justifies to suggest that in practice isotropic material properties are not needed to be considered when analysing wood-based composite girders.

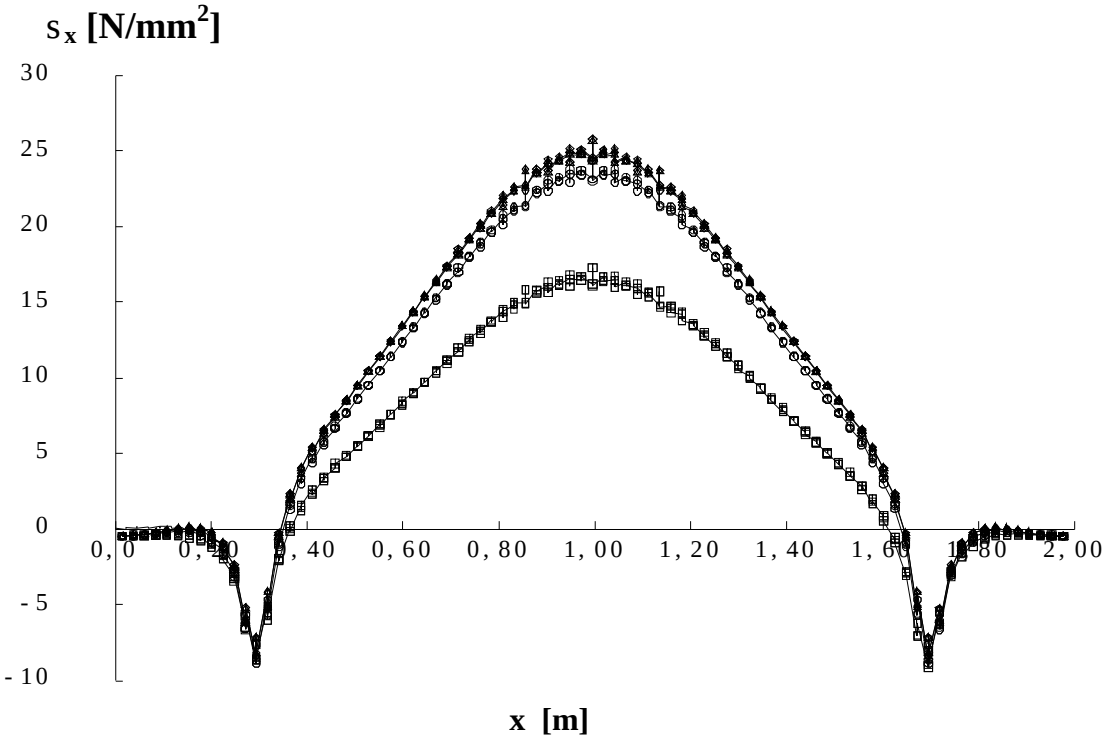


*Fig. 77. Distribution of the axial stress $s_x$ at the bottom layer as function of spring stiffness $k_y$ according to the parametric study with Specimen 2. The curves at the midsection listed from bottom represent $k_y$-values equal to $10^{15}$, 10, 1 and 0,4 MN/m, respectively. The applied load is 30 kN.*

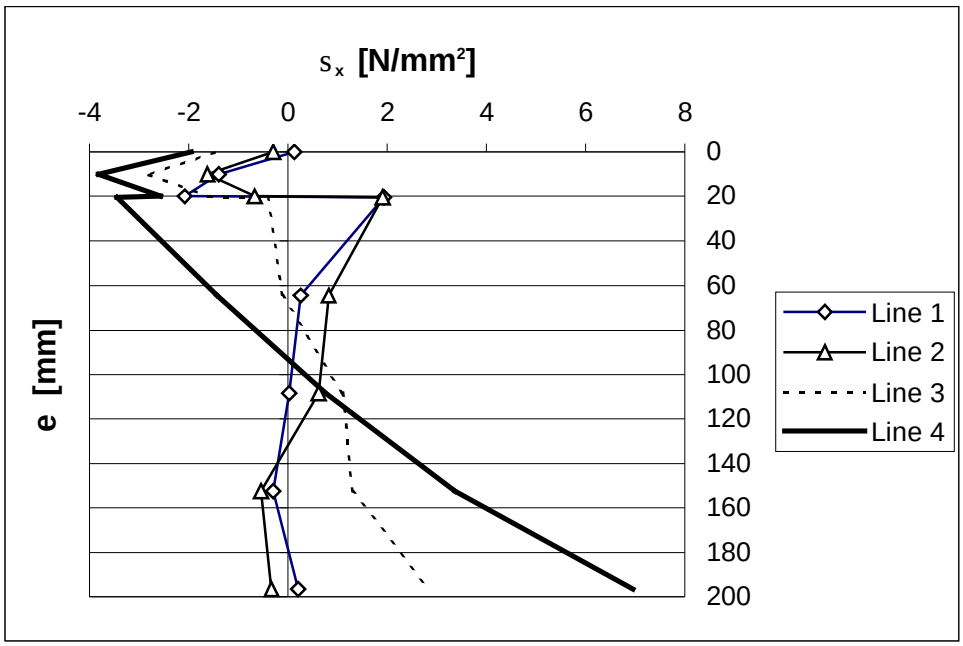


*Fig. 78. Vertical distribution of the axial stress $s_x$ near the support region with $k_y$=10 MN/m (Specimen 2). The curves from 1 to 4 are valid for x equal to 133, 333, 433 and 533 mm, respectively, when the global coordinate system shown in Fig. 69* is used. *The applied load is 30 kN.*

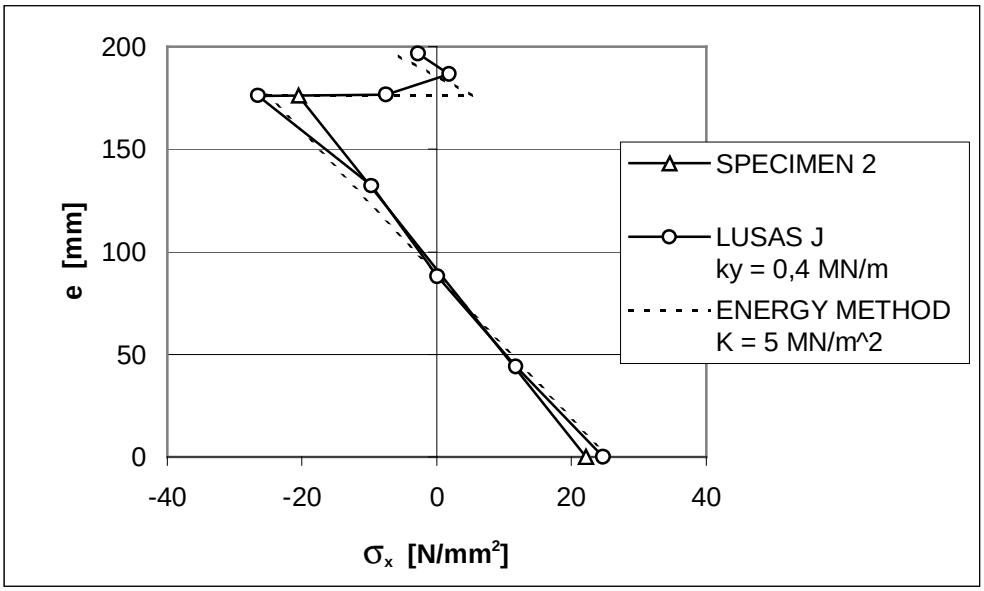


*Fig. 79. Comparison of normal stresses $s_x$ obtained by using different methods at mid-span at different heights **e** of Specimen 2 due to 30 kN concentrated load.*

### 7.4 Conclusions

From the experimental and numerical analyses, the following can be concluded:

- The state of stresses and deformations of the examined composite girders subjected to gravity loads can be determined precisely with the applied numerical models.
- The cantilever parts accumulate significant stresses and connector forces although not loaded violating the traditional bending theory.
- The connector carrying the maximum load is not the first but the second or third one measured from the support line towards the span. This result, although violating the traditional bending theory as well, is in accordance with the results obtained with other types of composite girders.

# 8 CONCLUSIONS AND RECOMMENDATIONS

The present study deals with the behaviour of connectors and their influence on the stress and strain condition of a composite girder. It is known, that the behaviour of the connectors may affect the entire composite girder. Therefore it was also necessary to review several other issues and tendencies concerning the investigation of the entire composite girder.

## 8.1 Analytical and numerical methods related to composite girders

Among analytical models, statical and energy methods, based on the beam theory, are considered. The so-called exact statical and energy methods assume that the connectors form an elastic layer in contrast to the redundant force method where discrete connectors are taken into consideration. Several investigations have shown that the Hawranek-Steinhardt method is quite conservative when calculating the shear force per unit length in the support region. The fact, that the traditional energy method does not provide a solution for composite girders subjected to temperature difference, inspired the author to develop a new kind of energy method based on variational calculation for determining the shear force distribution of connectors in composite girders. The new method is in compliance with the experimental and the latest theoretical investigations and can be processed using the latest engineering programs, e.g. MathCad or MathLab software applications.

The present study also summarizes the investigations carried out for composite girders using numerical methods. In this context the author has developed several FEM models for more precise numerical analysis of composite girders using three-dimensional i.e. shell-beam, solid and solid-spring models. Here the shear connectors were represented by beam elements, solid elements and springs. The models developed proved to be an effective tool when verifying the experimental results.

## 8.2 Experimental results on steel-concrete composite girders

The study presents several experimental tests with steel-concrete composite girders conducted by the author. Special emphasis was laid on the behaviour of shear connectors and their influence on the simply supported composite girders subjected to temperature difference between the steel beam and concrete slab. The temperature difference was provided directly by heating the steel beam or indirectly by prestressing it using external hydraulic jacks simulating the phenomenon. In the first case (direct way) the slip between steel and concrete was measured. Based on these measurements the spring stiffness values of the connectors could be determined using a solid-spring FEM model. Based on the various spring stiffness values the stress-deformation state of test girders could be checked (e.g. longitudinal normal stresses $\sigma_x$) and predicted. In the second case (indirect way) the normal force of the concrete slab was calculated from test measurements obtained by using strain gauges. Using implicit way the spring stiffness values were selected so that the resulting normal force diagram determined by the Hawranek-Steinhardt method would provide the best approximation of the experimental curve. In function of spring stiffness the internal forces can be calculated. These (indirect) tests were verified by FEM as well, using solid and solid-spring models. However, the solid model contains only stress values. But the solid spring model provides a link to the LUSAS Solid model and to Hawranek-Steinhardt method and the Author's Energy Method as well. For practical calculations of shear flow due to temperature difference, the Author's Energy Method is recommended because these results proved to be in close proximity to the numerical values.

When comparing mid-span longitudinal normal stress $\sigma_x$ and mid-span deflection values, every calculation method (including FEM as well) shows good accordance with the experimental test data. Concerning the other parts of a simply supported beam, the solid FEM model produces most reliable results compared to test results.

The section of the study presenting experimental tests on steel-concrete composite girders was terminated by a photoelastic measurement where the support region stresses were examined. When comparing shear stresses due to temperature difference discovered during the experiments, the test results are in good accordance with the calculated Author's Energy Method, except for those obtained by the LUSAS Solid FEM.

### 8.3 Parametric studies on composite girders with isotropic material

The present investigation includes parametric studies that extend the experimental results. In addition, they also provide a good tool to estimate the elastic shear flow at the support line of simply supported composite girders subjected to uniformly distributed load. The formula covers all the practical deformability characteristics K values of common headed stud connections for each span and cross-section variations of composite girders with isotropic material. The process used can be applied to other load cases as well.

### 8.4 Experimental tests and numerical analysis of wood-based composite girders

The study also presents experimental and FEM analysis results related to shear flow distribution between deformable connectors in a wood-based composite girder. Special emphasis is laid on those connectors that are located behind the end bearing line. The effect of these connectors is normally neglected in practical design. The modelling of the composite girders studied is based on an orthotropic material law.

From the experimental and numerical analyses it can be concluded that the state of stresses and deformations of the examined composite girders subjected to gravity loads can be determined precisely with the applied numerical models. In addition, cantilever parts accumulate significant stresses and connector forces although unloaded, violating the traditional bending theory. Furthermore, the connector carrying the maximum load is not the first but the second or third one measured from the support line towards the span. This result, although violating the traditional bending theory as well, is in accordance with result obtained with other types of composite girders.

### 8.5 New contributions of the present study and suggestions for further research

The major contributions of the present study are summarised as follows:

- A new kind of energy method based on variational calculation for determining the shear force distribution between the connectors in a composite girder is presented. This method, that proves to be in good compliance with the experimental and the latest theoretical investigations, provides a tool to cover temperature difference and gravity loading problems, too.
- Experimental tests with steel-concrete composite girders are carried out to study mainly the shear connector behaviour and its influence along the entire girder due to gravity loadings and temperature difference. In these tests a photoelastic method is also used to verify shear stresses near the beam end.
- Appropriate numerical models (FEM) for steel-concrete composite girders are developed to verify and extend the experimental results using parametric study.

- Parametric studies are carried out based on analytical and finite element analyses. As a result, new design formulas are developed for design practice in order to determine elastic shear flow at the support line. These formulas cover all the practical deformability characteristics values of common headed stud connections for each span and cross-section variations of composite girders with isotropic material.
- Experimental tests, FEM analysis and parametric studies with wood-based composite girders are carried out. The test specimens were modelled using an orthotropic material law. The state of stresses and deformations of the examined composite girders subjected to gravity loads could be precisely determined with the applied numerical models. The connector carrying the maximum load proved to be not the first but the second or third one measured from the support line towards the span.
- At the end of the new contributions it can be declared that the aims of the study (Section 1.4) have been reached.

**Suggestions for further research:**

- Unlike beam-to-column connections in Eurocode 3 and composite joints in frames for buildings in Eurocode 4 where rigid, semi-rigid and pinned connections are defined, for connections of steel-concrete composite girders in Eurocode 4 there is no definition of deformable connections. Limitations of “deformability” are not stated either. This problem should be addressed in further studies.
- Interaction formulae between shear and axial forces of shear connectors need to be developed further.
- Further research on the effect of shrinkage and creep in wood-concrete composite girders is needed.
- Long-term behaviour (creep, mechanosorptive creep, shrinkage/swelling) and temperature variations of wood-concrete girders are suggested to be addressed and considered in the standards.
- The principle of partial and full shear connection should be applied to wood-concrete composite girders in the same way as it is applied to steel-concrete composite structures.

## REFERENCES


[1] ARIBERT, J. M. & AL BITAR, A., Optimisation du dimensionnement en connection partielle de poutres de planchers mixtes réalisés avec un bac de tôle mince nervurée (Optimization of the dimensioning in the case of partial connection of beams of composite floors carried out with a thin ribbed sheet vat). Construction Métallique 4 (1989) 12, pp. 4-33.

[2] ARIBERT, J. M. & AZIZ, A. K., Modéle général pour le calcul des poutres mixtes hyper statiques jusqu'á la ruine (General model for the calculation of composite hyperstatic beams until failure). Construction Métalligue 4 (1986) 12, pp. 3-41.

[3] ARIBERT, J. M., Dimensionnement de poutres mixtes en connection partielle. In: Mixed Structures including New Materials (Dimensioning of composite beams with partial connections). IABSE Reports, Nr. 60, 1990, pp. 215-220.

[4] ARIBERT, J. M. & AZIZ, A K., Calculation of composite beams up to ultimate state with the effect of uplift at steel-concrete interface. Revue Construction Métallique n° 4 – 1985, pp. 3-36.

[5] ARIBERT, J. M. & AZIZ, A K., General model for the ultimate state design of statically indeterminate composite beams. Revue Construction Métallique n° 4 – 1986, pp. 3-41.

[6] ARIBERT, J. M. et al., Etude numérique et experimentale de l'influence d'une connection partielle sur le comportement de poutres mixtes (Numerical and experimental study of the influence of a partial connection on the behavior of composite beams). Journées. Association Francaise des Ponts et Charpentes, 1983, March, pp. 68-89.

[7] ARIBERT, J. M., Span limitations in design of composite steel and concrete beams with a partial shear connection. IABSE Symposium Brussels, Belgium - Theme 1 - September 5-7, 1990, pp. 148-154.

[8] ARIBERT, J. M., RAOUL, J. & TERPEREAU, O., Test and analyses of a bridge continuous composite beam. Proceedings “Composite Construction – Conventional and Innovative,” International Conference Innsbruck, Austria, 1997, pp. 271-276.

[9] AYOUB, A. & FILIPPOU, F. C., Mixed formulation of nonlinear steel-concrete composite beam element. Journal of Structural Engineering, ASCE, 126 (2000) 3, pp. 371-381.

[10] BAŽANT, Z. P., Comparison of approximate linear methods for concrete creep. Journal of Structural Engineering, ASCE, 100 (1974) 9, pp. 1851-1874.

[11] BODE, H. & SCHANZENBACH, J., Das Tragverhalten von Verbundträgern bei Berücksichtigung die Dübelnachgiebigkeit (Load-carrying capacity of composite girders by considering the elasticity of connectors). Der Stahlbau 58 (1989) 3, pp. 65-74.

[12] BORBÁS, L., Some problems of data evaluation of photoelastic coating technique in case of small-size, fibre-optics fitted equipment. ICEM 12, Bari, Italy, Proceedings:

Advances in Experimental Mechanics, McGraw-Hill, 2004, pp. 595-596.

[13] BUSEMANN, R., Kriechberechnung von Verbundträgern unter Benützung von zwei Kriechfasern (Calculation of creep effects in composite beams by two creep fibres). Der Bauingenieur 25 (1950), 2, pp. 418-420.

[14] CEB-FIP Model Code for concrete structures, Paris, London, Berlin, 1978.

[15] CEB-FIP Model Code 1990. Comitté Euro-International du Beton, Lausanne, 1990.

[16] CEB Model Code 90 Bulletin d'Information n. 213, Printed version, Thomas Telford. 1993.

[17] CHAPMAN, J. C., Composite construction in steel and concrete - the behaviour of composite beams. The Structural Engineer, London, England, 42 (1964) 4, pp. 115-125.

[18] Community Programme in Education and Training for Technology (COMETT), ESDEP Working Group 10. Composite Construction. The Steel Construction Institute. UK. 1993.

[19] COSENZA, E. & MAZZOLANI, S., Composite steel-concrete structures and Eurocode 4. New Research Results, Behaviour in Service of Beams with Partial Shear Connectors. Eurocodes 3 and 4 in the Light of (I) Other Design Rules (II) New Research Results. International Advanced School. Technical report. Budapest, 1994, pp. 345-374.

[20] CRISFIELD, M. A., Non-linear finite element analysis of solids and structures. Vol,. I: Essentials. Chichester, 1991. 345 p.

[21] DALL'ASTA, A. & ZONA, A., Non-linear analysis of composite beams by a displacement approach. Computers and Structures 80 (2002) 27-30, pp. 2217-2228.

[22] DALL'ASTA, A. & ZONA, A., Comparison and validation of displacement and mixed elements for the non-linear analysis of continuous composite beams. Computers and Structures 82 (2004) 23-26, pp. 2117-2130.

[23] DALL'ASTA, A. & ZONA, A., Finite element model for externally prestressed composite beams with deformable connection. Journal of Structural Engineering, ASCE, 131 (2005) 5, pp 706-714.

[24] DANIELS, B. J. & CRISINEL, M., Composite slab behavior and strength analysis. Part I: Calculation procedure. Journal of Structural Engineering, ASCE, 119 (1993) 1, pp.16-35.

[25] DAO XUAN, L., The vibro-creep of composite bridges. Ph.D. Thesis. 1977. Budapest. Supervisor: P. PLATTHY, 70 p.

[26] DAVIES, C., Tests on half-scale steel-concrete composite beams with welded stud connectors. The Structural Engineer, London, England, 47 (1969) 1, pp. 29-40.

[27] DEFRIES-SKENE A. & SKORDELIS, A. C., Direct stiffness solution for folded

plates. Journal of Structural Division of American Society of Civil Engineers, 90 (1964) ST 4, Aug., pp. 15-48.

[28] DEZI, L. & TARANTINO, A. M., Creep in composite continuous beams. I: Theoretical treatment. Journal of Structural Engineering, ASCE, 119 (1993) 7, pp. 2095-2111.

[29] DEZI, L. & TARANTINO, A. M., Creep in composite continuous beams. II: Parametric study. Journal of Structural Engineering, ASCE, 119 (1993) 7, pp. 2112-2133.

[30] DEZI, L., GARA, F. & LEONI, G., Time-dependent analysis of shear-lag effect in composite beams. Journal of Structural Engineering, ASCE, 127 (2001) 1, pp. 71-79.

[31] DISCHINGER, F., Elastische und plastische Verformungen der Eisenbeton Tragwerke und insbesondere der Bogenbrücken (Elastic and plastic deformations of reinforced concrete load-carrying structures and especially that of arch bridges). Der Bauingenieur, 1939, H. 5-6, pp. 53-63; H. 21-22, pp. 286-294; H 31-32, pp. 426-437; H. 47-48, pp. 563-572.

[32] DISCHINGER, F., Untersuchungen über die Knicksicherheit, die elastische Verformung und das Kriechen des Betons bei Bogenbrücken (Investigations on buckling safety, elastic deformation and creep of concrete in arch bridges). Der Bauingenieur, 1937, H. 33-34, pp. 487-520; H. 35-36, pp. 539-552; H 39-40, pp. 595-621.

[33] ENGLAND, G. L. & ILLSTON, J. M., Methods of computing stress in concrete from a history of measured strain. Civil Engineering and Public Works Review 1965, pp. 513-517, 692-694 and 846-847.

[34] EUROCODE 3, Design of steel structures, EN 1993-1-1, Part 1.1, General rules and rules for buildings. CEN. 2004.

[35] EUROCODE 4, Design of composite steel and concrete structures, EN 1994-1-1, Part 1.1, General rules and rules for buildings. CEN. 2004.

[36] FABBROCINO, G., MANFREDI, G. & COSENZA, E., Analysis of continuous composite beams including partial interaction and bond. Journal of Structural Engineering, ASCE, 126 (2000) 11, pp. 1288-1294.

[37] FABER, O., Plastic Yield, Shrinkage and other Problems of Concrete and their Effect on Design. Minutes of Proceedings of the Institution of Civil Engineers, Vol. 225, London, England (1927-1928), Nov. 1927, pp. 27-76.

[38] FAELLA, C., CONSALVO, V. & NIGRO, E., An “exact” finite element model for the linear analysis of continuous composite beams with flexible shear connections. Proc, 4th International Conference on Steel and Aluminium Structures, Espoo, Finland, 1999, pp. 761-770.

[39] FAELLA, C., MARTINELLI, E. & NIGRO, E., Steel and concrete composite beams with flexible shear connection: "exact" analytical expression of the stiffness matrix and applications. Computers and Structures 80 (2002) 11, pp.1001-1009.

[40] FAELLA, C., MARTINELLI, E. & NIGRO, E., Shear connection nonlinearity and deflections of steel-concrete composite beams: Simplified method. Journal of Structural Engineering, ASCE, 129 (2003) 1, pp.12-20.

[41] FENWICK, R. C. & PAULAY, T., Mechanism of Shear Resistance of Concrete Beams. ASCE Journal of the Structural Division, 94 (1968) ST10, pp. 2235-2350.

[42] FEA LTD., LUSAS USER MANUAL. Versions 12-13.6. Kingston upon Thames, UK.

[43] FORRAY, M. J., Variational Calculus in Science and Engineering. McGraw-Hill. New York-San Francisco-Toronto-London-Sydney, 1968, pp. 32-33.

[44] FRAGIACOMO, M., AMADIO, C. & MACORINI, L., Finite-element model for collapse and long-term analysis of steel concrete composite beams. Journal of Structural Engineering, ASCE, 130 (2004) 3, pp. 489-497.

[45] FRAGIACOMO, M. & CECOTTI, A., Long-term behaviour of timber-concrete composite beams. I: Finite element modelling and validation. Journal of Structural Engineering, ASCE, 132 (2006) 1, pp. 13-22.

[46] FRAGIACOMO, M., Long-term behaviour of timber-concrete composite beams. II: Numerical analysis and simplified evaluation. Journal of Structural Engineering, ASCE, 132 (2006) 1, pp. 23-33.

[47] FRITZ, B., Verbundträger. Berechnungsverfahren für die Brückenbaupraxis (Composite girder. Calculation methods for bridge engineering pactice). Springer-Verlag. Berlin-Göttingen-Heidelberg, 1961, 149 p.

[48] GALERKIN, B. G., Rods and plates. Series occuring in various questions concerning the elastic equlibrium of rods and plates (in Russian). Vestn. Inghenerov, Vol. 19, 1915, pp. 897-908.

[49] GATTESCO, N., Analytical modelling of nonlinear behaviour of composite beams with deformable connection. Journal of Constructional Steel Research 52 (1999) 11, pp. 195-218.

[50] GILBERT, R. I. & BRADFORD, M. A., Time-dependent behaviour of continuous composite beams at service loads. Journal of Structural Engineering, ASCE, 121 (1995) 2, pp. 319-327.

[51] GOLDBERG, J. E. & LEVE, H. L., Theory of prismatic folded plate structures. IABSE Publications 17 (1957) No. 87, pp. 59-86.

[52] HAWRANEK, A. & STEINHARDT, O., Theorie und Berechnung der Stahlbrücken (Theory and analysis of steel bridges). Springer – Verlag. Berlin - Göttingen - Heidelberg. 1958. Pp. 381 - 414.

[53] HOISCHEN, A., Verbundträger mit elastischer und unterbrochener Verdübelung (Composite girder with discrete elastic connectors). Der Bauingenieur 29 (1954) 7, pp. 241-244.

[54] HOLISTER, G. S., Experimental stress analysis. Cambridge University Press, 1967. Pp. 138-248.

[55] HOMBERG, H., Brücke mit elastischem Verbund zwischen den Stahlhauptträgern und der Betonfahrbahntafel (Composite bridge with elastic connection between steel main beam and concrete slab). Der Bauingenieur 27 (1952) 7, pp. 213-216.

[56] JASIM, N. A., Deflections of partially composite beams with linear connector density. Journal of Constructional Steel Research 49 (1999) 3, pp. 241-254.

[57] JASIM, N. A.& ATALLA, A., Deflections of partially composite continuous beams: a simple approach. Journal of Constructional Steel Research 49 (1999) 3, pp. 291-301.

[58] JOHNSON, R. P. & OEHLERS, D. J., Analysis and design for longitudinal shear in composite T-beam. Proceedings of the Institution of Civil Engineers 71 (1981), Part 2, pp. 909-1021.

[59] JOHNSON, R. P. & OEHLERS, D. J., Design for longitudinal shear in composite L-beams. Proceedings Institution of Civil Engineers 73 (1982), Part 2, pp. 147-170.

[60] JOHNSON, R. P. & MOLENSTRA, N., Partial shear connection in composite beams for buildings. Proceedings of the Institution of Civil Engineers 91 (1991), Part 2, pp. 679-704.

[61] JURKIEWIEZ, B., DESTREBECQ, J. F. & VERGNE, A., Incremental analysis of time-dependent effects in composite structures. Computers and Structures 73 (1999) 1-5, pp. 425-435.

[62] JUTILA, A., Load-carrying structures. Helsinki University of Technology, Laboratory of Bridge Engineering. Lecture notes. 1990.

[63] KÁLLÓ, M., Korszerű méréselemzési eljárások alkalmazása acélszerkezeteken. (Application of modern measurement techniques on steel structures). Dr. Universitas Thesis. Budapest, 1984. 70 p.

[64] KLINGENBERG, W., Verbundbauveise im Strassenbrückenbau, gegenwärtiger Stand und Überlick über laufende Versuche (Composite construction in highway bridge construction, present state and review of the ongoing tests). Der Bauingenieur 27 (1952) 6, pp. 186-194.

[65] KOLLMANN, F. & CôTÉ, W., Principles of wood science and technology, Part I, Solid Wood. Berlin - Heidelberg - New York 1968. Springer Verlag. 592 p.

[66] KÖRÖNDI, L., Comparison of strain measurement on a railway bridge with the results of a model experiment. The 5$^{th}$ Danubia-Adria Symp. on "Exp. Methods in Solid Mechanics". Udine 1988. pp. 98-99.

[67] KŘÍSTEK, V., Theory of box girders. Wiley, New York, 1979. 371 p.

[68] KŘÍSTEK, V. & STUDNIČKA, J., Analysis of composite girders with deformable connectors. Proceedings of Institution of Civil Engineers 73 (1982), Part 2, pp. 699-

712.

[69] KŘÍSTEK, V., VÍTEK, I. L. & WRIGHT, H. D., The affect of connector stiffness on composite beam design. International symposium. Bratislava 1987.

[70] KNOWLES, P. R., Composite steel and concrete construction, Butterworths, London, 1973. 200 p.

[71] KULLMAN, R. B. & HOSAIN, M. U., Shear capacity of stub-girders: Full scale tests. Journal of Structural Engineering, ASCE, 111 (1985) 1, pp. 56-75.

[72] KWAK, H. G. & SEO, Y. J., Long-term behaviour of composite girder bridges. Computers and Structures 74 (2000) 5, pp. 583-599.

[73] LAM, D. & EL-LOBODY, E., Behaviour of headed stud shear connectors in composite beam. Journal of Structural Engineering, ASCE, 131 (2005) 1, pp. 96-107.

[74] LESKELÄ, M., Calculation models for concrete-steel composite beams, considering partial interaction. Department of Civil Engineering, University of Oulu, Acta. Univ. Oulu. C 36.7986. Artes Constr. 8. Oulu, Finland, 1986, 158 p.

[75] LESKELÄ, M., Intentional and unintentional shear connections in shallow floor composite structures. RILEM Proceedings, Connections between steel and concrete. Stuttgart, 2001, pp. 1392-1401.

[76] LESKELÄ, M., Acconting effects of non-linear shear connections in composite beams. Proceedings of 5th International Conference, Composite Construction in Steel and Concrete V. South-Africa. 2004. Pp. 293-303.

[77] MÄKIPURO, R., TOMMOLA, J., SALOKANGAS, L. & JUTILA, A., Wood-Concrete Composite Bridges. Nordic Timber Bridge Project. Stockholm 1996. 71 p.

[78] MANDER, J. B., PRIESTLEY, M. J. N. & PARK, R., Theoretical stress-strain model for confined concrete. Journal of Structural Engineering, ASCE, 114 (1988) 8, pp.1804-1826.

[79] MANFREDI, G., FABBROCINO, G. & COSENZA, E., Modeling of steel-concrete composite beams under negative bending. Journal of Engineering Mechanics, ASCE, 125 (1999) 6, pp. 654-662.

[80] McMACKIN, P.J., SLUTTER, R.G. & FISHER, J.W., Headed steel anchor under combined loading. Engineering Journal, AISC 10 (1973) 2, pp. 43-53.

[81] NEUERHOFER, A. & FILIPPOU, F. C., Geometrically non-linear flexibility based frame finite element. Journal of Structural Engineering, ASCE, 124 (1998) 6, pp. 704-711.

[82] NIE, J. & CAI, C. S., Steel-concrete composite beams considering shear slip effects. Journal of Structural Engineering, ASCE, 129 (2003) 4, pp. 495-506.

[83] NIE, J., FAN, J & CAI, C. S., Stiffness and deflection of steel-concrete composite beams under negative bending. Journal of Structural Engineering, ASCE, 130 (2004) 11, pp.

1842-1851.

[84] NIELSEN, L. F., Kriechen und Relaxation des Betons (Creep and relaxation of concrete). Beton- und Stahlbetonbau 65 (1970) 11, pp. 272-275.

[85] NEWMARK, N. M., SIESS, C. P. & VIEST, I. M., Test and analyses of composite beams with incomplete interaction. Proc., Society for Experimental Stress Analysis. Vol. 9, New York 1951. Pp. 75-92.

[86] ODEN, J. T. & REDDY, J. N., Variational methods in theoretical Mechanics. Springer-Verlag. Berlin-Heidelberg-New York. 1976. Pp. 7-8.

[87] OEHLERS, D. J., Splitting induced by shear connectors in composite beams. Journal of Structural Engineering, ASCE, 115 (1989) 2, pp. 341-362.

[88] OEHLERS, D. J. & PARK, S. M., Shear connectors in composite beams with longitudinally cracked slabs. Journal of Structural Engineering, ASCE, 118 (1992) 7, pp. 2004-2022.

[89] OEHLERS, D. J. & PARK, S. M., Shear connection in haunched composite beams with sloping sides. Journal of Structural Engineering, ASCE, 120 (1994), pp. 2227-2232.

[90] OEHLERS, D. J. & BRADFORD, M.A., Composite Steel and Concrete Structural Members: Fundamental Behaviour, Pergamon, 1995. 549 p.

[91] OLLGARD, J.O., SLUTTER, R.G. & FISHER, J.W., Shear strength of stud connectors in light-weight and normal-weight concrete. Engineering Journal, AISC (1971) 8, pp. 55-64.

[92] PAULAY, T. & LOEBER, P. J., Shear transfer by aggregate interlock. Shear in reinforced concrete. ACI Special Publication SP 42 (1974), Detroit.

[93] PLATTHY, P., SZABÓ, B. & FEKETE, L., Hőmérsékleti hatás laboratóriumi szimulálása öszvértartónál (Experimental simulation of temperature difference effect in composite beams), Közlekedésépités- és Mélyépitéstudományi Szemle, XLIII. (1993), No. 11, pp. 429-439.

[94] PLATTHY, P., Rugalmas kapcsolatú folytatólagos öszvértartók számitása (Calculation of continuous composite girders having elastic connectors). ÉKME Tud. Közl. (Scientific Publications of BUTE) XI. No. 3-4. Budapest 1965. Pp. 261-270.

[95] PLUMM, D. R. & HORNE, M. R., The analysis of continuous composite beams with partial interaction. Proceedings of Institution of Civil Engineers 59 (1975) 12, Part 2, pp. 625-643.

[96] RITZ, W., Über Eine Neue Methode zur Lösung gewisser Variationsprobleme der matematischen Physik (About a new method on solving certain variational problems of mathematical physics). Journal Reine Agnew. Math. 135 (1909) 1, p. 1.

[97] RÜSCH, H., JUNGWIRTH, D. & HILSDORF, H., Kritische Sichtung der Verfahren zur Berücksichtigung der Einflüsse von Kriechen und Schwinden des Betons auf das

Verhalten der Tragwerke (A critical evaluation on the methods for considering the influence of creep and shrinkage of concrete on the behaviour of load-carrying structures). Beton und Stahlbetonbau 68 (1973) 3, pp. 49-60; 4 pp. 76-85; 6, pp.152-158.

[98] SALARI, M. R., SPACONE, E., SHING, P. B. & FRANGOPOL, D. M., Nonlinear analysis of composite beams with deformable shear connectors. Journal of Structural Engineering, ASCE, 124 (1998) 10, pp. 1148-1158.

[99] SATTLER, K., Theorie der Verbundkonstruktionen (Theory of composite structures). W. Ernst und Sohn, Berlin. 1959. 280 p.

[100] SATTLER, K., Ein allgemeines Berechnungsverfahren für Tragwerke mit elastischem Verbund (A general calculation method for load-carrying structures with elastic connectors). Köln, Stahlbau-Verlag. 1955. 53 p.

[101] SEVERIN, Z., Mereni teploty na sprazenych acelbetonovych silnicnich mostech. (Temperature measurements on steel-concrete composite bridges). Ocelové konstrukce. Vitkovice 1983. Pp. 25-35.

[102] SEBASTIAN, W. M. & McCONNEL, R. E., Nonlinear FE analysis of steel-concrete composite structures. Journal of Structural Engineering, ASCE, 126 (2000) 6, pp. 662-674.

[103] SLUTTER, R. G. & DISCROLL, G. C., Test results and design recommendations for composite beams. Lehigh University, Fritz Engineering Laboratory, Report No. 279. 10, January 1962.

[104] STÜSSI, F., Beiträge zur Berechnung und Ausbildung zusammengesetzter Vollwandträger. (Contributions to analysis and detailing of riveted plate girders). Schweizerische Bauzeitung 121 (1943) 9, pp. 87-89, 102-104.

[105] SZABÓ, B. & SZIKORA, M., Vasbetonlemezzel együttdolgozó acéltartók változó merevségű fogazásának viselkedése egyenlõtlen hõmérséklet-változás és zsugorodás hatására (The influence of temperature difference and shrinkage on the behaviour of steel-concrete composite structures with connectors of varying stiffness). Közlekedésépítés- és Mélyépítéstudományi Szemle. Vol. XL. 12. 1990. Pp. 458-464. (In Hungarian).

[106] SZABÓ, B., Sajátfeszültségekkel és súlyteherrel terhelt öszvértartók vizsgálata (Experimental analysis of composite beams subjected to temperature difference, shrinkage and patch load). VI. Magyar Mechanikai Konferencia. Miskolc 1991. Pp. 116-117. (In Hungarian).

[107] SZABÓ, B. & PLATTHY, P., The influence of temperature difference on the behaviour of steel-concrete composite Structures. The 7th Czech and Slovak International Conference on Steel Structures and Bridges, Bratislava, Slovakia, 1994. Pp. II-189-II-193.

[108] SZABÓ, B., Öszvértartó numerikus analízise **(**Numerical analysis of composite girder). BETON szakmai havilap. A Magyar Epitöanyagipari Szövetség Beton Tagozatának hivatalos lapja. Vol. V. 11. 1997. Pp. 16-19. (In Hungarian).

[109] SZABÓ, B., Hőmérsékleti hatásnak kitett öszvértartó numerikus analízise (Finite Element Analysis of Composite Bridge Subjected to Temperature Difference). Közúti Közlekedés- és Mélyépítéstudományi Szemle Vol. XLVIII. 3. 1998. Pp. 110-116. (In Hungarian).

[110] SZABÓ, B., Shear force distribution of headed studs of composite simply supported beams subjected to temperature difference. Proceedings of Conference Eurosteel "99 Praha. 1999. Pp. 557-560.

[111] SZABÓ, B., Fa-vasbeton öszvérhidak Finnországban (Wood-concrete composite bridges in Finland). Közúti Közlekedés- és Mélyépítéstudományi Szemle Vol. 50.1. 2000. Pp. 36 - 38. (In Hungarian).

[112] SZABÓ, B., Súlyterhekkel igénybevett öszvértartók nyírt kapcsolóelemeinek viselkedése (Behaviour of shear connectors of composite girders subjected to gravity loading). Közúti Közlekedés- és Mélyépítéstudományi Szemle Vol. 51. 2. 2001. Pp. 75 -78. (In Hungarian).

[113] SZABÓ, B. & JUTILA, A., Behaviour of shear connectors in wood-based composite girders. Proceedings of IABSE Conference LAHTI 2001 (Innovative Wooden Structures and Bridges). Finland. 2001. Pp. 143–148.

[114] TAYLOR, R. P., PLUM, D. R. & PAPASOZOMENOS, A. G., Investigations on the use deep haunches in composite construction. Proceedings of the Institution of Civil Engineers 47 (1964), Part 2, pp. 115-125.

[115] TIMOSHENKO, S. P., and GODIER, J. N., Theory of elasticity. 2nd ad., McGrav- Hill Book Co., New York, N.Y. 1970. 567 p.

[116] TOMMOLA, J. & JUTILA, A., Test results on shear connectors used in wood-concrete composite bridges. International Scientific Conference, Use of Timber and Steel Structures in Construction. Bratislava. November 18-20, 1998. 10 p.

[117] TOMMOLA, J., SALOKANGAS, L. & JUTILA, A., Tests on shear connectors. Nordic Timber Bridge Project. Stockholm 1999. 19 p.

[118] TOMMOLA, J. & JUTILA, A., Analysis of wood-concrete composite girder with discrete shear connectors. Proceedings of IABSE Conference LAHTI 2001 (Innovative Wooden Structures and Bridges). Finland. 2001. Pp. 489 – 494.

[119] TOPRAC, A. A. & DALE, G. E., Composite beams with a hybrid Tee steel section. Journal of Structural Engineering, ASCE, 93 (1967) 5, pp. 309-322.

[120] TROST, H., Zur Berechnung von Stahlverbundträgern im Gebrauchszustand auf Grund neuerer Enkenntnisse des Viskoelastischen Verhaltens des Betons (Analysis of composite steel girders in serviceability state on the basis of recent knowledge of the viscoelastic behaviour of concrete), Der Stahlbau 37 (1968) 11, pp. 321-331.

[121] TROST, H., Auswirkungen des Superpositionsprinzips auf Kriech-und Relaxationsprobleme bei Beton und Spannbeton (Influence of superposition principle of creep and relaxation in concrete and prestressed concrete). Beton und Stahlbetonbau 62 (1967) 10, pp. 230-238; 11, pp. 261-269.

[122] TROST, H., MAINZ, B. & WOLFF, H., Zur Berechnung von Spannbetontragwerken im Gebrauchszustand unter Berücksichtigung des zeitabhängigen Betonverhaltens (On analysing of prestressed concrete structures in serviceability state taking into consideration the time-dependent behaviour of concrete). Beton und Stahlbetonbau 66 (1971) 9, pp. 220-225; 10, pp. 241-244.

[123] TROST, H. & WOLFF, H., Zur wirklichkeitsnahen Ermittlung der Beanspruchungen in abschnittsweise hergestellten Spannbetontragwerken (On determination of realistic stresses of prestressed concrete structures fabricated in parts). Der Bauingenieur 45 (1970) 5, pp. 155-169.

[124] VÁSÁRHELYINÉ, Sz. A., A Treftz-módszer és véges elemes módszer összeépítése alapozási probléma megoldásánál (Amalgamation of Treftz and finite element method for solution of foundation problem). Építés-Építészettudomány. Vol. X. (3-4). Pp. 331- 340. (Additionally consultation with the paper author.)

[125] WANG, Y. C., Deflection of steel-concrete composite beams with partial shear interaction. Journal of Structural Engineering, ASCE, 124 (1998) 10, pp. 1159-1165.

[126] WRIGHT, H. D., The deformation of composite beams with discrete flexible connection. Journal of Constructional Steel Research 15 (1990) 1, pp 49-64.

[127] ZSILÁK, ZS. & FEKETE, L., Experimental analysis of residual stresses of composite beams. Scientific Student Circle Work. Budapest 1992. Pp. 64-76.

[128] YAM, L. C. P., Design of composite steel-concrete structures. London, Surrey University Press, 1981. 168 p.

# APPENDIX

## Calculation of a simply supported beam subjected to 40 °C temperature difference using the Author's Energy Method

The Author's Energy Method is here applied to a simply supported steel-concrete composite girder with 2 m span (Fig. 37, Specimen S4) subjected to 40 °C temperature difference. The beam is a 140 mm high welded plate girder with 100 mm x 10 mm flanges and 120 mm x 6 mm web. The slab cross-section was 250 mm x 80 mm. The layers were connected by 16 pieces "D" type connectors (Fig. 33). The connectors had equal spacing of 130 mm. The elastic modulus value was 205000 MN/m$^2$ for steel and 29550 MN/m$^2$ for concrete. The coefficient of thermal expansion $a_T$ for steel is 0,000012 1/°C. The geometrical properties of the composite girder (Specimen S4) and constants for calculation are summarised in Table A1 and Table A2.

*Table A1. Geometrical properties of Specimen S4.*

| Distance [m] | | | Area of cross-section [m$^2$] | | | Moment of inertia [m$^4$] | | |
|---|---|---|---|---|---|---|---|---|
| $d_{ai}$ | $d_{ci}$ | $d$ | $A_a$ | $A_c$ | $A_i$ | $I_a$ | $I_c$ | $I_i$ |
| 0,057 | 0,053 | 0,110 | $2{,}72\cdot10^{-3}$ | $20{,}0\cdot10^{-3}$ | $5{,}603\cdot10^{-3}$ | $9{,}36\cdot10^{-6}$ | $10{,}67\cdot10^{-6}$ | $27{,}83\cdot10^{-6}$ |

*Table A2. Constants for calculation.*

| Spring stiffness value | Constants of HAWRANEK-STEINHARDT equation | |
|---|---|---|
| $K$ [N/mm$^2$] | $w^2$ [m$^{-2}$] | $g$ [m$^{-3}$] |
| 2600 | $2{,}314\cdot10^{-3}$ | 128,02 |

The moment due to temperature difference $DT$ = 40 °C (the steel beam has positive strain) can be calculated using the following formula (page 46 of Ref. [70]):

$$M = 2\frac{a_T \cdot DT \cdot E_c \cdot A_c \cdot d_{ci}}{I_i}\cdot\left(I_a + \frac{E_c \cdot I_c}{E_a}\right) = 2\frac{1{,}2\cdot10^{-5}\cdot 40\cdot 29550\cdot 20{,}0\cdot10^{-3}\cdot 0{,}053}{27{,}83\cdot10^{-6}}\cdot$$

$$\left(9{,}36\cdot10^{-6} + \frac{29550\cdot 10{,}67\cdot10^{-6}}{205000}\right) = 0{,}012\ MNm$$

In order to obtain the normal force $N(x)$ Equation (87) can be used to determine Fourier coefficients $a_i$, where $i = 1, 2, \ldots 12$. (In practice is usual to take into consideration up to 12 Fourier members.) The calculation can be carried out by using MathCad software, for instance. Some steps of the process are shown below.

Determining of $a_1$

$n := 1$

$a_1 := 1$

Given

$$a_1 \cdot \int_0^L \left( n \cdot \frac{\pi^2}{L^2} \cdot \cos\left( n \cdot \frac{\pi \cdot x}{L} \right) \right)^2 dx + \omega^2 \cdot a_1 \cdot \int_0^L \sin\left( n \cdot \frac{\pi \cdot x}{L} \right)^2 dx = \gamma \cdot M \cdot \int_0^L \sin\left( n \cdot \frac{\pi \cdot x}{L} \right) dx$$

$a_1 := \text{Find}(a_1)$

$a_1 = 66{,}148$

Determining of $a_2$

$n := 2$

$a_2 := 1$

Given

$$a_2 \cdot \int_0^L \left( n \cdot \frac{\pi^2}{L^2} \cdot \cos\left( n \cdot \frac{\pi \cdot x}{L} \right) \right)^2 dx + \omega^2 \cdot a_2 \cdot \int_0^L \sin\left( n \cdot \frac{\pi \cdot x}{L} \right)^2 dx = \gamma \cdot M \cdot \int_0^L \sin\left( n \cdot \frac{\pi \cdot x}{L} \right) dx$$

$a_2 := \text{Find}(a_2)$

$a_2 = 0$

Determining of $a_3$

$n := 3$

$a_3 := 1$

Given

$$a_3 \cdot \int_0^L \left( n \cdot \frac{\pi^2}{L^2} \cdot \cos\left( n \cdot \frac{\pi \cdot x}{L} \right) \right)^2 dx + \omega^2 \cdot a_3 \cdot \int_0^L \sin\left( n \cdot \frac{\pi \cdot x}{L} \right)^2 dx = \gamma \cdot M \cdot \int_0^L \sin\left( n \cdot \frac{\pi \cdot x}{L} \right) dx$$

$a_3 := \text{Find}(a_3)$

$a_3 = 8{,}27$

.

.

Determining of $a_{12}$

$a_{12} := 1$

$n := 12$

Given

$$a_{12} \cdot \int_0^L \left( n \cdot \frac{\pi^2}{L^2} \cdot \cos\left( n \cdot \frac{\pi \cdot x}{L} \right) \right)^2 dx + \omega^2 \cdot a_{12} \cdot \int_0^L \sin\left( n \cdot \frac{\pi \cdot x}{L} \right)^2 dx = \gamma \cdot M \cdot \int_0^L \sin\left( n \cdot \frac{\pi \cdot x}{L} \right) dx$$

$a_{12} := \text{Find}(a_{12})$

$a_{12} = 0$

The Fourier coefficients $a_i$ and the vector of Fourier components (formulation and values) $p(x)_i$ are summarised in Table A3.

*Table A3. Fourier coefficients $a_i$ and components $p(x)_i$.*

| | | | | | | |
|---|---|---|---|---|---|---|
| $a_i$ | $a_1$ | 66,148 | $p(x)_i = \begin{pmatrix} \sin 1 \cdot \frac{p \cdot x}{L} \\ \sin 2 \cdot \frac{p \cdot x}{L} \\ \sin 3 \cdot \frac{p \cdot x}{L} \\ . \\ . \\ \sin 12 \cdot \frac{p \cdot x}{L} \end{pmatrix}$ | $p(x)_i$ | $p(x)_1$ | 0 |
| | $a_2$ | 0 | | | $p(x)_2$ | 0 |
| | $a_3$ | 8,27 | | | $p(x)_3$ | 0 |
| | $a_4$ | 0 | | | $p(x)_4$ | 0 |
| | $a_5$ | 2,206 | | | $p(x)_5$ | 0 |
| | $a_6$ | 0 | | | $p(x)_6$ | 0 |
| | $a_7$ | 0,859 | | | $p(x)_7$ | 0 |
| | $a_8$ | 0 | | | $p(x)_8$ | 0 |
| | $a_9$ | 0,416 | | | $p(x)_9$ | $1{,}102 \cdot 10^{-15}$ |
| | $a_{10}$ | 0 | | | $p(x)_{10}$ | $-1{,}225 \cdot 10^{-15}$ |
| | $a_{11}$ | 0,231 | | | $p(x)_{11}$ | $4{,}900 \cdot 10^{-15}$ |
| | $a_{12}$ | 0 | | | $p(x)_{12}$ | $-1{,}470 \cdot 10^{-15}$ |

The normal force $N(x)$ from MathCad equation (see also Equation (76))

$$N(x) := \sum_{i=0}^{11} \left( a_{i,0} \cdot p(x)_{i,0} \right)$$

can be obtained. Derivation of normal force $N(x)$ provides the shear flow $T(x)$ (in N/mm unit)

$$T(x) := \frac{d}{dx} \sum_{i=0}^{11} \left( a_{i,0} \cdot p(x)_{i,0} \right)$$

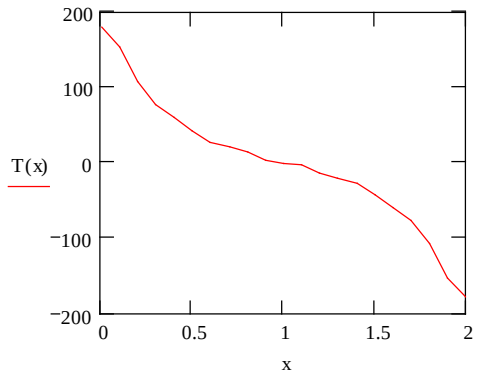


From the non-uniform curve of shear force per unit length $T(x)$ it can be concluded that for the precise calculation of shear flow more terms of the Fourier series need to be considered.

Programming a cycle for the Fourier coefficients $a_i$

$$a := \left| \begin{array}{l} \text{for } \ value \in 1..n \\ \quad a_{value-1} \leftarrow \dfrac{\gamma \cdot M \cdot \displaystyle\int_0^L \sin\left( value \cdot \frac{\pi \cdot x}{L} \right) dx}{\displaystyle\int_0^L \left( value \cdot \frac{\pi^2}{L^2} \cdot \cos\left( value \cdot \frac{\pi \cdot x}{L} \right) \right)^2 dx + \omega^2 \cdot \int_0^L \sin\left( value \cdot \frac{\pi \cdot x}{L} \right)^2 dx} \\ \quad a \end{array} \right.$$

the normal force *N(x)* and shear flow *T(x)* can be obtained from MathCad equations

$$N(x) := \sum_{i=0}^{n-1} \left[ a_i \cdot \sin\left[ (i+1) \cdot \frac{\pi \cdot x}{L} \right] \right] \qquad \text{and} \qquad T(x) := \frac{d}{dx} \sum_{i=0}^{n-1} \left[ a_i \cdot \sin\left[ (i+1) \cdot \frac{\pi \cdot x}{L} \right] \right]$$

when a reasonable number of cycles (e.g. *n = 400*) are used. The perfect diagrams *N(x)* and *T(x)* shown below can then be demonstrated.

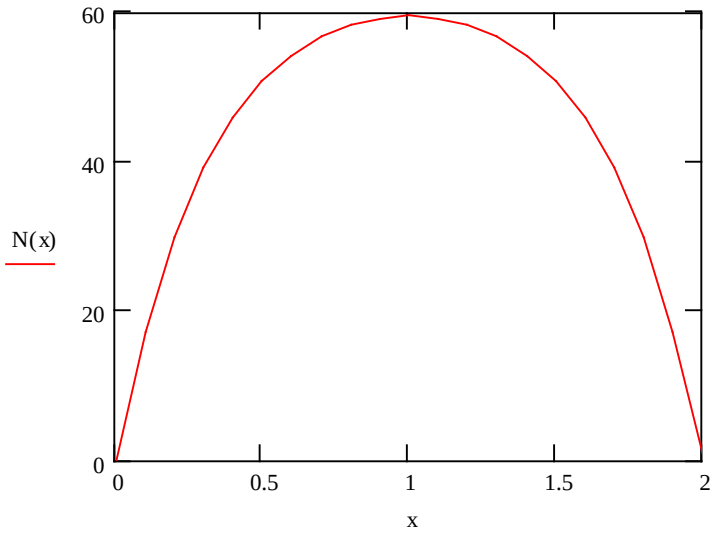


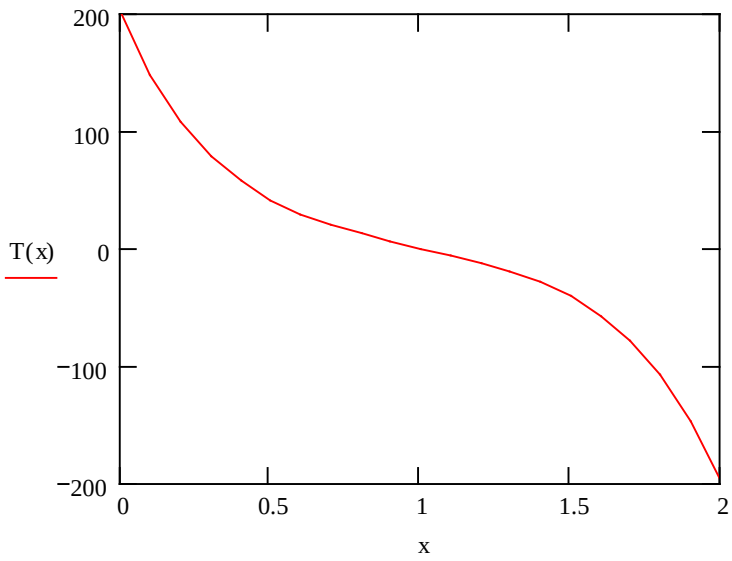

TKK-SRT-1 Tesár, A.,
Advanced analysis of thin-walled structures in bridge and structural engineering. Editor: Jutila, A. 1992. 83 p.

TKK-SRT-2 Haakana, P., Jutila, A., Rautakorpi, H. & Salokangas, L.,
Tutkimusprojekti puusiltojen kehittäminen, taustatietojen selvittäminen. 1993. 78 p.

TKK-SRT-3 Haakana, P., Jutila, A., Rautakorpi, H. & Salokangas, L.,
Research project development of wood bridges, survey of source documents. Excerpt of the Finnish Report Survey of background information (Publication no. 2). 1993. 46 p.

TKK-SRT-4 Kiviluoma, R.,
Vinoköysisillan analyysi tuulikuormalle. Editor: Jutila, A. 1993. 112 p.

TKK-SRT-5 Rautakorpi, H., Tesár, A., Jutila, A., Mäkipuro, R., Haakana, P. & Salokangas, L.,
Research project development of wood bridges, prospects of wood in various types of bridges. 1993. 54 p.

TKK-SRT-6 Tesár, A., Jutila, A., Rautakorpi, H., Haakana, P. & Salokangas, L.,
Research project development of wood bridges, numerical and experimental analysis of static and dynamic behaviour of wood bridges. 1993. 47 p.

TKK-SRT-7 Wiio, M., Jutila, A., Mäkipuro, R., Haakana, P., Salokangas, L. & Wistbacka, J.,
Research project development of wood bridges, literature survey of shear connections of wood-concrete composite bridges. 1994. 14 p.

TKK-SRT-8 Rautakorpi, H., Jutila, A., Mäkipuro, R., Haakana, P. & Salokangas, L.,
Research project development of wood bridges, literature survey of wooden arch bridges. 1994. 34 p.

TKK-SRT-9 Haakana, P., Jutila, A., Kiviluoma, R., Mäkipuro, R., Rautakorpi, H. & Salokangas, L.,
Tutkimusprojekti puusiltojen kehittäminen, puusiltojen suunnitteluperusteet ja -menetelmät. 1994. 66 p.

TKK-SRT-10 Rautakorpi, H., Jutila, A., Mäkipuro, R., Haakana, P. &, Salokangas, L.,
Research project development of wood bridges, scale model tests of a wooden arch bridge. 1994. 26 p.

TKK-SRT-11 Mäkipuro, R., Jutila, A., Rautakorpi, H., Haakana, P. &, Salokangas, L.,
Research project development of wood bridges, experimental studies of wood-concrete shear connections. 1994. 26 p.

TKK-SRT-12 Wistbacka, J.,
Puu-betoni-liittopalkki. Editor: Jutila, A. 1994. 73 p.

TKK-SRT-13 Rusila, J.,
Liittopalkkisiltojen tietokoneohjelmat ja niiden kehittäminen. Editor: Jutila, A. 1995. 101 p.

TKK-SRT-14 Torkkeli, M.,
Literature survey on fatigue of bond between prestressed steel and concrete. Editor: Jutila, A. 1996. 53 p.

TKK-SRT-15 Noponen, S. & Jutila, A.,
Reiällisen vanerilevyn tarttuvuus betoniin. 1997. 91 p.

TKK-SRT-16 Paavola, E.,
Teräslevyn varaan ruiskubetonoitu holvisilta. Editor: Jutila, A. 1997. 126 p.

TKK-SRT-17 Rissanen, T.,
Picada Varela –sillan uudistamistyö osana Uruguayn kantatieverkon parantamista. Editor: Jutila, A. 1998. 81 p.

TKK-SRT-18 Noponen S., Jutila A.,
Puu-betoni-liittopalkkisiltojen muotti- ja telineratkaisut. Dec 1998. 20 p.

TKK-SRT-19 Noponen S., Jutila A.,
Puu-betoni-liittopalkkisiltojen tyyppipiirustukset. Dec 1998. 39 p.

TKK-SRT-20 Savolainen A., Rautakorpi H., Jutila A.,
Puisen kevyen liikenteen kaarisillan kehittäminen. Dec 1998. 93 p.

TKK-SRT-21 Mäkipuro R., Jutila A.,
Puuta sisältävän liittopalkkisillan laskentamenetelmät. Dec 1998. 25 p.

TKK-SRT-22 Torkkeli M., Rautakorpi H., Jutila A.,
Puisen ajoneuvoliikenteen kaarisillan kehittäminen. Dec 1998. 57 p.

TKK-SRT-23 Salokangas L., Jutila A.,
Puu-betoni-liittopalkkisillan seurantatutkimus. Dec 1998. 20 p.

TKK-SRT-24 Mäkipuro R., Jutila A.,
Elementtikantisten puusiltojen prototyyppimallit. Dec 1998. 27 p.

ISBN 951-22-8446-4

ISBN 951-22-8447-2 (PDF)

ISSN 1456-6273